2015

DEFORMATION-BASED EXCAVATION SUPPORT SYSTEM DESIGN METHOD

Sekyi K. Intsiful
University of Kentucky, ksin222@uky.edu

STUDENT AGREEMENT:

I represent that my thesis or dissertation and abstract are my original work. Proper attribution has been given to all outside sources. I understand that I am solely responsible for obtaining any needed copyright permissions. I have obtained needed written permission statement(s) from the owner(s) of each third-party copyrighted matter to be included in my work, allowing electronic distribution (if such use is not permitted by the fair use doctrine) which will be submitted to UKnowledge as Additional File.

I hereby grant to The University of Kentucky and its agents the irrevocable, non-exclusive, and royalty-free license to archive and make accessible my work in whole or in part in all forms of media, now or hereafter known. I agree that the document mentioned above may be made available immediately for worldwide access unless an embargo applies.

I retain all other ownership rights to the copyright of my work. I also retain the right to use in future works (such as articles or books) all or part of my work. I understand that I am free to register the copyright to my work.

REVIEW, APPROVAL AND ACCEPTANCE

The document mentioned above has been reviewed and accepted by the student's advisor, on behalf of the advisory committee, and by the Director of Graduate Studies (DGS), on behalf of the program; we verify that this is the final, approved version of the student's thesis including all changes required by the advisory committee. The undersigned agree to abide by the statements above.

Sekyi K. Intsiful, Student

Dr. L. Sebastian Bryson, Major Professor

Dr. Y.T. (Ed) Wang, Director of Graduate Studies

DEFORMATION-BASED EXCAVATION SUPPORT SYSTEM DESIGN METHOD

THESIS

A thesis submitted in partial fulfillment of the

requirements for the degree of Master of Science in

Civil Engineering in the College of Engineering

at the University of Kentucky

By

Sekyi Kobina Intsiful

Lexington, KY

Director: Dr. L. Sebastian Bryson, Associate Professor of Civil Engineering

Lexington, KY

ABSTRACT OF THESIS

DEFORMATION-BASED EXCAVATION SUPPORT SYSTEM DESIGN METHOD

Development in urban areas around the world has steadily increased in recent years. This rapid development has not been matched by the ever decreasing open space commonly associated with urban centers. Vertical construction, thus, lends itself a very useful solution to this problem. Deep excavation is often required for urban construction. Unfortunately, the ground movements associated with deep excavation can result in damage to adjacent buildings. Thus, it is critically important to accurately predict the damage potential of nearby deep excavations and designing adequate support systems.

A new design method is proposed, as an attempt, to address the problem. The method is semi-empirical and directly links excavation-induced distortions experienced by nearby buildings and the components of the excavation support system. Unlike, the traditional limit equilibrium approach, the method is driven by the distortions in adjacent buildings. It goes further to propose a preliminary cost chart to help designers during the design phase. The benefit is that initial cost is known real time and will help speed up making business decisions. A new design flowchart is proposed to guide the designer through a step-by-step procedure.

The method is validated using Plaxis 2D (the finite element program) simulation. Though the nature of deep excavation is three-dimensional, a plane strain condition is valid when the length of the excavation is long. Hence, two-dimensional finite element simulation was considered appropriate for this effort. Five hypothetical cases were compared and the model performed very well. The lack of available literature on this approach made verification difficult. It is hoped that future case histories will be used to ascertain the veracity of the deformation-based design method.

KEYWORDS: Deep Excavation; Excavation Support System; Crack Width; Cost
                 Estimate; Ground Settlement Profile; 2D Finite Element
                 Simulation; Deformation.

Sekyi Kobina Intsiful

05/08/2015

DEFORMATION-BASED EXCAVATION SUPPORT SYSTEM DESIGN METHOD

By

Sekyi Kobina Intsiful

_____

L. Sebastian Bryson, Ph.D., P.E.

Director of Thesis

_____

Dr. Yi-Tin Wang

Director of Graduate Studies

05/08/2015

ACKNOWLEDGEMENTS

I use this opportunity to firstly express my gratitude to my advisor, L. Sebastian Bryson, Ph.D., P.E. Through the opportunity he gave me as a research assistant and his continuous support and guidance along the entire journey. Working with him has offered me an opportunity to learn a whole lot in both regular course work and in the field of research.

Secondly, I would use this opportunity to express my thankfulness to my family, especially my older brother, Kwame Wilson Intsiful, for coming through for me when I needed it the most.

Lastly, I am grateful to all the lecturers, working staff of UK, colleagues and friends, who in diverse ways contributed to my successful completion.

TABLE OF CONTENTS

LIST OF TABLES

LIST OF FIGURES

xiv

CHAPTER 1

1.0   Introduction

1.1   Background

Developmental projects involving deep excavation have become very popular worldwide. Especially in urban and densely populated areas, vertical construction lends itself as a solution to the ever the growing constraint on the availability of space above the ground. The closeness to adjacent structures, therefore requires that these excavation support systems be rigid to limit ground movements induced damages. Stiff excavation support systems (such as secant pile walls, diaphragm walls, or tangent pile walls) have been used successfully to limit ground movement-induced damages. Several case histories exist for the use of stiff excavation support systems; examples such as the use of secant pile walls for the construction of a subway station (Finno and Bryson, 2002), cut-and-cover tunnel excavation (Koutsoftas et al., 2000), and deep basement excavations (Ou et al., 2000; Ng, 1992); inter alios. The problem of excessive excavation-induced damage associated with underground construction in urban areas is a major concern, especially in soft clays and adjacent buildings with shallow foundation. Excessive ground movements can lead to significant displacements and rotations in adjacent structures, thereby causing damages ranging from cosmetic to structural. Hence, an accurate prediction of the ground movements related to deep excavation a critical step in the design and analysis of excavation support systems.

1

Traditionally, structural limit equilibrium controls the design of excavation support systems. Despite the fact that this method prevents structural failure of the support system, it however, does not limit ground movements. Thus, this approach does not necessarily minimize the levels of damages in walls and structural members of adjacent buildings. These limit equilibrium methods are based on expected apparent earth pressure diagrams developed by Peck (1969) or Tschebotarioff (1951).These pressure diagrams were from field measurement of strut loads, thus represent conservative enveloped values. Using this approach, the support system is defined in terms of the maximum anticipated earth pressure and governed by overall structural stability. Therefore, the approach may not necessarily meet maximum horizontal or vertical deformation limiting criterion.

Current state-of-the-art design methods relate excavation induced ground movements to the stiffness of the support system, and then relate those ground movements to damage estimates. However, these approaches are iterative in nature. They require the designer to choose a wall design based on structural stability considerations, and then estimate the ground movements. Severity of the possible damage is then inferred from the estimated ground movements. The entire process is iterated until acceptable damage levels are obtained. Very few authors have proposed methods to quantify excavation-induced damage to adjacent structures (Boscardin and Cording, 1989; Boone, 1996; Son and Cording, 2005; Bryson and Kotheimer, 2011).

The method proposed in this thesis will invert the aforementioned limit equilibrium-based design approach. It presents a means to directly design excavation support systems based on an approach that first considers acceptable excavation-induced

2

damage and the corresponding deformations, and then satisfies the structural stability requirements.

1.2   Proposed Method

Previously mentioned is the fact that current methods satisfy structural stability first and then check for deformation compliance. The difficulty with this is that it does not guarantee acceptable levels of damage in adjacent buildings due to excavation-induced ground movements.

In this research, a new deformation-based method (inverse design approach) is proposed to design excavation support systems which will ensure limited damages in adjacent buildings. In essence, it first achieves deformation compliance and then structural stability, as opposed to the converse. The approach was developed from parametric studies of several configurations of deep excavation support systems. This approach also addresses the issue of the iterative process associated with the traditional approach, and provides a streamlined excavation support system design option. Additionally, it provides insight into the cost implications of choices that the designer will be faced along the design process by providing a preliminary cost estimate. Thus, yielding not only an acceptable design, but also a cost-effective one.

1.3   Objectives of Research

The aim of the research is to propose a deformation-based approach (i.e. inverse design) that will produce acceptable levels of damage in adjacent structures while controlling cost.

3

To achieve this goal, the following will be done:

- Develop a design flow chart that will guide the designer through the entire process. It will allow the engineer/designer to achieve acceptable damage to adjacent buildings, size walls and supports and develop preliminary cost estimates during the design the process.

- Develop a two-dimensional simulation in Plaxis 2D as a basis for evaluating the validity of the proposed method.

- Develop a new deformation-based methodology using existing formulations that will link deformations in adjacent structures to the components of the excavation support system.

- Develop a new cost chart that will be used as a guide to inform the designer about cost-benefit analysis with respect to options available during design.

1.4   Relevance of Research

The uncertainty associated with the traditional approach of designing for structural stability and then checking for deformation leaves much to be desired. In essence, a structurally stable excavation support system may still lead to costs associated with unacceptable damage in adjacent buildings. Failure costs associated with deep excavations is estimated in monetary terms to be between 5-10 percent loss of effectiveness compared to 2-3 percent net profit (Van Staveren, 2006). This is understandable given the complicated nature of the soil-structure interaction of excavation support systems and the excavation-induced ground movements (Ou et al., 2000; Lin et al., 2003; Zdravkovic et al., 2005; Finno et al., 2007). Although much

4

research has been done concerning crack width measurements; excavation-induced deformation; ground settlement profiles related to deep excavation and tunneling; soil-structure interaction and building stiffness and geometry, these efforts tend to be stand-alone in nature. This research, therefore, attempts to put all the various components together in a more coherent manner. It is highly anticipated that this new approach will prove useful in designing excavation support systems that yields acceptable damage in adjacent buildings. Finally, it is intended that this study will directly link cost of an excavation support system to induced damages in adjacent buildings.

1.5   Content of Thesis

In Chapter 2, the current state-of-practice is presented. It reviews available literature on excavation-induced deformation; soil-structure interaction; stiffness of adjacent buildings; stiffness of excavation support systems; crack width measurements and ground settlement profiles. Additionally, it will attempt to highlight the deficiencies with current practices which can be improved.

Chapter 3 presents the analytic approach and development of the deformation-based design approach. All the formulations and charts developed are presented within this chapter as well.

Chapter 4 focuses on the sensitivity analyses of the various parameters used in the development process. Various elements of the excavation support system are varied and the effects on pertinent items are presented.

5

Chapter 5 presents the evaluation of the performance of the proposed method. This is done by comparing the output of a finite element model of a two-dimensional deep excavation using the Plaxis 2D software package. Additionally, a simple statistical inference is constructed using the data from the predicted deformation values.

Chapter 6 summarizes the research and presents the overall conclusions. This chapter also presents recommendations on how to further research in damage to adjacent structures caused by nearby excavations.

2.0   Technical Background

2.1   Current State-of-Practice of Excavation Support System Design

Typically, excavation support system design starts by first sizing all the elements of the support system to satisfy limit equilibrium requirements; and then checks are conducted for excavation-induced ground movements. By the traditional approach, pre-determined limits of acceptable ground movements are set prior to performing the support system design. These limits are usually set in accordance with the governing building codes being enforced for the excavation or are based on an approach that is specific to the design engineer. In the scenario where the pre-defined ground movement is exceed by the support system, available options are to increase various structural sections of the system or to reduce the vertical and horizontal support spacing, or a combination of the two. Figure 2.1 is a schematic of the iterative process involved in the traditional design of excavation support system.
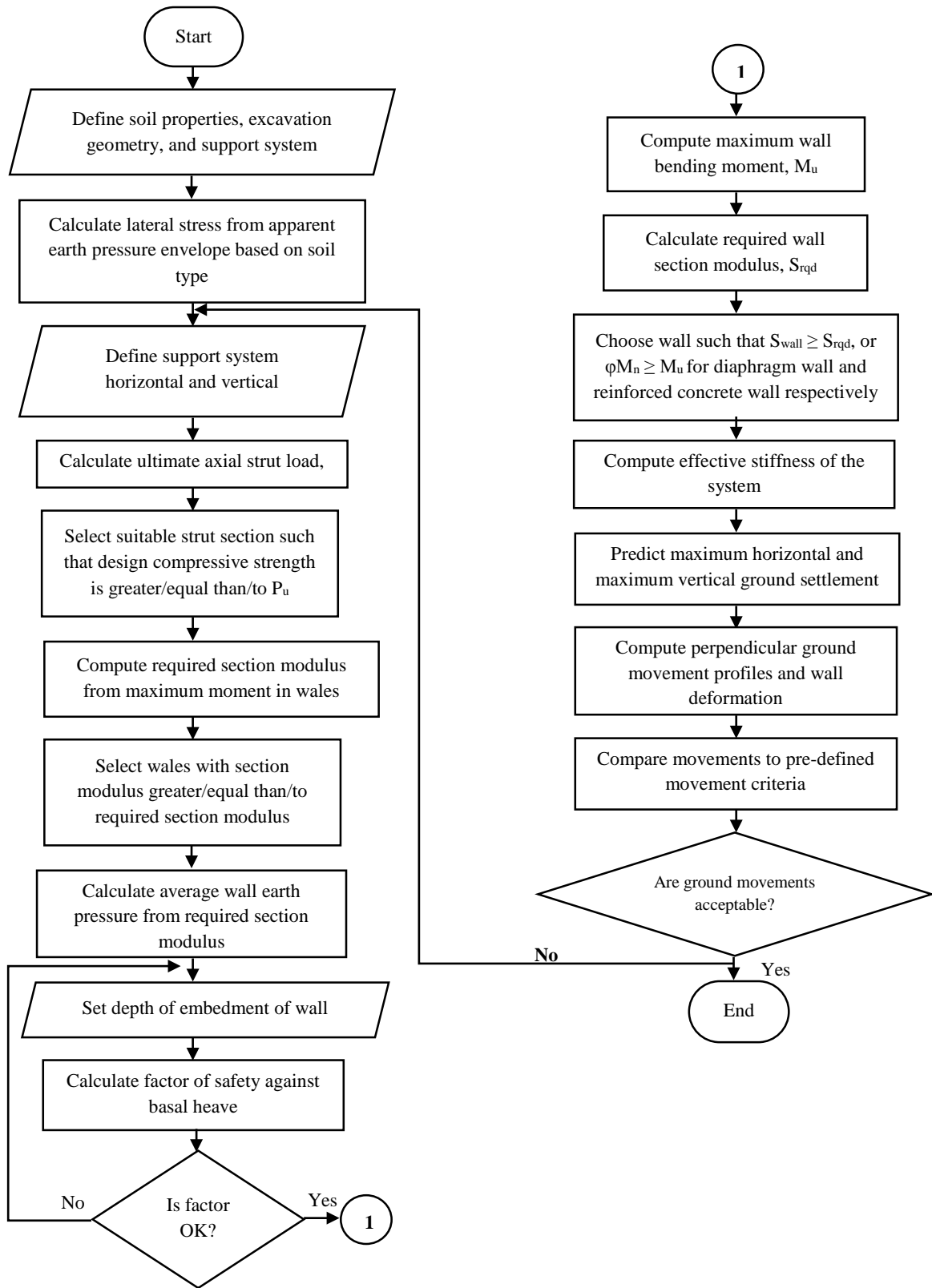
Figure 2.1 Schematic of traditional excavation support system design.

8

where P_u is ultimate strut load; S_{wall} is section modulus of support wall; φM_n is design moments of reinforced concrete wall; M_u is applied wall moments.

2.2   Excavation Related Damage

The current state of excavation support system design methods, first and foremost, satisfy structural stability and then check for deformation compliance. Inherently, this approach does not guarantee the safety of nearby infrastructure. The most efficient method, thus, will be to design the excavation support system in such a way as to prevent damage to adjacent infrastructure. Several researchers (Boone, 1996; Finno et al., 2005; Son and Cording, 2005, 2008; Bryson and Kotheimer, 2011) have linked damage in buildings adjacent to excavations, to vertical ground movements. Of particular concern are buildings on shallow foundations (Son and Cording 2008). The aforementioned researchers' approach typically relate semi-empirical damage criteria to building distortions. These excavation-induced distortions are then related to the changes in ground slope. Using settlement profiles, changes in ground slope can be predicted given the maximum settlement value.

2.3   Basal Stability of Excavations in Clays

Ground movements adjacent to deep excavations occur in response to lateral deflections of the excavation support system. In soft clay, these movements are influenced by the stiffness of the support system, the soil and groundwater conditions, the earth and pore-water pressures, and the construction procedures. Additionally, lateral movements of an excavation support system tend to increase dramatically as a result of

plastic yielding in the soil beneath and surrounding the excavation. The extent of the plastic yielding can be quantified with the use of factor of safety against basal heave. Basal stability analyses can be carried out using limit equilibrium methods that assume two-dimensional conditions and are based on bearing capacity (Terzaghi, 1943) (Figure 2.2).
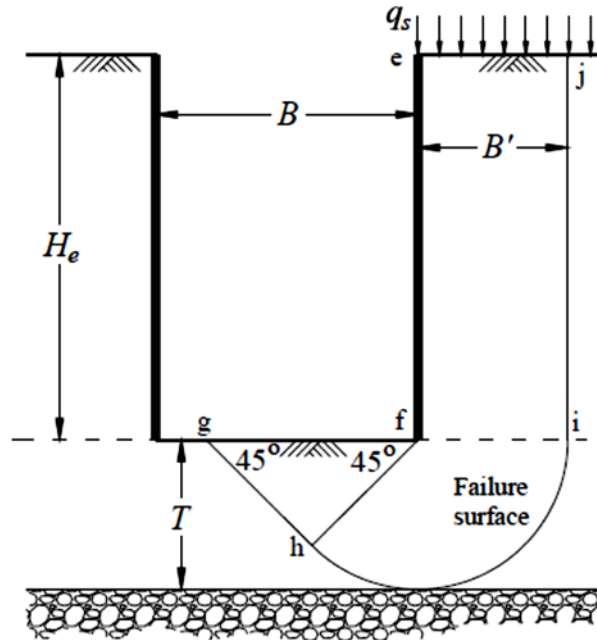
Figure 2.2 Factor of safety against bottom heave without wall embedment depth (Terzaghi, 1943a).

Based on section *jihg* in Figure 2.2, Terzaghi (1943a) assumed a failure surface of infinite length for wide excavation and provided the following as the factor of safety against bottom heave:

$$FS_{(heave)} = \frac{s_u N_c}{(\gamma_s + q_s/H_e - s_u/B')H_e}$$

(2-1)

where s_u is undrained shear strength of soil; N_c is bearing capacity factor for clay (which is equal to 5.7 thus assumes perfectly rough interface between soil and

foundation); γ_s is unit weight of soil; q_s is surface surcharge; H_e is depth to bottom of excavation; T is thickness of the clay below the base of the excavation; B is width of cut; and B' is limited to $B/\sqrt{2}$ or T, whichever is smaller. Clough et al. (1989) used Equation (2-1) to relate maximum lateral movement to excavation support system stiffness. The most common bearing capacity methods were developed before the introduction of stiffer in situ wall systems such as diaphragm walls and secant piles. As a result, these methods ignore the effect of the depth of the wall penetration below the base of excavation, soil anisotropy, and other factors. Ukritchon et al. (2003) presented a modified version of the Terzaghi (1943) factor of safety against basal heave that included the effects of the wall embedment (Figure 2.3).
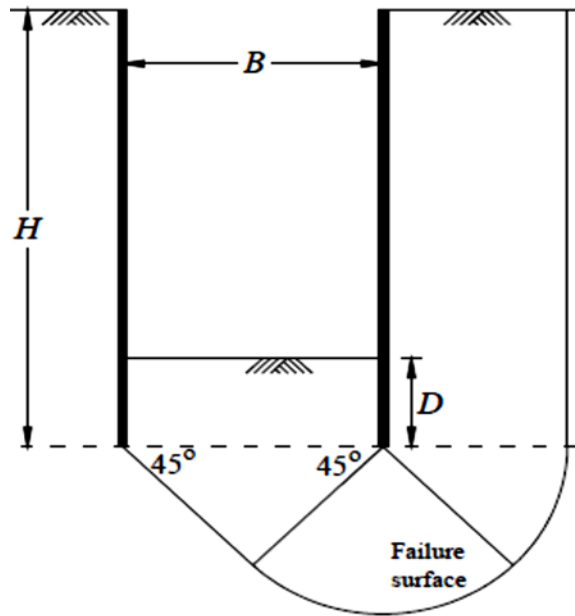
Figure 2.3 Factor of safety against bottom heave with wall embedment (Ukritchon et al., 2003).

11

The expression for the factor of safety against basal heave is given by:

$$FS_{bh} = \frac{s_{ub}N_c + (H/B)\sqrt{2}s_{ueq} + 2s_{ub}(D/B)}{\gamma_s H_e}$$ (2-2)

where D is depth of embedment; H is height of support wall; s_{ub} is shear strength of soil below bottom of cut; s_{ueq} is the equivalent undrained shear strength if soil is layered; all other terms have their previous meaning. The terms $s_{ub}N_c$ and $(H/B)\sqrt{2}s_{ueq}$ represent the shear capacity and the shear resistance of the soil mass, respectively, and $2s_{ub}(D/B)$ represents the adhesion along the inside faces of the wall assuming a rough surface.

2.4   Ground Movement Distributions

Several researchers have proposed methods for estimating ground movement distributions around deep excavations (Clough and O'Rourke 1990; Hsieh and Ou 1998; Kung et al., 2007; Ou and Hsieh, 2001). Clough and O'Rourke (1990) described the general deflection behavior of the wall in response to the excavation and the resulting surface settlement profile adjacent to the excavation. At early phases of the excavation, when the first level of lateral support has yet to be installed, the wall will deform as a cantilever. Settlements during this phase may be represented by a triangular distribution having the maximum value very near to the wall. As the excavation activities advance to deeper elevations, horizontal supports are installed restraining upper wall movements. At this phase, deep inward movements of the wall occur. The combination of cantilever and deep inward movements results in the cumulative wall and ground surface displacements. If deep inward movements are the predominant form of wall deformation, the settlements tend to be bounded by a trapezoidal displacement profile as in the case with deep

12

excavations in soft to medium clay; and if cantilever movements predominate, as can occur for excavations in sands and stiff to very hard clay, then settlements tend to follow a triangular pattern. Similar findings were presented by Ou et al. (1993) and Hsieh and Ou (1998), who based on observed movements of case histories in clay, proposed spandrel and concave settlement profiles. Ground movements parallel to the excavation are often not looked when designing the excavation support system. Smaller ground movements at the corners of the excavation and larger movements at the center of the excavation are often found due to the higher stiffness value at the corners of the excavation. Roboski and Finno (2006) proposed parallel distributions of settlement and lateral ground movement for deep excavations in soft to medium clays. The parallel distribution profiles were based on optical survey data obtained around a 12.8-m-deep excavation in Chicago supported by a flexible sheet pile wall and three levels of regroutable anchors. They found that when using the complementary error function (erfc), just geometry and maximum movement parameters are necessary for defining the parallel distributions of ground movement. Although the distribution was derived from observations of flexible wall excavations, it has been reported by Roboski and Finno (2006) that it can predict with reasonable agreement the ground movement profiles for stiffer walls. Special attention is needed in excavations where there are larger diameter utility pipes, buildings with stiff floor systems, buildings supported on deep foundations, and deep foundations between the building and the excavation because they provide restraint for the movements and consequently will affect their distribution. Roboski and Finno (2006) concluded that the complementary error function approach is applicable to excavations where the induced ground movements can develop with little restraint.

13

2.4.1 Maximum Lateral Wall Deflection

Maximum wall deflection, induced by excavation, is commonly estimated through empirical and semi-empirical methods (Mana and Clough, 1981; Clough et al., 1989; Wong and Broms, 1989; Hashash and Whittle, 1996; Addenbrooke et al., 2000; Kung et al., 2007). The current state-of-the-practice for preliminary estimation of the maximum lateral wall deflection for clays employs the Clough et al. (1989) design chart. It allows the user to estimate lateral movements in terms of effective system stiffness $\left(EI/\gamma_w s_v^4\right)$ and the factor of safety against basal heave. where E is Young's modulus of elasticity; I is moments of inertia; γ_w is unit weight of water; and s_v is average vertical strut spacing. The factor of safety against basal heave used in the Clough et al. (1989) work is that given by Terzaghi (1943). The Clough et al. (1989) chart was created from parametric studies using two-dimensional plane strain finite element analyses of sheet pile and slurry (i.e. diaphragm) walls. Unfortunately, the chart was developed using a limited number of wall types and configurations. Furthermore, the chart does not take into consideration the three-dimensional nature of the excavation. Bryson and Zapata-Medina (2012) proposed a new relative stiffness ratio to address the deficiencies of the Clough et al. (1989) chart. Although the ratio was originally termed relative stiffness, it actually describes the flexibility of the support system. This new ratio was formulated using dimensional analysis of the excavation support system stiffness problem and is given as:

$$R = \frac{E_s}{E} \cdot \frac{s_h \cdot s_v \cdot H}{I} \cdot \frac{\gamma_s H_e}{s_u} \tag{2-3}$$

14

where R is relative stiffness ratio; E_s is reference secant Young's modulus at the 50 percent of the stress level, E_{50}^{ref} in Appendix A; s_h is average horizontal support spacing; all others have their previous definitions. The terms E_s/E, $s_h s_v H/I$ and, $\gamma_s H_e/s_u$ in Equation (2-3), represent the relative stiffness resistance, the relative bending resistance, and the excavation stability number, respectively. The relative stiffness ratio was compared with data obtained from a three-dimensional finite element parametric study. The parametric study consisted of a three-dimensional system model and three-dimensional ground movements. Figure 2.4 presents the maximum lateral wall displacements obtained from the parametric study versus R for different factors of safety against basal heave. In the figure, the lateral movements are normalized with respect to the height of the wall, H, and the factors of safety are calculated using Equation (2-3), which includes the effects of the wall embedment depth below the base of excavation. Figure 2.4 allows the designer to predict maximum lateral wall movements for deep excavations in cohesive soils based on simple soil data and excavation geometry.
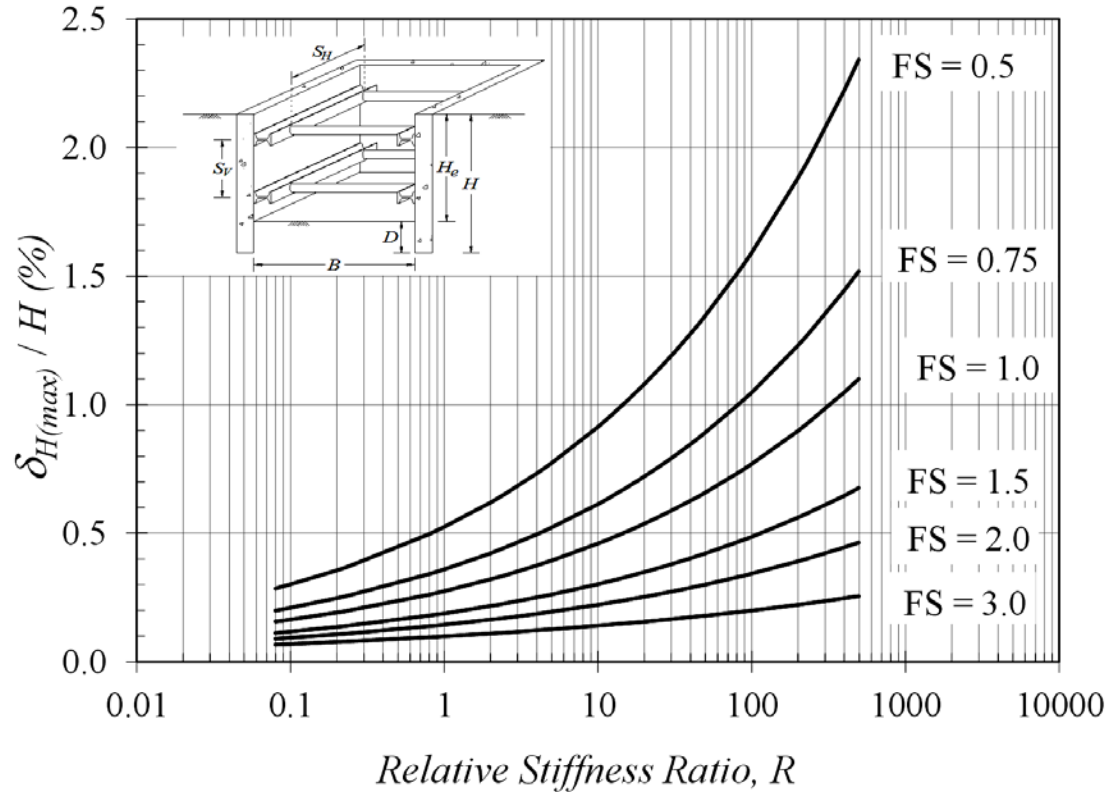
Figure 2.4 Relative Stiffness Ratio Design Chart (Bryson and Zapata-Medina 2012).

where $\delta_{H(\max)}$ is maximum horizontal ground movement.

2.4.1.1 Ground Settlement Profile as a Function of Wall Stiffness

Bryson and Zapata-Medina (2012) proposed a relationship between relative stiffness ratio and the excavation-induced vertical deformation profile. Figure 2.5 pictures the proposed perpendicular settlement profiles at the centerline of the excavation for stiff, medium, and soft clays, respectively. In the figures, the settlement and distance axes are normalized with respect to the maximum settlement and depth of excavation, respectively. Note that the coordinates that define the settlement profiles are dependent of the relative flexibility of the system represented by, R. It was observed that excavations with similar relative stiffness ratio have similar settlement distributions.

16
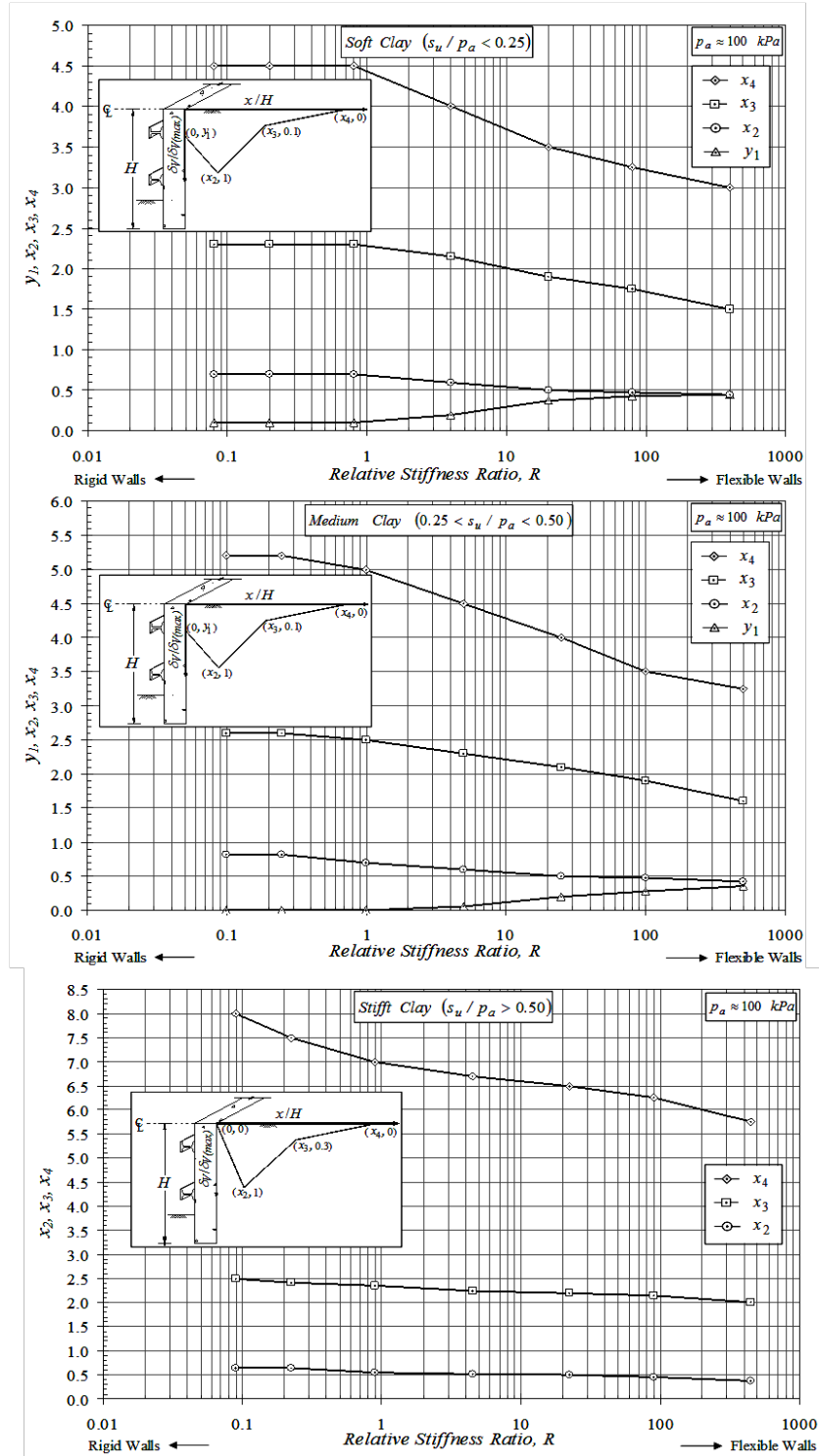
Figure 2.5 Prediction of perpendicular settlement profiles for (from top to down) soft clay, medium clay, and stiff clay (Bryson and Zapata-Medina 2012).

17

2.4.2 Maximum Vertical Ground Settlement

Correlation can be drawn between excavation-induced settlement and lateral wall deformations can be made by evaluating case history data. Researchers (Clough et al., 1989; Hsieh and Ou, 1998; Finno and Roboski, 2005; Kung et al., 2007; Ou and Hsieh, 2011) have reported that the maximum ground settlement adjacent to deep excavations is directly related to the maximum lateral displacement of the support system. These researchers generally conclude that the maximum excavation-induced ground settlement can be estimated from the maximum from the maximum lateral displacement from the relationship:

$$\delta_{V(\max)} = \alpha \delta_{H(\max)} \tag{2-4}$$

where $\delta_{V(\max)}$ is maximum vertical settlement of ground; $\delta_{H(\max)}$ is maximum lateral displacement of excavation support system; α is deformation ratio. Both Clough and O'Rourke (1990); and Hsieh and Ou (1998) reported that the ratio varied between 0.5 and 1.0 (Figure 2.6). The value depends on the soil conditions, construction method, and wall stiffness. Figure 2.6 represents case history plot of the maximum wall deflection versus maximum ground surface settlement, with both axes normalized with respect to the height of the excavation, H_e.
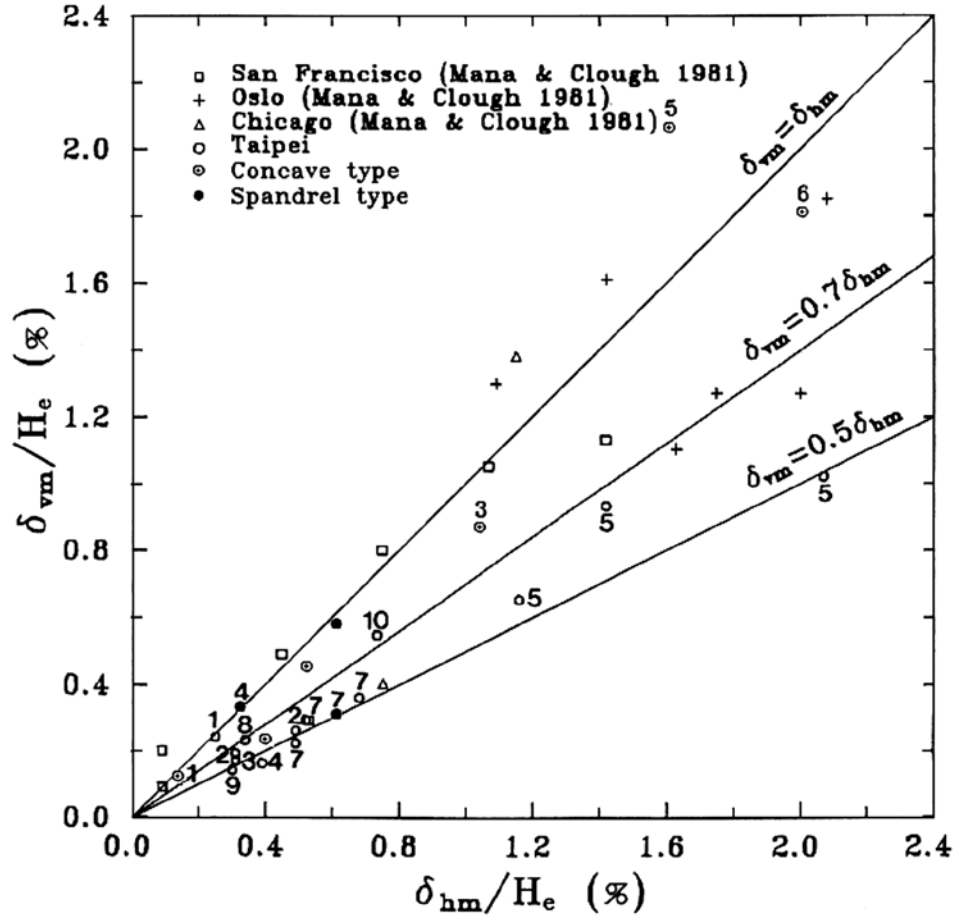
Figure 2.6 Relationship between maximum ground settlement and maximum lateral wall deflection (Ou et al., 1993; Hsieh and Ou, 1998).

Finno et al. (2002) found that for undrained unloading conditions in saturated soils the lateral deformation envelop closely matched that of the ground settlement. For the current study, a relationship between maximum settlement and maximum lateral deformation, based on case history data, was sought for input into the proposed design methodology. Bryson and Zapata-Medina (2007) presented a case history data for several excavations found in literature. A listing of the case history information is given in Table 2.1. Note that the case data presented in Table 2.1 is divided into stiff, medium, and soft clay on the basis of undrained shear strength found at the bottom of the excavations. Soft clay is

19

defined as clay deposits with undrained shear strengths between 0 kPa to 25 kPa. Medium clay is defined as undrained shear strengths between 25 kPa and 50 kPa, and stiff clay are deposits with undrained shear strengths greater than 50 kPa. Table 2.2 is a summary of the geometric, soil and support system parameters for the case histories. Additional details of the case history data can be found in Zapata-Medina (2007).

Table 2.1 Case History Data (Bryson and Zapata-Median 2007).

Soil Type	Case	Reference	Wall Type	S_v [m]	S_H [m]	γ_s [kN/m³]	s_u [kPa]	I [m⁴/m]	E [GPa]	FS_{bh}
Stiff Clay	St1	Ng (1992)	Diaph.	3.2	1.5	20	120	0.01800	31	3.73
	St2	Burland and Hancock (1977)	Diaph.	3.2	3.2	20	170	0.06075	27.6	3.99
	St3	Hsieh and Ou (1998)	Diaph.	3.3	3.3	19	76.5	0.06075	27.6	1.26
	St4	Poh et al. (1997)	Diaph.	4.3	6	20.75	80	0.01800	NA	2.05
	St5	Ou and Shiau (1998)	Diaph.	3.3	3.3	19.7	50	0.01800	12	1.51
	St6	Whittle et al. (1993)	Diaph.	3	slab	20.24	91	0.06075	23	1.32
	St7	Liao and Hsieh (2002)	Diaph.	2.65	1.92	20	77.5	0.04267	27.6	1.38
	St8	Liao and Hsieh (2002)	Diaph.	2.33	1.85	20	65	0.14400	27.6	0.99
	St9	Becker and Haley (1990)	Diaph.	3.35	slab	18	70	0.03516	23.2	1.21
	St10	Ulrich (1989)	Secant	2.45	2.45	20.1	140	0.03516	27.6	3.62
Medium Clay	M1	Ou et al. (1998)	Diaph.	3.4	slab	18.9	50	0.06075	27.6	0.96
	M2	Finno and Roboski (2005)	Sheet	4	2.29	19	36	0.00025	200	1.08
	M3	Finno and Roboski (2005)	Sheet	4	2.29	20	36	0.00025	200	0.80
	M4	Hsieh and Ou (1998)	Diaph.	2.85	2.85	19	47.5	0.04267	27.6	0.97
	M5	Miyoshi (1977)	Steel-Conc.	2.7	2.7	19	42	0.04267	27.6	0.99
	M6	Finno et al. (1989)	Sheet	2.5	2.5	19	30	NA	200	1.10
	M7	NGI (1962)	Sheet	1.7	1.7	19	30	NA	200	1.16
	M8	Clough and Buchignani (1981)	Diaph.	3	3	17	44	0.08333	25	0.98
	M9	Wang et al. (2005)	Diaph.	4	3	18	35	0.04267	NA	0.85
	M10	Peck (1969)	Sheet	1.68	1.68	19	27.5	NA	200	1.35

Table 2.1 cont.

Soil Type	Case	Reference	Wall Type	S_V [m]	S_H [m]	γ_s [kN/m³]	s_u [kPa]	I [m⁴/m]	E [GPa]	FS_{bh}
Soft Clay	So1	Finno et al. (2002)	Secant	3.8	6.1	19.1	20	0.06075	12.65	0.59
	So2	Goh et al. (2003)	Diaph.	2.5	9	17.6	10	0.04267	30	0.31
	So3	Hu et al. (2003)	Diaph.	3.5	9	18	22	0.04267	21.7	0.73
	So4	Gill and Lukas (1990)	Sheet	2.5	2.5	19	22.7	NA	200	1.93
	So5	Teparaksa (1993)	Sheet	2.5	2.5	16	13.5	0.00025	200	0.62
	So6	Baker et al. (1987)	Diaph.	2.75	2.75	19	21.5	0.03658	26	0.93
	So7	Konstantakos (2000)	Diaph.	3.65	3.65	19	45	0.03658	26	1.25
	So8	Clough and Buchignani (1981)	Soldier	3	3	17	25	0.03516	26	1.69
	So9	Kort (2002)	Sheet	7.75	7.2	14	20	NA	200	1.63
	So10	Koutsoftas et al. (2000)	Soldier	3.3	6	16.5	25	0.06280	27.6	1.42

where s_v is average vertical strut spacing; s_h average horizontal strut spacing; γ_s is unit weight of soil; s_u is undrained shear strength of soil; I is moments of inertia of support wall; E is Young's modulus of inertia of support wall; and FS_{bh} is factor of safety against bottom heave. Table 2.2 presents further information about the excavation support systems given in Table 2.1. Figure 2.6 shows the maximum lateral movements as a function of the maximum vertical movements for the case histories. In Figure 2.7 the maximum lateral deformations are normalized with respect to the depth of wall and the maximum vertical movements are normalized with respect to the depth of the excavation. Bryson and Zapata-Medina (2007) reported that lateral deformations tended to be more influenced by the physical characteristics of the support system (i.e. length of wall, wall stiffness, etc.) while vertical deformations tended to be more influenced by the soil behavior.

21

Table 2.2 Case History Data (Bryson and Zapata-Median 2007).

Soil Type	Case	Reference	Wall Type	I [m^4/m]	E [GPa]	$\delta_{H(max)}$ [mm]	$\delta_{V(max)}$ [mm]	$\delta_{H(max)}$/H [%]	$\delta_{V(max)}$/He [%]	FS$_{bh}$
Stiff Clay	St1	Ng (1992)	Diaph.	0.01800	31	17.66	10.13	0.108	0.106	3.73
	St2	Burland and Hancock (1977)	Diaph.	0.06075	27.6	24.06	19.53	0.080	0.106	3.99
	St3	Hsieh and Ou (1998)	Diaph.	0.06075	27.6	124.76	77.76	0.378	0.389	1.26
	St4	Poh et al. (1997)	Diaph.	0.01800	NA	10.02	NA	0.072		2.05
	St5	Ou and Shiau (1998)	Diaph.	0.01800	12	44.53	NA	0.194		1.51
	St6	Whittle et al. (1993)	Diaph.	0.06075	23	53.61	45.00	0.209	0.223	1.32
	St7	Liao and Hsieh (2002)	Diaph.	0.04267	27.6	81.37	NA	0.301		1.38
	St8	Liao and Hsieh (2002)	Diaph.	0.14400	27.6	54.30	NA	0.143		0.99
	St9	Becker and Haley (1990)	Diaph.	0.03516	23.2	47.26	101.60	0.182		1.21
	St10	Ulrich (1989)	Secant	0.03516	27.6	14.75	NA	0.074		3.62
Medium Clay	M1	Ou et al. (1998)	Diaph.	0.06075	27.6	106.51	77.18	0.304	0.392	0.96
	M2	Finno and Roboski (2005)	Sheet	0.00025	200	43.23	NA	0.262		1.08
	M3	Finno and Roboski (2005)	Sheet	0.00025	200	63.48	74.00	0.334	0.578	0.80
	M4	Hsieh and Ou (1998)	Diaph.	0.04267	27.6	62.61	43.16	0.202	0.235	0.97
	M5	Miyoshi (1977)	Steel-Conc.	0.04267	27.6	176.56	152.42	0.552	0.897	0.99
	M6	Finno et al. (1989)	Sheet	NA	200	172.64	255.70	0.899	2.096	1.10
	M7	NGI (1962)	Sheet	NA	200	223.58	200.00	1.397	1.818	1.16
	M8	Clough and Buchignani (1981)	Diaph.	0.08333	25	28.25	NA	0.093		0.98
	M9	Wang et al. (2005)	Diaph.	0.04267	NA	48.12	30.90	0.127	0.150	0.85
	M10	Peck (1969)	Sheet	NA	200	228.87	210.00	1.635	2.471	1.35
Soft Clay	So1	Finno et al. (2002)	Secant	0.06075	12.65	38.13	27.43	0.208	0.225	0.59
	So2	Goh et al. (2003)	Diaph.	0.04267	30	38.55	NA	0.124		0.31
	So3	Hu et al. (2003)	Diaph.	0.04267	21.7	15.39	7.00	0.073	0.061	0.73
	So4	Gill and Lukas (1990)	Sheet	NA	200	83.27	NA	0.496		1.93
	So5	Teparaksa (1993)	Sheet	0.00025	200	123.65	NA	0.687		0.62
	So6	Baker et al. (1987)	Diaph.	0.03658	26	37.39	37.00	0.204	0.435	0.93
	So7	Konstantakos (2000)	Diaph.	0.03658	26	3.63	NA	0.026		1.25
	So8	Clough and Buchignani (1981)	Soldier	0.03516	26	107.06	NA	0.351		1.69
	So9	Kort (2002)	Sheet	NA	200	385.38	NA	2.028		1.63
	So10	Koutsoftas et al. (2000)	Soldier	0.06280	27.6	48.10	30.20	0.117	0.231	1.42

where $\delta_{H(max)}$ is maximum lateral wall movement; and $\delta_{V(max)}$ is maximum vertical ground settlement.

22

Subsequently, the soil behavior at deep excavations is typically influenced by the depth of excavation.
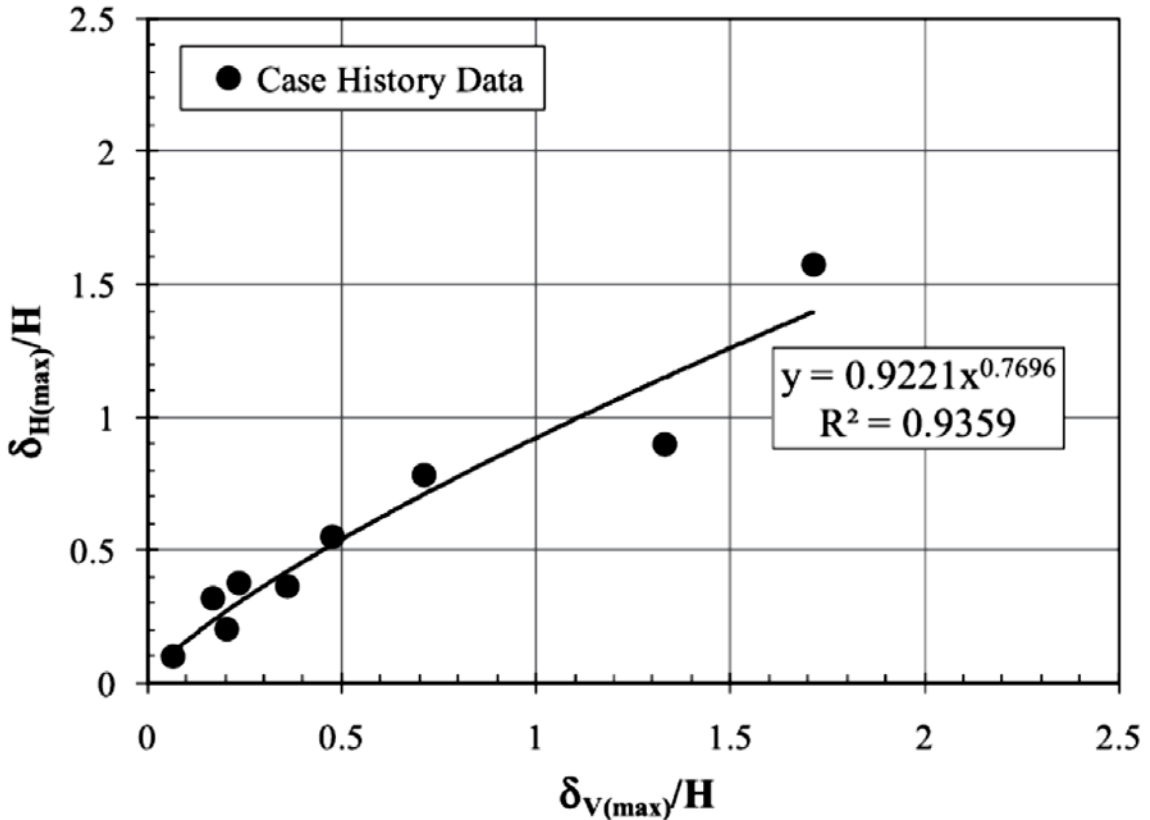
Figure 2.7 Case history plot of $\delta_{H(\max)}/H\,(\%)$ **vs** $\delta_{V(\max)}/H_e\,(\%)$ **(Bryson and Zapata-Medina, 2012).**

The purpose of Figure 2.7 is to show that it is possible to predict maximum lateral deformation based on input values of the maximum settlement. Subsequently, the maximum lateral deformations can be used to estimate the required support wall stiffness. This is a reasonable approach given the fact that other researchers (open excavations: Peck, 1969; Clough and O'Rourke, 1990; settlement troughs above tunnels: Attewell et al., 1986), have shown that settlement and horizontal strain profiles may be imposed on the foundation slab. It is, however, noted that estimating excavation-induced settlement

23

from lateral deformations may yield conservative results since many of the studies were based on free-field condition; whereas the existence of the building may reduce the effect of both the slope and maximum settlement compared with the greenfield condition (Namazi and Mohamad 2013).

Alternatively, the maximum excavation-induced settlement and lateral wall deformation can be correlated through R and FS_{bh} using the numerical data produced by Bryson and Zapata-Medina (2012) as shown in Figure 2.8.
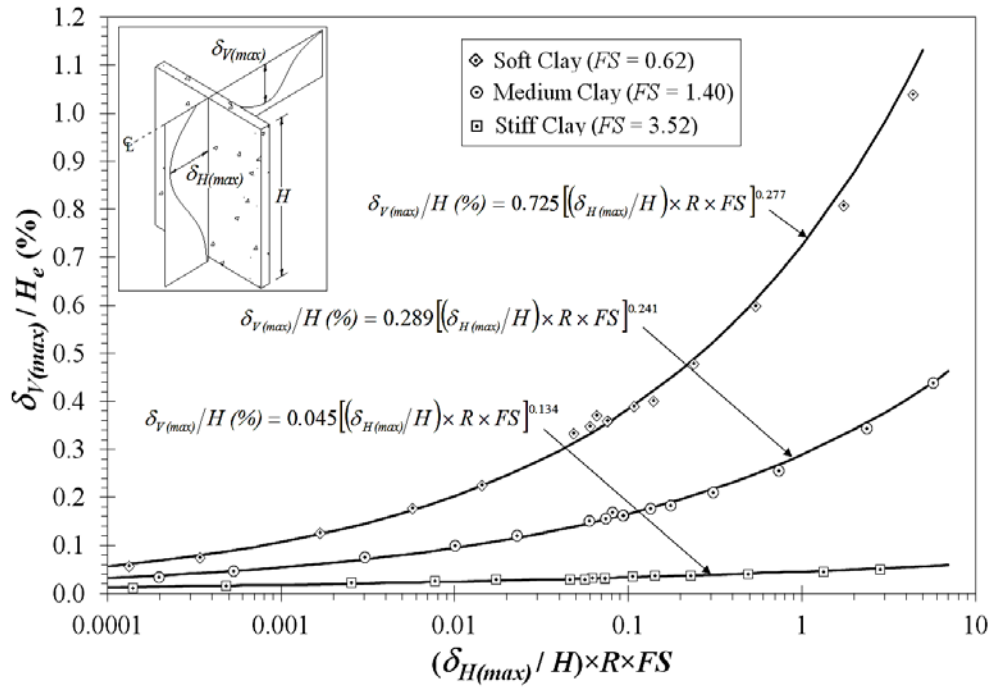
Figure 2.8 Correlation between $\delta_{H(\max)}$ and $\delta_{V(\max)}$ as a function of R and FS_{bh} (Bryson and Zapata-Medina 2012).

where all the symbols have their previous definitions.

The maximum settlements and lateral wall movements computed from the FE simulations were plotted as shown in Figure 2.3(b) where the x and y-axes are

$(\delta_{H(\max)}/H) \times R \times FS_{bh}$ and $\delta_{V(\max)}/H_e$ (%), respectively, and condensed into a single equation:

$$\frac{\delta_{V(\max)}}{H_e}(\%) = \left(\frac{0.507}{FS_{bh}} - 0.088 \right) \cdot \left[\frac{\delta_{H(\max)}}{H} \times R \times FS_{bh} \right]^{(0.309 - 0.05 \cdot FS_{bh})} \tag{2-5}$$

Equation (2-5) relates $\delta_{V(\max)}$ and $\delta_{H(\max)}$ at the center line of deep excavations in cohesive soils including the effects of the factor of safety against basal heave and the relative stiffness ratio, which takes into account the three-dimensional nature of the excavation.

2.5   Quantifying Deformation

Skempton and MacDonald (1956) established correlations between maximum angular distortion, maximum settlement, and maximum differential settlement. These relationships were based on case history data of 98 steel and reinforced concrete frame buildings, out of which 40 experienced damage. Their damage criterion was "angular distortion", which is the ratio of the differential settlement, δ, between two points divided by the distance between them, *l*, minus the rigid body tilt of the structure. Empirical limits of 1/300 for preventing cracks and 1/150 for avoiding structural damage were selected. Skempton and MacDonald (1956) further recommended that angular distortions in excess of 1/500 is detrimental and should be avoided when possible, and that the limit be decreased to 1/1,000 to rule out all damage.

Son and Cording (2005) proposed an amendment to the concept of angular distortion as a direct damage criterion. By dividing angular distortion (*β*) by the relative ground slope, the relative behavior of the building and the ground is, thusly, accounted for. They

25

reasoned that buildings with high stiffness will have deformation path, which may differ from ground deformation. In a similar fashion as Burland and Wroth (1975), Son and Cording (2005) measured angular distortion by deducting the tilt effect from the slope of the bay under consideration. Son and Cording (2007) report that the onset of cracking in structures with relatively high bending to shear-stiffness ratios; (i.e. masonry structures with openings, such as windows and doors), is predominantly controlled by shear deformation. Supplemental recommendations on angular distortion, which related the magnitude of angular distortion to various damage types, was provided by Bjerrum (1963).

Burland and Wroth (1974) used beam-bending theory to develop limiting relative deflections of masonry and brick walls at critical tensile strains of 0.075% for varying length to height (L/H) ratios and building stiffness. Relative deflection, Δ/L, is defined as the ratio of the deflection to the length of the deflected portion. The deformed shapes of buildings subjected to ground settlement, Burland and Wroth (1974), defined "hogging" for concave downward deflection profiles and "sagging" for concave upward profiles. Finno and Bryson (2002) noted that self-weight movements of buildings generally result in sagging profiles; while, movement due to excavation may result in sagging, hogging, or both in adjacent buildings. They also indicate that the type of settlement profile will lead to more prohibitive limits in a structure, particularly for hogging buildings. Finno and Bryson (2002) reasoned to this end citing the Canadian Foundation Engineering Manual (1992), which recommends limiting angular distortions to 1/1,000 for unreinforced load bearing wall that sags and 1/2,000 for a hogging one. Furthermore they noted that, the aforementioned results may not, necessarily, be applicable to excavation-

26

induced movements within adjacent buildings. Table 2.3 provides a summary of these studies.

Table 2.3 Damage criteria based only on self-weight settlement.

Type of structure	Damage Type	Angular Distortion(β)				
		Meyerhof (1947)	Meyerhof (1956)	Skempton and MacDonald (1956)	Polshin and Tokar (1957)	Bjerrum (1963)
Frame structures and reinforced bearing walls	Structural	1/250		1/150	1/200	1/150
	Cracks in walls	1/500		1/300	1/500	1/500
Unreinforced load bearing walls	Onset of cracking		1/1,000			

		Relative Deflection(Δ/L)				
Unreinforced load bearing walls	Onset of cracking		1/2,500			

		Polshin and Tokar (1957)
Load bearing brick or concrete block walls	Onset of cracking	
	For L/H>5	1/2,000 to 1/1,400
	For L/H<3	1/3,300 to 1/2,500

Polshin and Tokar (1957) used the concept that the onset of visible cracking (the start of observable damage) maybe associated with a limiting or critical strain. Later, Burland and Wroth (1974) applied the idea of a critical tensile strain to the initial visible cracking of a simple beam. They proposed a damage criteria, based on visible cracks, following the work of other researchers (such as economic consequences of heave of buildings on swelling clays: Jennings and Kerrich 1962; simplified classification of subsidence

27

damage: The U.K. National Coal Board 1975; MacLeod and Littlejohn 1974). Table 2.4 is a summary of the criteria which was developed with emphasis on ease of repair.

Table 2.4 Damage criterion based on visible crack width (after Burland et al., 1977).

Category	Degree of damage	Δl_c (mm)
0	Negligible	< 0.1
1	Very Slight	$\not> 1$
2	Slight	$\not> 5$
3	Moderate	5 to 15
4	Severe	15 to 25
5	Very Severe	> 25

Boscardin and Cording (1989) also used angular distortion to quantify excavation-induced damage to adjacent structures. Their method, unlike previous studies, took into consideration the importance of horizontal strains. Based on damage severity criteria proposed by Burland and Wroth (1977), they utilized case history data to correlate angular distortion and horizontal strains as shown in Figure 2.9.
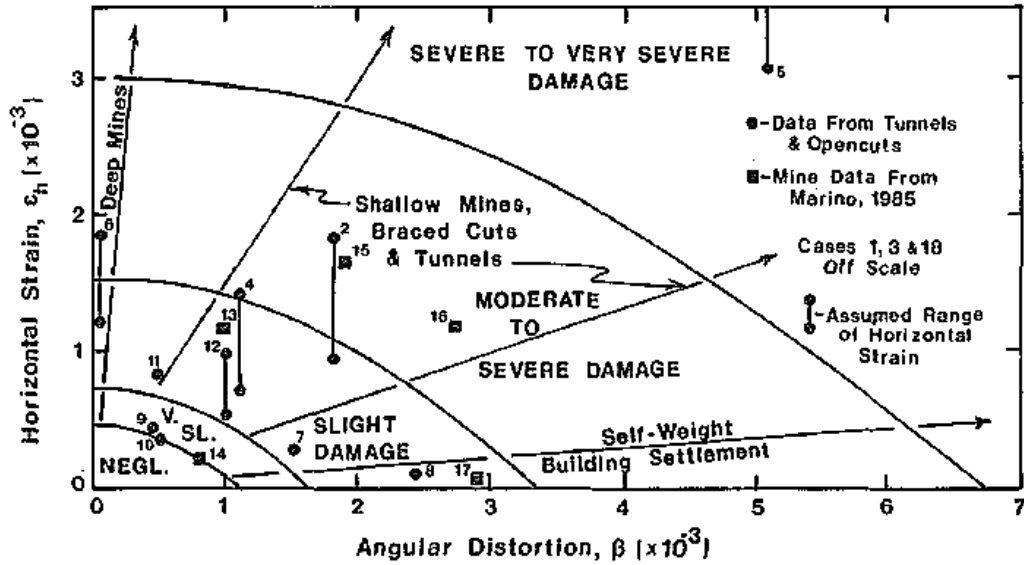
Figure. 2.9 Relationship of damage to angular distortion and horizontal extension strain (Boscardin and Cording, 1989).

The corresponding values for angular distortion and horizontal extension strains are tabulated on the basis of the severity criteria proposed by Burland and Wroth (1974) and presented by Boone et al., (1998) and shown on Table 2.5.

Table 2.5 Damage criteria based on angular distortion and horizontal extension strain (after Boone et al., 1998).

Damage category	Angular distortion β x 10^{-3}	Horizontal strain ε_h x 10^{-3}
Negligible	$> \approx 1.1$	> 0.5
Very Slight	$\approx 1.1 < \beta < \approx 1.6$	$0.5 < \varepsilon_h < 0.75$
Slight	$\approx 1.6 < \beta < \approx 3.3$	$0.75 < \varepsilon_h < 1.5$
Moderate	$\approx 3.3 < \beta < \approx 6.7$	$1.5 < \varepsilon_h < 3.0$
Severe	$> \approx 6.7$	> 3.0

29

Boone et al. (1998) argue that the concept of angular distortion, as well as deflection ratio, is simple and do not consider real differences in structure responses, which depend on building height, length, and construction materials.

2.6   Deformation Models

Current methods used in analyzing damage caused to adjacent buildings due to ground displacement from nearby excavation include; Deep Beam; Laminate Beam; and Thick Plate Models. The oldest and most popular of these analytical approaches is the deep beam model. The full development of the deep beam model will be presented and utilized in subsequent sections of this research, while the other two will be touched upon slightly.

Finno et al. (2005) proposed the laminate beam model, pictured in Figure 2.10, which utilizes an extension of the equations from Burland and Wroth (1975. Finno et al., (2005) used the concept of complementary virtual work to relate deflection ratio to tensile strains.
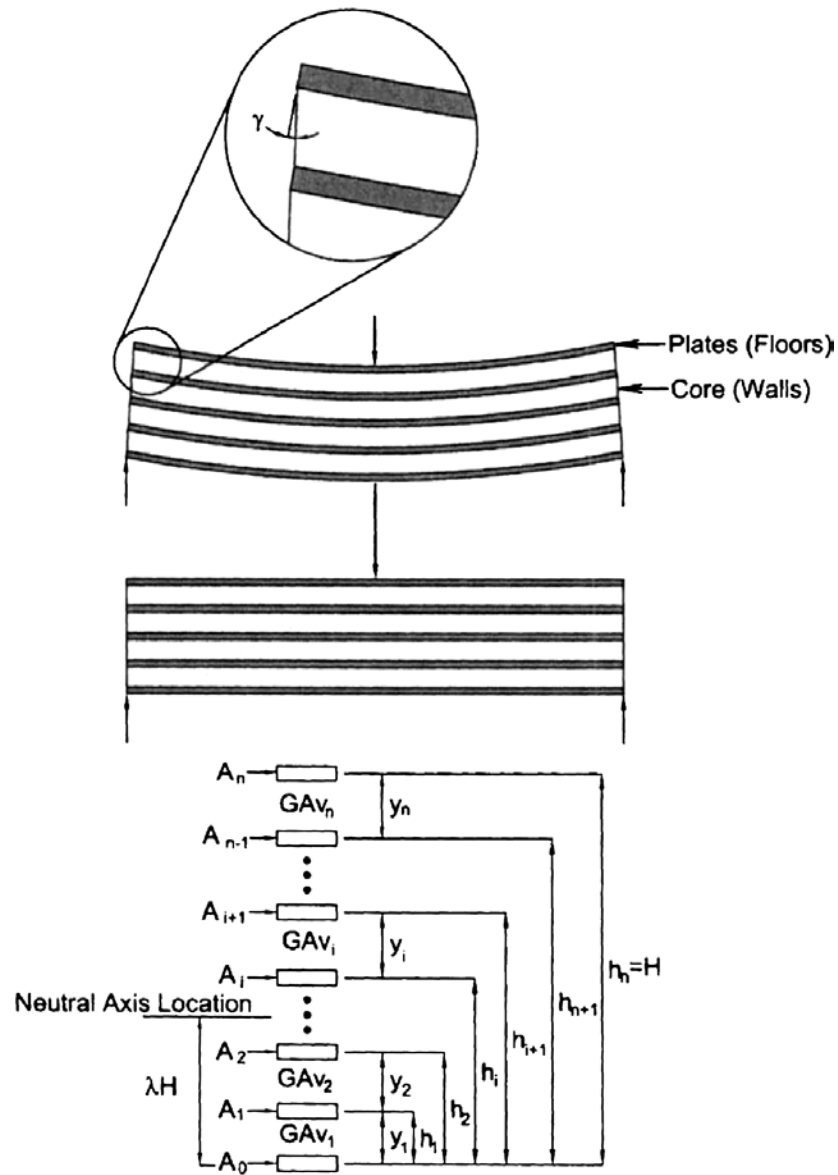
Figure 2.10 Laminate beam of structure (Finno et al., 2005).

The model comprises of a multistory building with floor slab, infill wall, and columns in analyzing a building's response to excavation-induced ground movement. Within the model, infill walls resist shear deformation while the floor resist the bending moment deformation.

31

Using the case of simply supported beam, Finno et al. (2005) related limiting deflection

ratio to bending strain at the top, $\varepsilon_{b(top)}$, bottom, $\varepsilon_{b(bottom)}$, and the maximum diagonal

tensile strain, ε_{di}:

$$\frac{\Delta}{L} = \left[\frac{1}{12(1-\lambda)} \left(\frac{L}{H} \right) + \frac{EI}{\overline{GA_v}L(1-\lambda)H} \right] \varepsilon_{b(top)} \qquad (2\text{-}6)$$

$$\frac{\Delta}{L} = \left[\frac{1}{12\lambda} \left(\frac{L}{H} \right) + \frac{EI}{\overline{GA_v}L\lambda H} \right] \varepsilon_{b(bottom)} \qquad (2\text{-}7)$$

$$\frac{\Delta}{L} = \left[\frac{L^2(GA_v)_i}{24EI\dfrac{V_i}{V}} + \frac{(GA_v)_i}{2\dfrac{V_i}{V}\overline{GA_v}} \right] \gamma_i \qquad (2\text{-}8)$$

where i is floor number; H is height of building; A_i is area of floor slab contributing to

bending resistance; h_i is location of the floor measured from the bottom of the laminate

beam; A_v is the area contributing to shear resistance; l is moment of inertia of the beam;

V_i is the ratio of shear in each story; V is the total shear in the laminate beam; and λ is

the ratio of the distance from the neutral axis to the bottom on the beam to its height. The

interested reader is referred to Finno et al. (2005) for further details on the development

of the method. Finno et al. (2005) noted the simply supported beam assumption does not

hold for all situations or excavation-induced ground movements, including conditions

such that the building undergoes both sagging and hogging modes of deformation shown

in Figure 2.11. To correct this, an additional strain term, γ_{add} (i.e. the difference between

the slope and the rigid body rotation), was added to the shear strain due to the simply

supported beam condition. Thus, they modified Equation (2-8) to Equation (2-9):

32
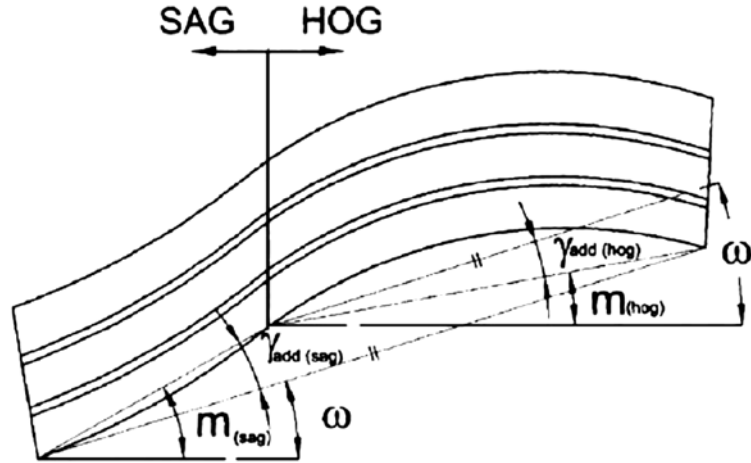
Figure 2.11 Dual modes of deformation of a beam (Finno et al., 2005).

$$\frac{\Delta}{L} = \left[\frac{L^2 (GA_v)_i}{24EI \frac{V_i}{V}} + \frac{(GA_v)_i}{2 \frac{V_i}{V} GA_v} \right] (\gamma_{crit\,i} - \gamma_{add})$$ (2-9)

where $\gamma_{add} = |m - \omega|$ (m is the slope; and ω is the rigid body tilt); and $\gamma_{crit\,i}$ is the critical shear strain. The output of the model is deflection ratio based on the bending and shear stiffness of the system. The difficulty in using the model is that, it uses specific material information which are usually absent from case history data. Also, some users may find it a bit complicated (Halim and Wong, 2012).

Namazi and Mohamad (2013) proposed the thick plate model to address two situations; namely when the building facades are not within the same plane as the retaining wall, and when path of the tunnel underneath an existing structure is oblique to the structure. In both cases, the model stipulates a 3D mode of deformation, with additional modes of deformation such as twisting or warping and horizontal extension in the out-of-plane

33

direction. The model assumes a simply support beam and the entire building (i.e. including components such as structural design, foundation, and geometry) is treated as a rectangular thick plate as shown in Figure 2.12. The maximum deflection,Δ, is measured at the center of the deformed parabolic surface.
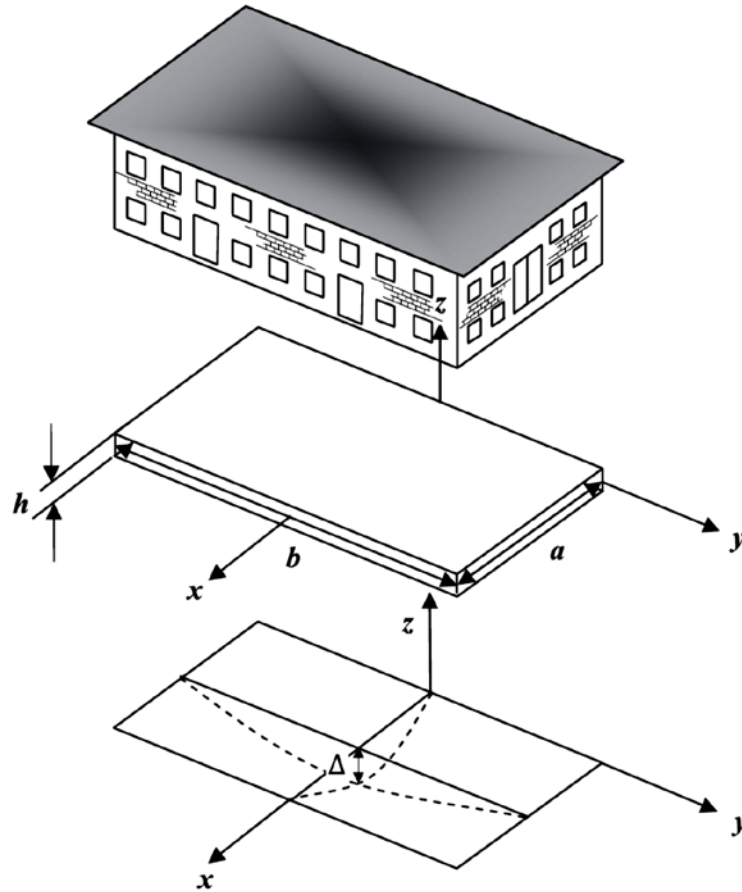
Figure 2.12 Thick plate model idealization of real building (after Namazi and Mohamad, 2013).

In the Figure 2.12, *b* is the length; *a* is the width; and *h* is the height. To establish the critical strain using a relationship between deflection ratio and beam geometry, Namazi and Mohamad (2013), following the findings of Burland (1995), assumed that the analysis is insensitive to the loading type. By employing third-order shear deformation

plate theory (TSDT) (Levinson, 1980), that enables the variation of shear strains across the depth of the structural panels unlike Timoshenko's first-order shear deformation theory (FSDT) [which assumes a constant shear strain across depth (Burland and Wroth, 1974; Finno et al., 2005; Netzel, 2009)], an expression for the deflection of the thick plate was derived .
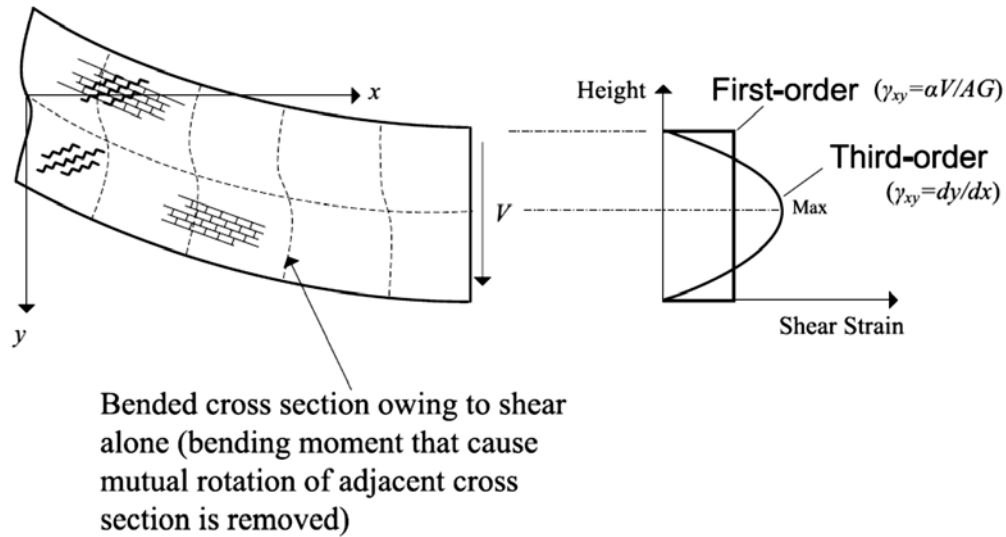
Figure 2.13 First-order and Third-order deformation theories (Namazi and Mohamad, 2013).

From Figure 2.13, the corresponding expressions for the total vertical displacement, *w*; rotations about the *y*- and *x*- axes respectively; using Levy's solution (Coke and Levinson, 1983) are given by:

$$w = \sum_{m=1}^{\infty} f_m(y)\sin\frac{m\pi x}{a} \tag{2-10}$$

$$\varphi_x = \sum_{m=1}^{\infty} g_m(y)\cos\frac{m\pi x}{a} \tag{2-11}$$

35

$$\varphi_y = \sum_{m=1}^{\infty} h_m(y)\sin\frac{m\pi x}{a} \qquad (2\text{-}12)$$

where $f_m(y)$, $g_m(y)$, and $h_m(y)$ are arbitrary constants that can be determined from boundary conditions. These constants also depend on the distance from the center of the plate in the longitudinal direction, y. After a series of derivations and application of the principle of superposition, the total bending strain and the resultant diagonal tensile strain in the longitudinal direction of the plate are respectively:

$$\varepsilon_{br} = \varepsilon_h + \frac{\delta_2\Delta}{\delta_1 a} + \frac{\varphi^3}{24}\left(\frac{b}{a}\right)^3 \qquad (2\text{-}13)$$

$$\varepsilon_{dr} = \varepsilon_h\left(\frac{1-\upsilon}{2}\right) + \sqrt{\varepsilon_h^2\left(\frac{1+\upsilon}{2}\right)^2 + \left(\frac{8\varphi}{\pi^2}\frac{h}{a} + \frac{\delta_3}{\delta_1}\frac{\Delta}{a}\right)^2} \qquad (2\text{-}14)$$

where ε_h is the horizontal strain; $\delta_2\Delta/\delta_1 a$ is the strain induced by deflection; $\varphi^3 b^3/24a^3$ is the strain induced by twist; δ_1, δ_2, and δ_3 are numerical factors that depend on the dimension ratios of b/a, h/a, and the mechanical properties of the plate; and υ is the Poisson's ratio. The effect of twist on the twist on the thick plate is shown on Figure 2.14.

36
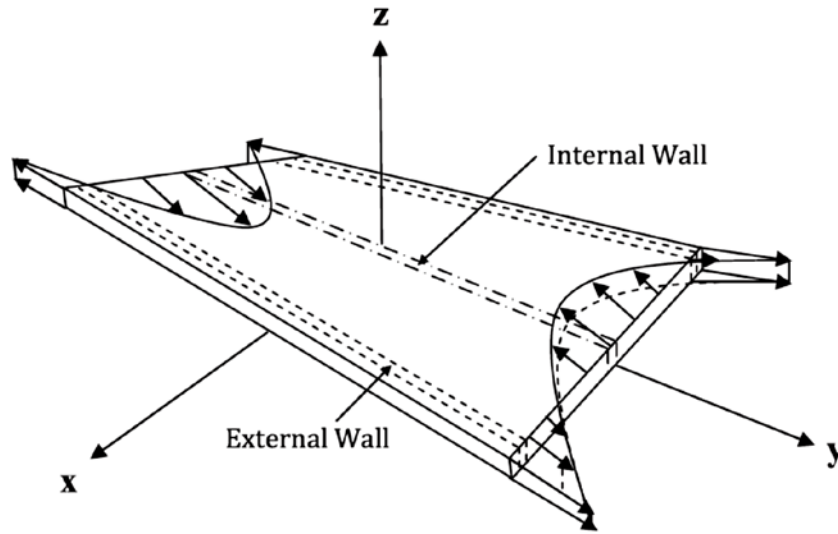
Figure 2.14 Distribution of axial strain due to twist (Namazi and Mohamad, 2013).

Thus by the method of superposition, the warping or twisting and horizontal displacement can be factored into the tensile strains. The model's damage criteria is based on deflection ratio, horizontal strain and twist. The approach compared favorably in comparison with existing methods when tested using 16 case history data. Despite the benefits it may provide, the very definition of the method [i.e. the method is proposed for out-of-plane ground movements (Namazi and Mohamad, 2013)] preclude it from being used in this research, since this research assumes a plane-strain condition.

2.6.1 Deep Beam Model

The concept of deep beam was proposed by Burland and Wroth (1974) to estimate damage in a building by modelling the building as a deep beam. They developed charts relating building damage to relative deflection ratio and the dimensions of the building (e.g. length over height ratio, *L/H*, of the building). Following this work, Boscardin and Cording (1989) proposed a new chart that considered horizontal strain as a major influencing parameter compared to building dimensions, thusly assuming *L/H* was

37

unity. The reason being that, their research showed that a structure's tolerance to differential settlement decreased with increasing lateral strains. Son and Cording (2005) subsequently furthered this approach by considering explicit values of building dimensions, *L/H*; percentage openings; soil-structure stiffness; and grade beams.

In the model, Boscardin and Cording (1989) imposed a convex deflected shape (i.e. a beam in a hogging mode) on a; weightless; linearly elastic; isotropic beam of length, *L*, and height, *H*; and unit thickness; load-bearing wall (beam). Modes of deformation of such beams included shearing, bending, and a combination of both bending and shearing. Figure 2.15 is an illustration of the deep beam model. Timoshenko (1957) provided the expression for total deflection at mid-span for simply supported beam, undergoing both shear and bending deformations in Equation (2-15).

$$\Delta = \frac{PL^3}{48EI}\left(1+\frac{18EI}{L^2HG}\right) \tag{2-15}$$

where *E* is the Young's modulus; *G* is the shear modulus; *P* is the point load; and *I* is the moment of inertia of the beam. In real structures, the foundation and soil provides considerable resistance to the deformation in the building. As a result, the condition in which the neutral axis is at the lower edge of the beam was adopted for the hogging mode of deformation (Burland and Wroth, 1974).
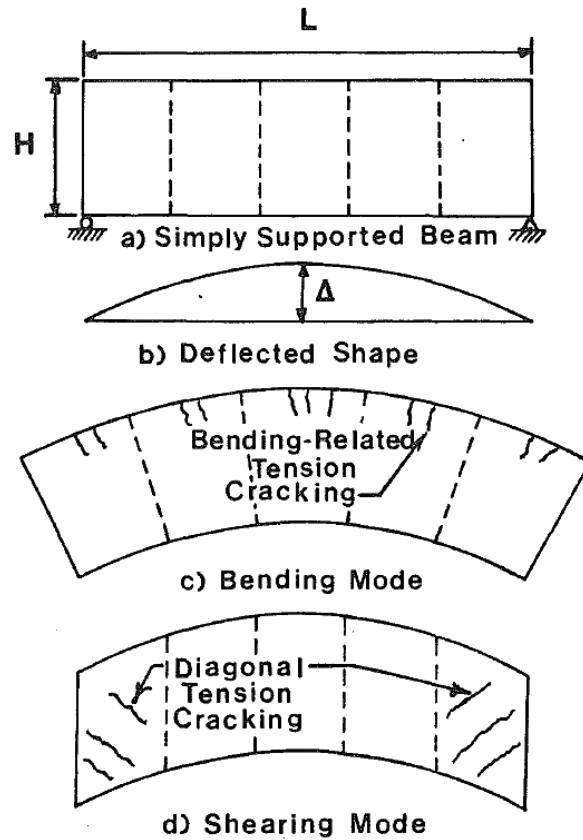
Figure 2.15 Deep Beam Model (Boscardin and Cording, 1989).

Subsequently, Burland and Wroth (1974) accounted for the soil-structure interaction effect by modifying the deflection expression into a deflection ratio, (Δ/L), and the maximum extreme fiber strain, ε_{bmax} in Equation (2-15) and assuming a Poisson's ratio of 0.3.

$$\frac{\Delta}{L} = \left[0.83\left(\frac{L}{H}\right) + 1.3\left(\frac{H}{L}\right) \right] \tag{2-16}$$

Furthering this research, Boscardin and Cording (1989) provided the relationship in Equation (2-17) for calculating the deflection ratio (Δ/L) in framed buildings, which takes into consideration the horizontal strain for the case of pure shear deformation.

39

$$\frac{\Delta}{L} = \left(0.064\frac{L^2}{H^2} + 1\right)\left(\frac{\varepsilon_{crit} - \varepsilon_h \cos^2\theta_{max}}{2\cos\theta_{max}\sin\theta_{max}}\right) \tag{2-17}$$

In the expression, Δ is the relative deflection of the beam; L and H are the same as previously defined; ε_{crit} is the critical strain of the beam, which is the strain level at which cracking begins; ε_h is the applied horizontal strain; and θ_{max} is the maximum inclination of the beam from the horizontal. Boone (1996) provides values of the critical strains for various materials as a function of the mode of deformation and the type of material. Figure 2.16 is a summary of the results.
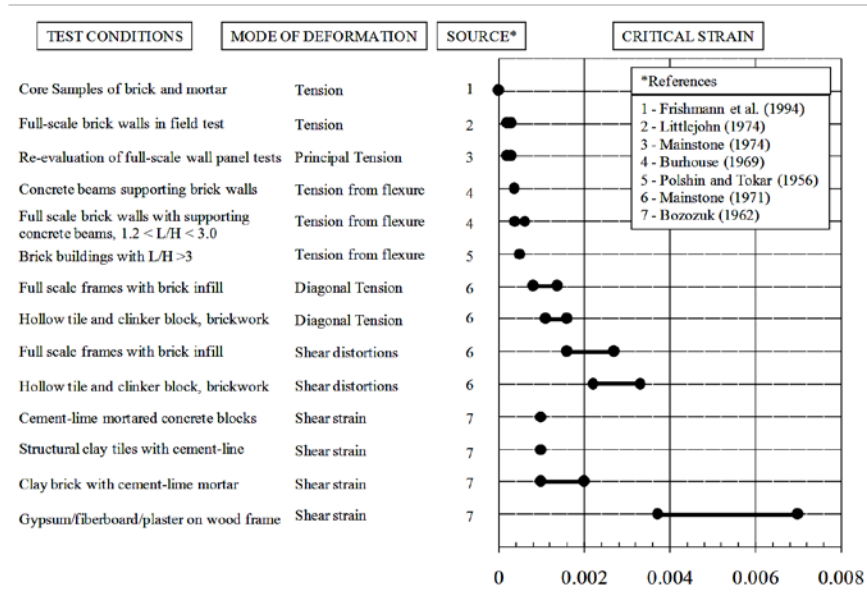
Figure 2.16 Critical Cracking Data (Bryson and Kotheimer, 2011).

The angular distortion, β (i.e. the maximum change in slope along the beam), is related to the deflection ratio by the expression:

$$\beta = \frac{3\Delta}{L} \left(\frac{1 + 4\left(\frac{E}{G}\right)\left(\frac{H^2}{L^2}\right)}{1 + 6\left(\frac{E}{G}\right)\left(\frac{H^2}{L^2}\right)} \right) \qquad (2\text{-}18)$$

By substituting Equation (2-17) into Equation (2-18), a direct relationship between the critical strain and the angular distortion, assuming a Poisson's ratio of 0.3 and an *E/G* of 2.6, is obtained. Equation (2-19) is the expression for the critical angular distortion (β_{crit}) at which cracking is initiated, at a given critical strain. It is noted that this expression allows an explicit input of length-to-height ratios.

$$\beta_{crit} = \frac{3}{125}\left(5\frac{L^2}{H^2} + 52 \right)\left[\frac{8\frac{L^2}{H^2} + 125}{5\frac{L^2}{H^2} + 78} \right]\left(\varepsilon_{crit} - \frac{\varepsilon_h}{2} \right) \qquad (2\text{-}19)$$

Bryson and Kotheimer (2011) provided a graphical representation of Equation (2-19) that allows the estimation of critical angular distortion from a known critical strain. This is shown in Figure 2.17.

41
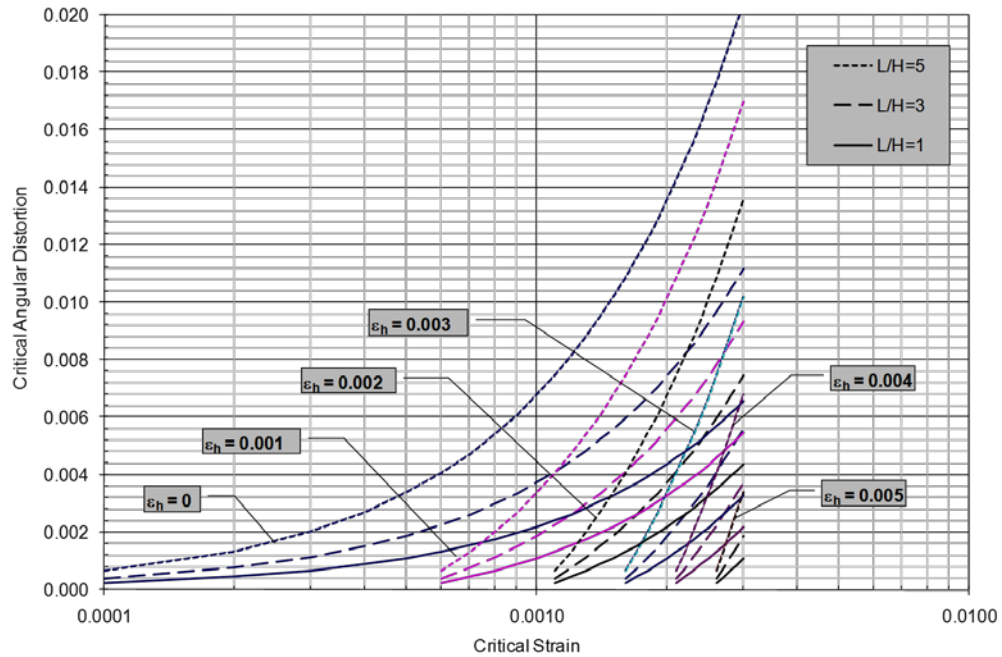
Figure 2.17 Relationship between critical angular distortion and critical strain. (Bryson and Kotheimer, 2011).

2.6   Crack Width Calculation

Burland and Wroth (1974) concluded that cracks in frame buildings are controlled by shear strain and not bending strain. Furthermore, the cracks are diagonally oriented (Fjeld, 1963). Son and Cording (2007) also reported that cracking in masonry structures with some percentage of openings (i.e. doors and windows) is predominantly as a result of shear deformation. The cracking can be aggravated if the frame structure is subjected to horizontal strains (Boscardin and Cording, 1989). Halim and Wong (2012) proposed Equation (2-20) for calculating the diagonal crack width, caused in the infill wall, as a result differential settlement between two columns.

$$\varepsilon_d = \frac{\delta_v}{L}\left(\frac{L}{\sqrt{L^2 + H^2}}\right)\cos\theta \qquad (2-20)$$

42

where θ is the angle shown in Figure 2.18(b) and is also given by $\tan^{-1}(L/H)$ in degrees; δ_v is the differential settlement; and L and H have their usual meanings.
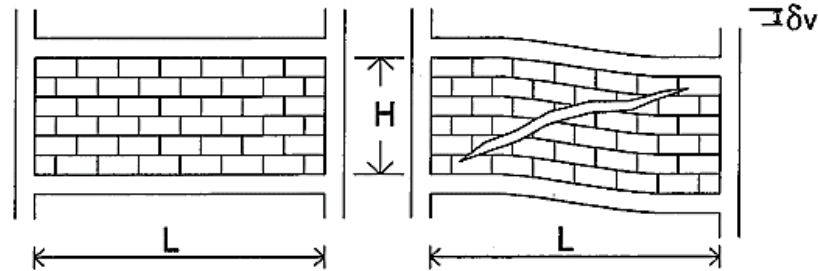
(a)
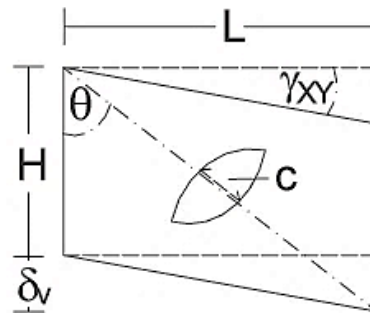
(b)

Figure 2.18 Deformation of a simple frame: (a) differential settlement between columns (b) development of diagonal crack (Halim and Wong, 2012).

It is noted that this approach only considered the differential settlement between the columns and the building dimensions. It does not account for the critical strain within the frame, thus assumed cracking was initiated once there was differential settlement. However, Boone (1996) indicate that cracking can only commence if the critical shear strain (for the case of diagonal cracks) is lower than the strains generated in the infill wall. Also, this approach does not account for horizontal strain, which has been shown by Boscardin and Cording (1989) to be pivotal in building deformation. Notwithstanding,

43

other researchers (Finno and Bryson, 2002; Son and Cording, 2005; Boscardin, 1980) have found that the presence of grade beams can significantly reduce the effect of horizontal strains.

Boone (1996) presented his first order method for assessment of excavation-induced damage to infill walls of adjacent building due to differential settlement. The considered ground movement profile geometry, structure geometry and design, strain superposition, and critical strains of building materials. Boone (1996) showed, using 20 case histories, that the method produces results which compare favorably with actual damage observations. Boone (1996) modeled the building walls as a simply supported deep beam as shown in Figure 2.19.
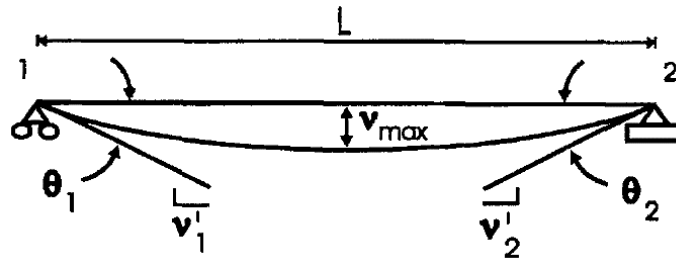
Figure 2.19 Deflection of simply supported beam (Boone 1996).

Then using beam deflection equations supplied by Gere and Timoshenko (1974), the maximum beam deflection, v_{max}, and angles of rotation at either end, θ_1 and θ_2, of a simply supported and uniformly loaded beam are given by:

$$v_{max} = \left(5qL^4\right)/\left(384EI\right) \tag{2-21}$$

$$\theta_1 = \theta_2 = \left(qL^3\right)/\left(24EI\right) \tag{2-22}$$

Re-arranging the two equations above yields,

44

$$\theta_1 = \theta_2 = (3.2 v_{max})/(L) \tag{2-23}$$

However, Boone (1996) noted that Equation (2-23) was only an approximation due to simplification assumptions and were only valid for small deflections and when shear effects are excluded. Gere and Timoshenko (1974) provided an expression that includes both bending and shear deflections for a centrally loaded simple beam with a rectangular cross section:

$$v_{max} = \frac{PL^3}{48EI}\left(1 + \frac{18EI}{GAL^2}\right) \tag{2-24}$$

where P is the point load; E is Young's modulus of elasticity of beam; G is shear modulus; A is cross-sectional area; I is moments of inertia; and L is length of deep beam.

Following other researchers (Boscardin et al., 1979; Boscardin and Cording, 1989), Boone (1996) assumed the shape of the deformed wall follows the approximate ground deformation as shown in Figure 2.20. Figure 2.20(a) shows the strains or elongation arising from bending, ε_M, and Figure 2.20(b) shows the elongation strain, ε_g, assuming no slip between foundation and ground.
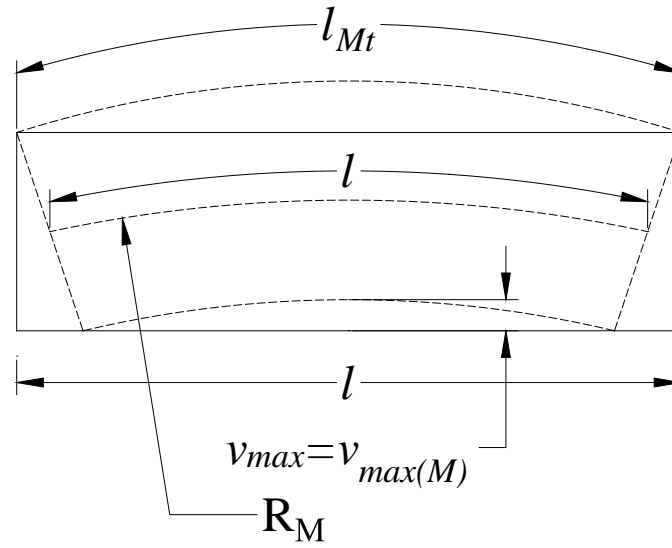
(a)
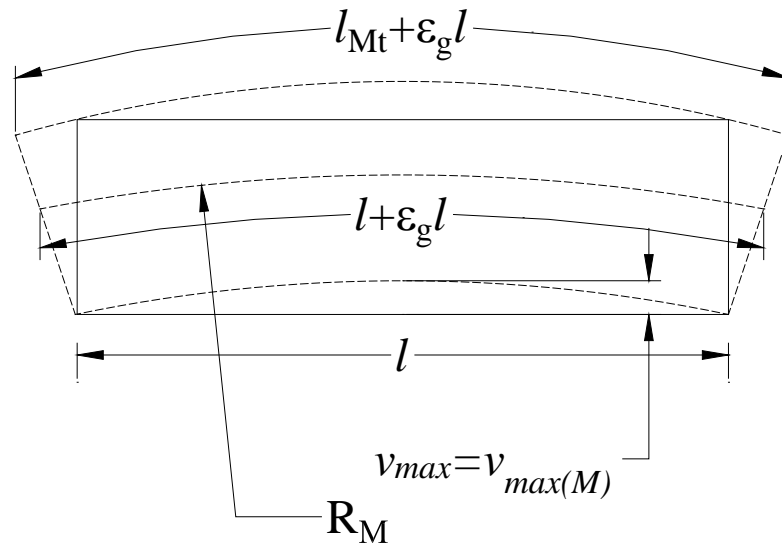
(b)

Figure 2.20 Modes of deformation and associated strains: (a) moment only (b) moment and ground elongation (after Boone, 1996).

The corresponding material deformation provided by Gere and Timoshenko (1974) is shown Figure 2.21.
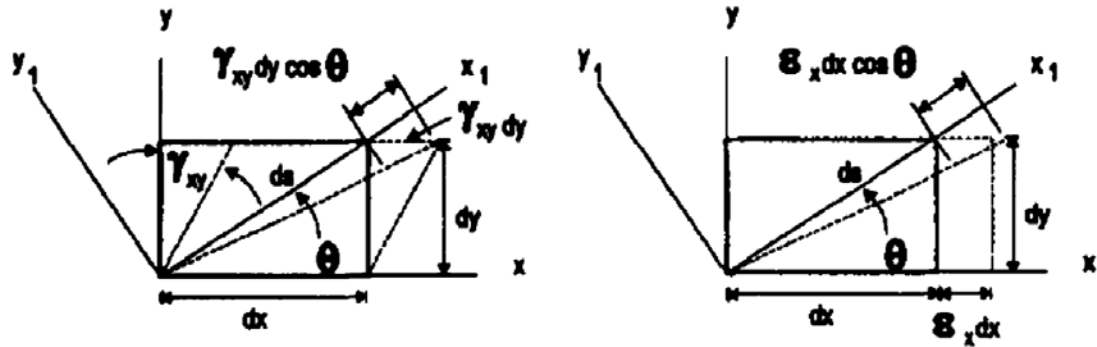
Figure 2.21 Deformation of material element (Boone. 1996).

Boone (1996) defined shear strain, γ, as the change in shape of a material element in units of radians and given by $\tan \gamma$ or $\tan^{-1} v'$ as shown in Figure 2.22.
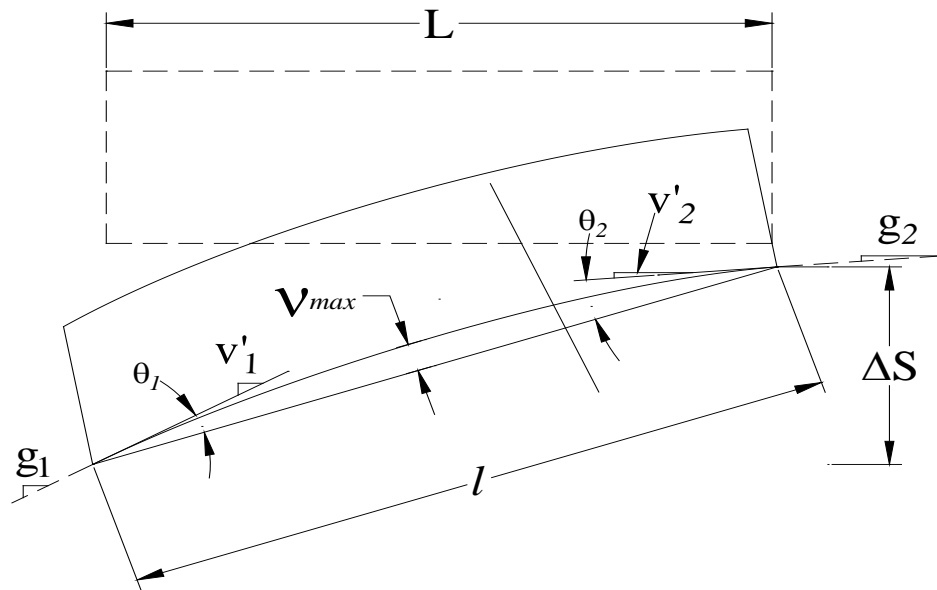
Figure 2.22 Wall in long settlement profile, general case (after Boone, 1996).

The bending strain, ε_M; elongation strain, ε_g; and the total tensile strain, ε_t, are given by:

$$\varepsilon_M = (l_{Mt} - l)/l \qquad (2\text{-}25)$$

47

$$\varepsilon_g = \left(l_g - l\right)/l \tag{2-26}$$

$$\varepsilon_t = \varepsilon_M + \varepsilon_g + \varepsilon_{le} \tag{2-27}$$

The total crack width can be estimated by multiplying the total tensile strain by length of the beam. For further details, the reader is directed to Boone (1996).

Despite the fact that the Boone (1996) approach checks to ascertain the likelihood of cracking, the value of the critical strains are not deducted from the total strains when calculating the crack width. This implicitly assumes that all the strains goes into crack propagation. However, this cannot be the case since the concept of critical strain stipulates that the critical strain has to be exceeded for cracking to begin.

2.6.1   Damage Approximation Method

Bryson and Kotheimer (2011) presented a damage approximation method that considered the effect of horizontal and critical strains. Their work followed research by Dulacska (1992), who suggested that crack width of interior infill wall panels can be estimated from the diagonal strain. The damage approximation method utilizes common mechanics of materials relationships. Figure 2.23 is an illustration of the resulting angular distortion, as experienced by the infill wall, due to differential settlement between the columns.
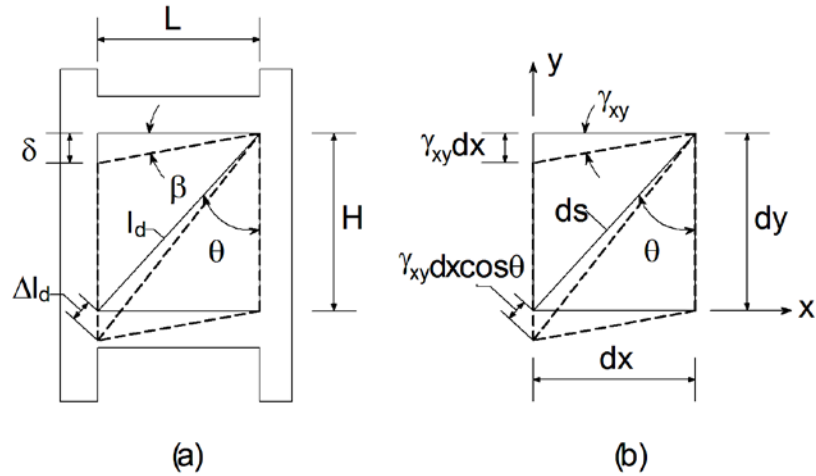
Figure 2.23 Deformation of a simple frame: (a) actual simple frame; (b) mechanics of materials approximation (Bryson and Kotheimer, 2011).

In both figures, δ is differential movement, β is angular distortion, l_d is original length of the diagonal, Δl_d is change in the length of the diagonal, θ is angle of rotation, dx is the elemental length along the x-axis, dy is the elemental length along the y-axis, ds is the elemental length along the diagonal, γ_{xy} is the shear strain in the xy-plane, and $\gamma_{xy}dx\cos\theta$ is the increase in the diagonal length. The mechanics of materials approximation, shown in Figure 2.23(b), illustrates the deformation of an element in plane strain due to shear strain. Bryson and Kotheimer (2011) suggested that increasing crack width in infill wall will be proportional to the increase in the length of the diagonal (Δl_d). Equation (2-28) represents the increase in crack width. The expression was obtained through the following substitutions: horizontal length of the wall (*L*) for the elemental horizontal length (dx); the vertical height of the wall of infill wall (*H*) for the

www.manaraa.com

elemental vertical length (dy); and finally the angular distortion (β) for the shear strain (γ_{xy}).

$$\Delta l_d = \gamma_{xy} dx \cos\theta = \beta L \cos\theta = \beta L \left(\frac{H}{\sqrt{H^2 + L^2}} \right) \tag{2-28}$$

It is immediately clear that Equation (2-28) makes the assumption that crack growth begins instantaneously as angular distortion is available in the infill wall. This makes the expression essentially the same as that proposed by Halim and Wong (2012), thusly failing to address the issue of critical strains as proposed by Boone (1996) and also violates its own fundamental assumptions (i.e. cracking is initiated when a critical angular distortion is exceeded). The logical progression from this point is, therefore, to reduce the excavation-induced angular distortion by the critical distortion in order to realistically represent the crack growth. Dulacska (1992) suggested that stiffer buildings are less affected by the ground distortions. Thus, as a result of the rigid body response of the building to the excavation-induced deformation, there may be variance in the measured building distortions and the measured ground distortions. He proposed the flexibility factor (η) to account for the stiffness of a building or a wall section when representing distortion developed within it. The flexibility factor is influenced by the percentage of opening in the wall section, and ranges from 0.5 for a stiff (solid) wall section to 1.0 for a highly punctured (flexible) wall section. To address the above discussed issues, Equation (2-28) was modified to account for these factors, thus the normalized crack width, $\Delta l_c / L$, is given by the equation:

50

$$\frac{\Delta l_c}{L} = \eta(\beta_{meas} - \beta_{crit})\left(\frac{H}{\sqrt{H^2 + L^2}}\right) = \mu\beta_{build} \qquad (2\text{-}29)$$

where β_{meas} is the measured or anticipated ground distortion; β_{build} is the building distortion (given by $\eta(\beta_{meas} - \beta_{crit}) \geq 0$); and μ is the geometric factor (given by $\left(H/\sqrt{H^2 + L^2}\right)$) and is dependent upon the *L/H* ratio. It is noted that this simplified relationship assumes that only one crack develops at a characteristic place within the wall element resulting in the widest cumulative crack width estimate. Bryson and Kotheimer (2011) compared crack width predicted using this method with crack gauge data reported by Bryson (2002) for a building adjacent to the Chicago Avenue and State street excavation. Figure 2.24 shows the method compared favorably with the crack gauge data. For additional details of the study, the reader is referred to Finno et al. (2002); Finno and Bryson (2002); and Bryson (2002).
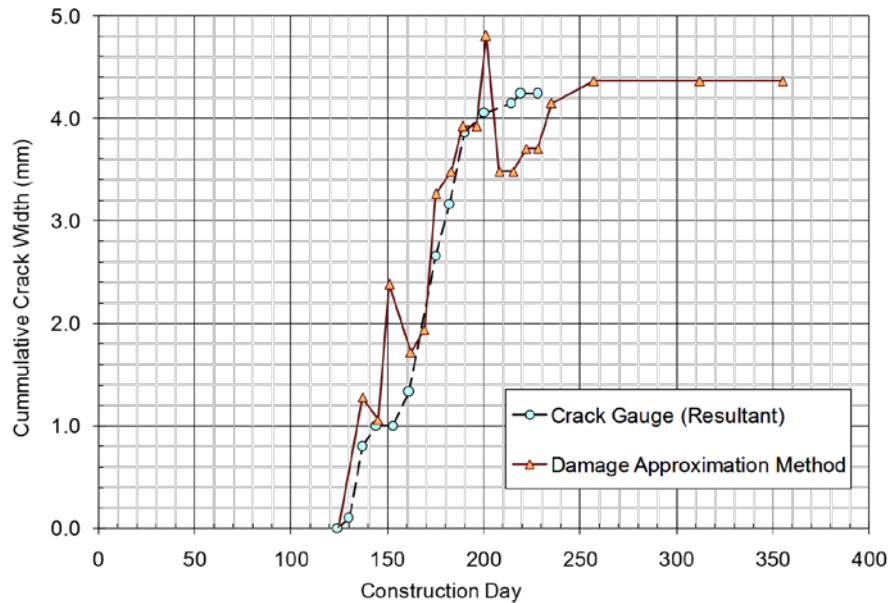
Figure 2.24 Cumulative crack width approximation (Bryson and Kotheimer, 2011).

51

2.7 Influence of Soil Types on Excavation-Induced Ground Movements in Adjacent Structures

In order to accurately predict distortions caused by excavation-induced ground settlements, it is essential to have a better understanding of the soil-structure interaction (Son and Cording, 2005; 2011). Despite the fact that several researchers (Breth and Chambosse, 1974; Attewell, 1978; Boscardin and Cording, 1989; Burland, 1995; Boone et al., 1999; Son and Cording, 2005) have provided very useful findings, there is a lot more be done. They attribute this shortfall to the difficulty and complexity of the processes involved in predicting soil-structure interaction.

To better understand soil-structure interaction, Son and Cording (2011) used numerical methods to evaluate the responses of single brick-bearing walls and frame structures under different soil conditions, structure conditions, and structural types. Figure 2.25 is a comparison of the structural responses of cases investigated. Son and Cording (2011) used different soil and structure conditions and a comparison was done on the basis of normalized angular distortion ($\beta/\Delta GS$). In the normalized angular distortion expression, β is the angular distortion in a bay; and ΔGS is the change in ground slope between two adjacent bays in a free-field ground settlement profile.

Among their findings, Son and Cording (2011) concluded that structures on stiffer soils are more susceptible to building damage, as a result of excavation-induced ground movements, than those on softer soil, given the same magnitude of ground movements. They attributed the observation to the tendency of structures on softer soils to modify the ground settlement profiles and this leads to less distortion.

52
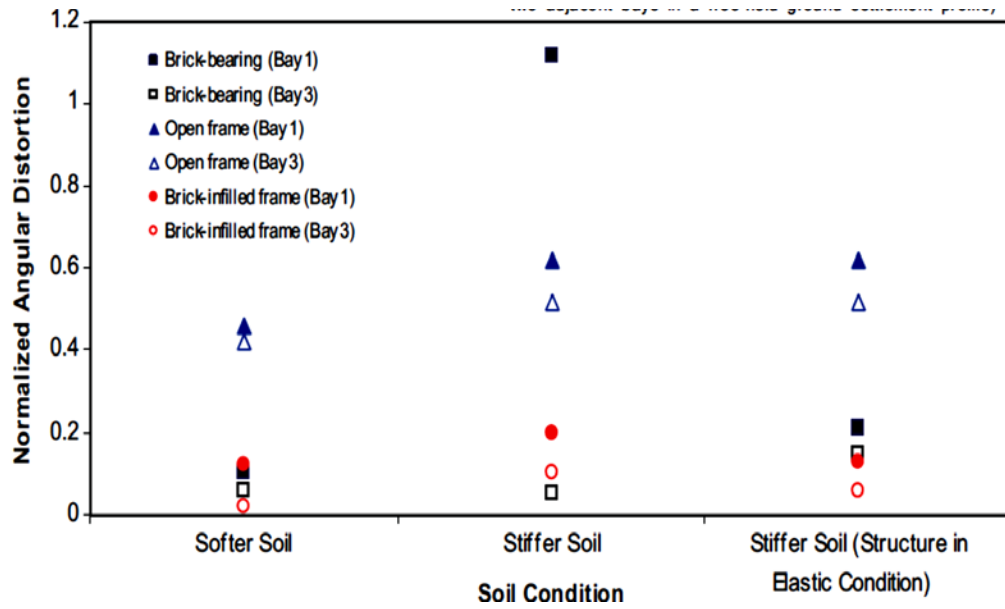
Figure 2.25 Comparison of normalized angular distortion for different soil conditions and structural configuration (after Son and Cording, 2011).

2.8   Cost Associated With Excavation Support Wall Movement

Several researchers (Boscardin and Cording, 1989; Boone, 2001; Finno et al., 2005; Cording et al., 2010; Son and Cording, 2011) have recognized that there are costs associated with excavation-induced ground movements. These costs are primarily due to the damages suffered by adjacent buildings. It is recognized that the sensitivity of the structure to damage, as well as the structure's significance should be considered when designing excavation support systems. Boone (2001) notes that the most sensitive cases involve structures with either masonry load bearing walls or frames with masonry infill walls. Son and Cording (2011) underscores the importance of a better understanding of the soil-structure interaction, a lack of which could lead to the implementation of unnecessary preventative measures which will increase the cost of the project. Preventive measures are those that are aimed at the root causes of building damage and may be less costly and disruptive than near surface measures. Little to nothing exist in current

53

literature about the relationship between cost of repair of excavation-induced damage in adjacent building and the stiffness of the excavation support wall.

North American Steel Sheet Piling Association (NASSPA), (2006) did cost comparisons of tied-back sheet piling versus five other excavation support systems (i.e. reinforced concrete cantilever, concrete modular unit, mechanically stabilized earth, soldier pile and concrete lagging, and slurry wall). They used designs based on AASHTO Standard Specifications for Highway Bridges, 17th Edition, 2002, ASD and costings were done using the 2006 edition of "RSMeans Heavy Construction Cost Data" and summarized on Table 2.6.

Table 2.6 Summary of cost comparison of excavation support types (NASSPA, 2006).

Retaining Wall Type	Construction duration (days)	Total Cost per 100ft ($)	Cost per Linear Ft. ($)	Cost per Square Ft. ($)
Grouted Anchor Steel Sheet Pile	13	90,607	906.07	47.69
Cast-In-Place Reinforced Concrete	47	258,572	2585.72	136.09
Concrete Modular Unit Gravity	31	144,741	1447.41	76.18
Mechanically Stabilized Earth	35	181,593	1815.93	95.58
Soldier Pile and Lagging	26	171,856	1718.56	90.45
Slurry Wall	64	400,145	4001.45	210.60

The study revealed the following:

i.   the sheet pile wall provided a minimum of 35% cost savings over other wall types and provided a 65% savings over a traditional cast-in-place concrete wall

ii.   the sheet pile had the shortest construction duration of all the options.

As has been presented in the foregoing sections, the current state-of-the-practice lacks a cost component embedded in the design process. Cost analyses, as shown in section 2.8, are conducted as a separate study. This research will propose a methodology that will make initial cost an intrinsic part of the design process. The method will be developed from an analytical study of damage to adjacent structures and the relationship with excavation-induced ground movement. The proposed method will also allow a juxtaposition of acceptable deformation and cost related to the chosen excavation support system. The approach will be validated using a finite element simulation of a two-dimensional deep excavation.

CHAPTER 3

3.0   Deformation-Based Method for Designing Excavation Support Systems

3.1   Introduction

As indicated earlier, the classical approach focuses on meeting limits equilibrium requirements and then checks for excavation-induced ground movements. These ground movements subsequently determine the kind of deformation that occur within adjacent infill walls (ceteris paribus). This is an iterative process as the designer may find out ground movements and damage to adjacent buildings are unacceptable, even though limits equilibrium requirements are fully met. Such an approach is both inefficient and could be costly due to unforeseen damages to adjacent buildings. Moreover, there is currently no literature on the design of excavation support systems with damage to adjacent buildings as the controlling factor.

This chapter focuses on the analytical and empirical techniques that were combined to create the inverse support system method for designing excavation support systems. This method can be viewed as an inverse process of the traditional method, except that both deformation and limits equilibrium requirements are fulfilled simultaneously. It should be noted that design is controlled by acceptable deformation to adjacent buildings. Additionally, the method provides the designer with preliminary costing information to guide the design process. In summary, the method makes use of in situ soil properties (i.e. wished-in-place wall condition), acceptable crack width, adjacent infill wall geometry, critical strains of infill wall, predicted horizontal and vertical ground

56

movements, and excavation geometry to design a cost effective support system that meets both limits equilibrium and deformation requirements.

3.2   Conceptual Overview of Problem

The deformation-based method can broadly be categorized into three stages or elements. Figure 3.1 is an illustration of the main stages and their interdependencies. In this method, the magnitude of the tolerable or acceptable deformation (i.e. diagonal crack width) (Element 1) is related analytically to the maximum vertical settlement caused by the nearby deep excavation (Element 2). The maximum horizontal movement (Element 3) can then be predicted using a relationship obtained from case history data.

3.2.1 Element 1 (Measure of Damage-Crack Width Criterion)

In this study, the measure of damage was based on diagonal tensile cracks. The diagonal crack width is a function of the material properties of both infill wall and building (i.e. $E/G=2.6$ assuming isotropy); critical diagonal tensile strain, ε_{crit}; the horizontal tensile strain the infill wall is subjected to, ε_h; geometry of the infill wall, L/H; soil-structure interaction, η; critical angular distortion, β_{crit}; and the differential settlement between the columns which bound the infill wall, δ, shown in Figure 2.22(a). Several researchers have acknowledged the difficulty and complexity involved measuring and assessing soil-structure interaction (Boscardin and Cording, 1989; Burland, 1995; Boone et al., 1999; Son and Cording, 2005; Finno et al., 2005; and Schuster et al.,2009). Son and Cording (2011) further emphasized the need for an adequate understanding and prediction of soil-structure interaction in order to accurately predict damage.

57
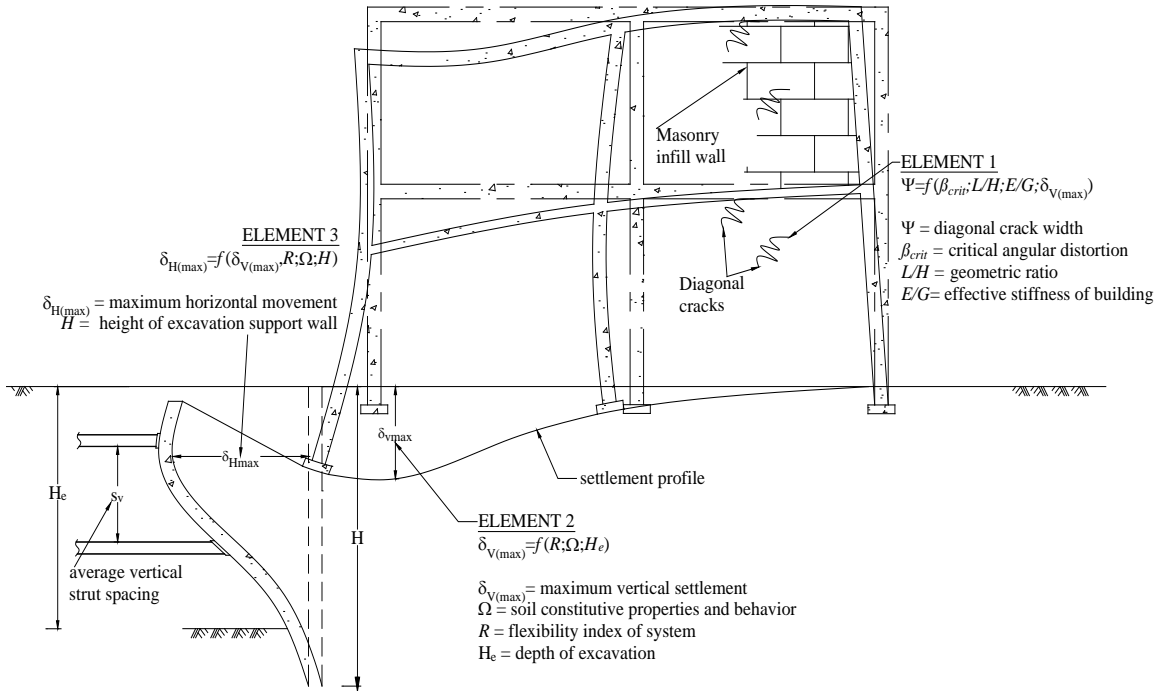
Figure 3.1 Conceptual approach to deformation-based excavation support system design.

Son and Cording (2011) concluded that all masonry-infilled frame structures suffered similar distortions regardless of soil and structure conditions. Dulacska (1992) suggested that the soil-structure interaction factor, η, is dependent on the amount of openings within the infill wall. It ranges from 0.5 for solid walls to 1.0 for highly punctured walls. Hence, it may be conservative to assume a value of 1.0.

As indicated earlier, several researchers have shown that the presence of grade beams will reduce the distortions within an infill wall. In this research, the focus of the analysis was on a single bay, with a length-to-height ratio of *L/H*. The bay was considered to be a simple frame supported by a shallow foundation. In that case Boone (1996) has shown that the length of the bay remains unchanged because the deformed shape is that of a rhombus as shown in Figure 3.2.

58
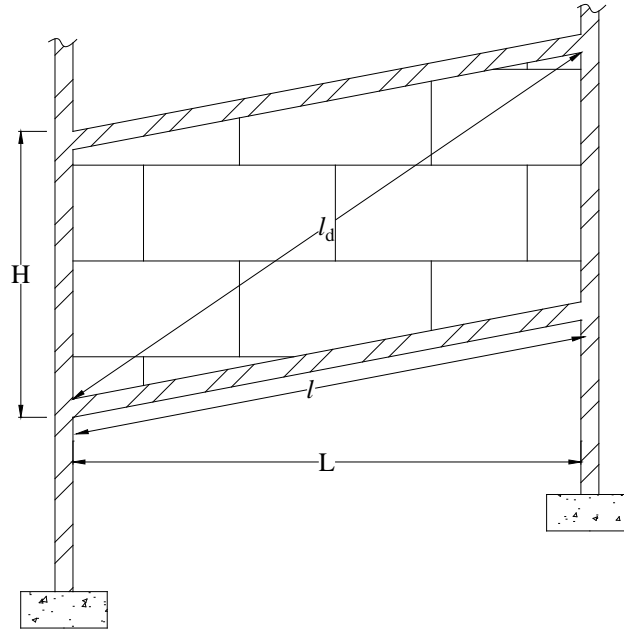
Figure 3.2 Deformation of a simple frame due to differential settlement (after Boone, 1996).

From the above figure, the deformed length of the bay is the same as the un-deformed length (i.e. $L = l$). Hence, in calculating the diagonal length, l_d, the actual bay dimensions was used. This also implies that the building distortions are equal to the ground distortions, thus $\eta = 1$.

From Element 1, the measured angular distortion, β_{meas}, can be related to the maximum vertical settlement, $\delta_{V\max}$ (Element 2). It should be noted that the term angular distortion, for the purposes of this study, refers to the slope of the deflected shape of the infill wall between the bounding columns (i.e. it does not account for rigid body tilt). For simplicity, this approach will suffice, even though it represents a more conservative interpretation of angular distortion and has been employed by other researchers (Boone et al., 1998), as shown in Figure 3.3.

59
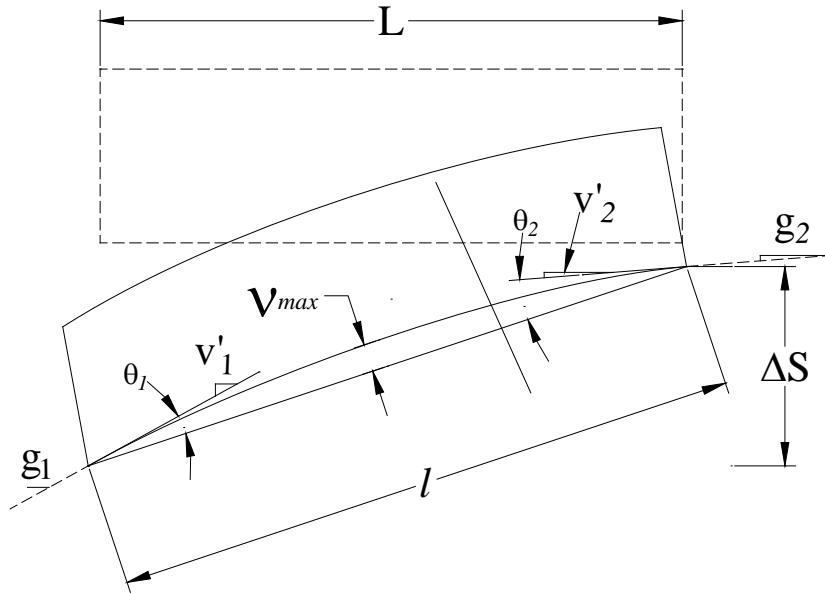
Figure 3.3 Angular distortion, *β*, as used in the application of the deep beam model (after Boone et al., 1998).

where ΔS is differential settlement; θ is rotation; $V_{\max}$ is maximum beam deflection; *g* is slope; *L* and *l* have their previous definitions.

3.2.2 Element 2 (Maximum Vertical Settlement)

Figure 3.4 shows the deformed shape of a frame structure subjected to ground movements behind the excavation support wall. Using the approximate distribution proposed by Bryson and Zapata-Medina (2012), shown in Figure 2.5, perpendicular settlement profile for any given flexibility index can be predicted. As was mentioned previously in Chapter 1, the relative stiffness ratio given by Bryson and Zapata-Medina (2012) actually describes the flexibility of the support system. Thus for this work, the ratio will be referred to as the "flexibility index".

60

Figure 3.4 Prediction of perpendicular settlement profile.

In this research only the case of Taipei silty clay ($s_u = 42kPa$) with a reference cohesion

of zero was considered, but the approach will be the same for any other types of clay. The

hardening soil properties for this medium clay was obtained from Bryson and Zapata-

Medina (2012). The undrained shear strength, s_u, was obtained by running a virtual

triaxial undrained compression test with initial effective stress, σ_3', of -100 kPa;

maximum strain, ε_1, of 10 percent; and a vertical preconsolidation stress of 0kPa.

Further details of the hardening soil properties is found in Appendix A. Figure 3.5 is the

illustration of the shear stress versus the mean effective principal stress. From the figure,

the value of the undrained shear strength is approximately 42 kPa. The essence of this

61

step is to illustrate that the research is staying consistent with the definition of medium clay as defined in Chapter 1.
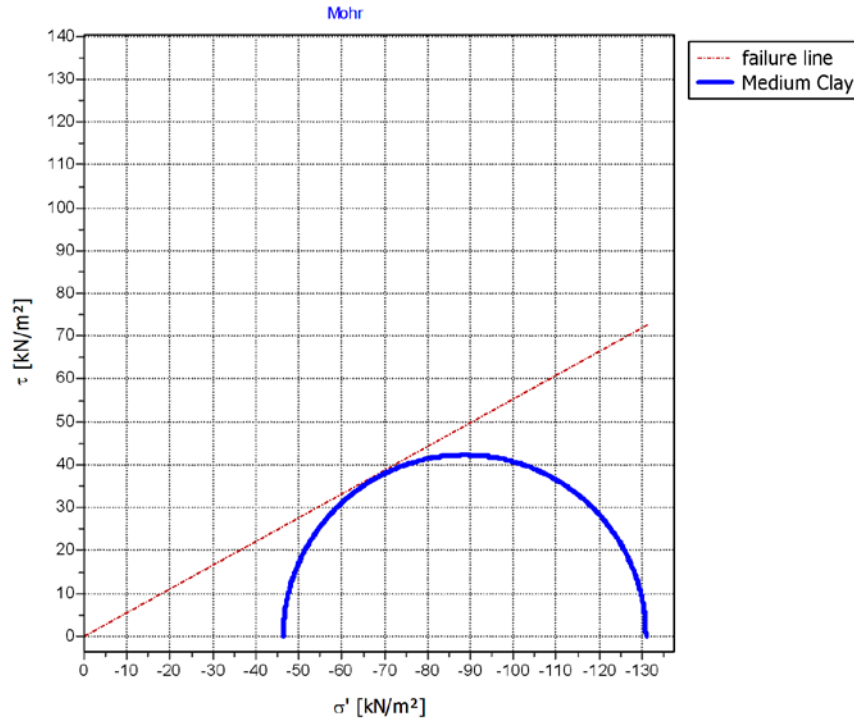
Figure 3.5 Undrained triaxial compressive strength test on Taipei silty clay.

Since the prediction of the perpendicular settlement is specific to soil type, it will be unnecessarily repetitive to use soils of differing undrained shear strength. At this stage, the research was focused on the influence of the geometrical arrangements of the excavation support system (i.e. s_v, and s_h) on the flexibility index, R, the soil properties; material type; and the factor of safety against basal heave were kept constant. The subsequent chapter will be used to assess the effect of changing soil type, as well as the other parameters held constant at this stage, on the proposed method. Table 3.1 is a summary of the parameters that will be held constant at this stage of the methodology.

62

Table 3.1 Soil properties and excavation geometry.

FS_{bh}	N_c	S_{ub} (kPa)	S_{ueq} (kPa)	Υ_{eq} (kNm^{-3})	H_e (m)	B (m)	q_s (kPa)	D (m)	E_{50} (kPa)	H (m)
1.5	5.14	42	42	18.1	12.2	25	0	15.06	12476	27.26

where FS_{bh} is factor of safety against basal heave; N_c is bearing capacity factor provided by Ukritchon et al., 2003; s_{ub} is the undrained shear stress below the bottom of the excavation; s_{eq} is the equivalent undrained shear stress of the layers of soil above the excavation; γ_{eq} is equivalent unit weight of layers of soil; H_e is depth of excavation; B is width of cut; q_s is applied surface surcharge; E_{50} is initial tangent modulus of the soil; H is the depth of the support wall and is equal to the sum of the depth of excavation and depth of embedment, D; and D is obtained by making it the subject in Equation (2-2):

$$D = \frac{B(FS_{bh}\gamma_s H_e - N_c s_{ub}) - \sqrt{2}s_{ueq}H_e}{\sqrt{2}s_{ueq} + 2s_{ub}} \tag{3-1}$$

Next step to be able to predict perpendicular settlement, was to calculate the flexibility index using Equation (2-3). An A36 steel sheet pile wall was assumed. Thus, the Young's modulus of elasticity, *E*, is 200.1 GPa. It should be noted that it does not matter what material the wall is made up of , the approach remains the same.

The parameters remaining in Equation (2-3) are the moments of inertia of the wall, *I*; horizontal strut spacing, s_h; and vertical strut spacing, S_v . For a given moments of

63

inertia of the support wall, the ratio of horizontal strut spacing to vertical strut spacing, s_h/s_v, was varied, this resulted in the generated flexibility indices, R. Then using the medium clay prediction chart in Figure 2.5, the vertical settlement profile was predicted at various values of R.

Now using the simplified assumption for the angular distortion, β, as the magnitude of the slope between points (x_2, y_2) and (x_3, y_3) and for small angles:

$$\tan \beta \approx \beta = \left(\frac{y_2 - y_3}{x_2 - x_3} \right) \tag{3-2}$$

It is implicit in the above equation that measurement of distortion is at plane strain point. Table 3.2 is a sample calculation leading to predicted perpendicular ground settlement, and subsequently angular distortion. In the table, $I = 8000\,cm^4/m$, and the s_h/s_v ratio was kept at 1.5. The s_h/s_v ratio of 1.5 is arbitrary but useful in the sense that it allows us to have a more realistic struts configuration. This because in reality, the ratio could be any value from one. Boone et al. (1998) provides a range of $2.4m$ to $5.8m$ for the vertical strut spacing. Das (2007) states that for construction works the minimum strut spacing is about $2.75m$. The importance of the randomness of s_h/s_v ratio will be explored further in latter sections.

In summary, varying the support configurations (i.e. s_v and subsequently S_h), resulted in different flexibility index values. Every flexibility index corresponded to different perpendicular settlement predictions, and subsequently different angular distortions.

64

Table 3.2 Angular Distortion at plane strain point along vertical settlement profile.

s_v (m)	$s_h=1.5s_v$ (m)	R	x_2 (mm)	y_2 (mm)	x_3 (mm)	y_3 (mm)	$\beta \times 10^{-3}$
2.75	4.13	1266.97	9629.99	83.45	52978.35	8.34	1.73
2.85	4.28	1360.79	9439.03	85.15	52916.26	8.51	1.76
2.95	4.43	1457.96	9249.13	86.82	52855.87	8.68	1.79
3.05	4.58	1558.48	9060.62	88.48	52797.07	8.85	1.82
3.15	4.73	1662.35	8873.78	90.10	52739.76	9.01	1.85
3.25	4.88	1769.57	8688.87	91.71	52683.84	9.17	1.88
3.35	5.03	1880.14	8506.11	93.30	52629.23	9.33	1.90
3.45	5.18	1994.06	8325.71	94.86	52575.86	9.49	1.93
3.55	5.33	2111.34	8147.85	96.40	52523.64	9.64	1.96
3.65	5.48	2231.96	7972.69	97.93	52472.52	9.79	1.98
3.75	5.63	2355.94	7800.35	99.44	52422.44	9.94	2.01
3.85	5.78	2483.26	7630.97	100.93	52373.35	10.09	2.03
3.95	5.93	2613.94	7464.61	102.40	52325.19	10.24	2.05
4.05	6.08	2747.96	7301.38	103.86	52277.92	10.39	2.08
4.15	6.23	2885.34	7141.32	105.30	52231.49	10.53	2.10
4.25	6.38	3026.07	6984.48	106.73	52185.88	10.67	2.13
4.35	6.53	3170.15	6830.89	108.14	52141.03	10.81	2.15
4.45	6.68	3317.58	6680.58	109.54	52096.92	10.95	2.17
4.55	6.83	3468.36	6533.54	110.92	52053.52	11.09	2.19
4.65	6.98	3622.49	6389.79	112.30	52010.80	11.23	2.22
4.75	7.13	3779.97	6249.31	113.65	51968.72	11.37	2.24
4.85	7.28	3940.80	6112.07	115.00	51927.27	11.50	2.26
4.95	7.43	4104.98	5978.06	116.34	51886.41	11.63	2.28
5.05	7.58	4272.52	5847.25	117.66	51846.14	11.77	2.30

Figure 3.6 is an illustration of the behavior of angular distortion with flexibility index, *R*. It should be noted that the relationship between angular distortion and flexibility index was developed for moments of inertia of the excavation support wall ranging from $I = 1000\,cm^4/m$ to $I = 125000\,cm^4/m$. It should be noted that the values of the moments of inertia of the support wall are arbitrary and were chosen within a range commonly found in sheet pile members. It can be observed that angular distortion increased with increased flexibility index. This behavior is to be expected, since a higher flexibility

65

index implies a less rigid excavation support system. Subsequently, a higher ground settlement would be expected.

The figure shows a plot of Angular Distortion, β ($\times 10^{-3}$) versus Flexibility Index with the fitted equation $y = 0.2791x^{0.2538}$.
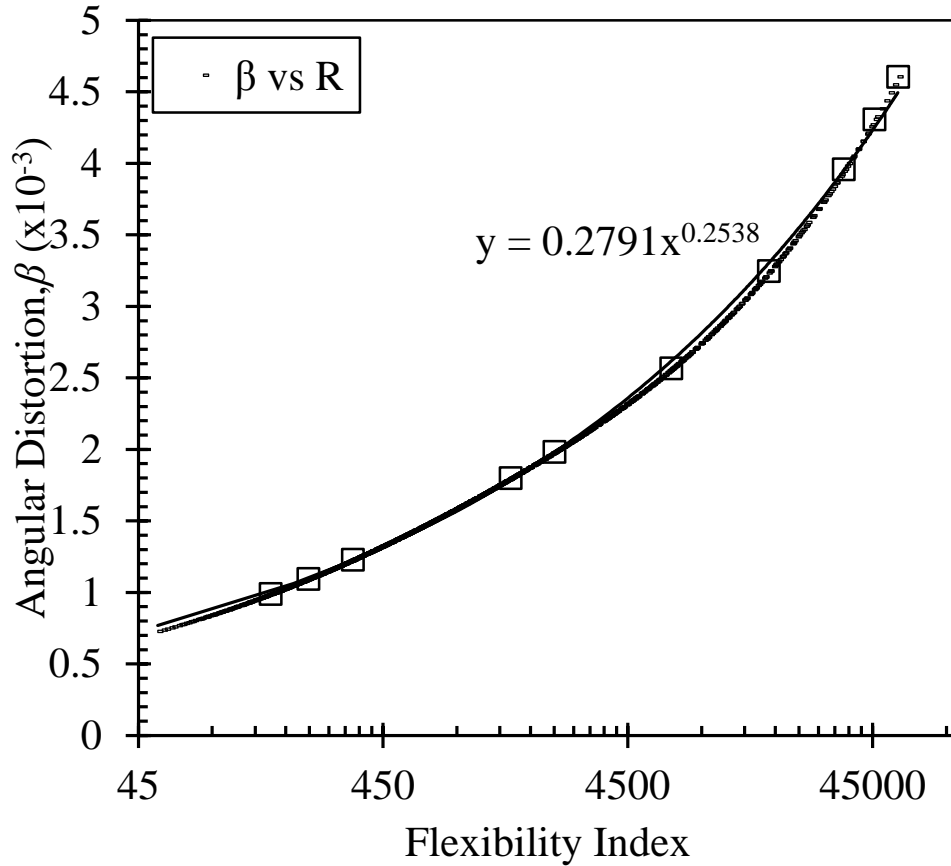
Figure 3.6 Variation of angular distortion with relative flexibility.

A power function was fitted to the data and the resulting equation is given by:

$$\beta = 0.2791 \times 10^{-3} R^{0.2538}$$

(3-3)

A closer look at the graph shows consistency with the concept of flexibility index. That is to say, when the value of flexibility index is null (i.e. as the rigidity of the excavation support system approaches infinity) no distortion is measured. Though practically impossible, theoretically such a system will not allow any movement.

66

3.2.3 Linking Element 1 to Element 2

This subsection will be used to show the link between the predicted angular distortion and Element 1 (damage criteria i.e. crack width). As earlier indicated, a simplified assumption has been made that the soil-structure interaction is rigid. This will ensure that distortion on adjacent structure is of the same magnitude as the amount of experienced by the greenfield, even though it may yield conservative values (Boone et al., 1998). Consider an isotropic infill wall with the following properties subjected to both tensile and horizontal strains:

Table 3.3 Infill wall properties.

E/G	L/H	μ	$\varepsilon_{crit}\times10^{-3}$	$\varepsilon_h\times10^{-3}$	$\beta_{crit}\times10^{-3}$
2.60	2.00	0.45	1.09	0.50	1.63

where ε_h is horizontal strain [the value on the table is assumed. A very small random number was chosen to reflect the presence of horizontal strains, which are commonly associated with open excavations (Boscardin and Cording, 1989)]; the critical diagonal tensile strain, ε_{crit}, is obtained by averaging the range of values for diagonal tensile on Figure 2.15; β_{crit} is obtained plugging the values on Table 3.3 into Equation (2-19); and μ is geometric factor given by $\left(H\big/\sqrt{H^2 + L^2}\right)$.

Next, substitute predicted angular distortions from Table 3.2 and a flexibility factor of $\eta = 1$ into Equation (2-29). This resulted in a generated normalized crack width, $\Delta l_c\big/L$, data for the respective flexibility index values. A sample calculation using angular

67

distortion values from Table 3.2 and a length-to-height ratio, L/H, of two is shown in Table 3.4. In this research, it is assumed that diagonal cracks are fully developed in the bay under consideration, thus an L/H of two is appropriate and represents a realistic field value. Boscardin and Cording (1989) noted that the L/H ratio increases from zero at the onset of excavation-induced ground movement (and behaves as travelling wave that gradually impinges on the structure), until cracks are fully developed. Flexibility index values were plotted against normalized crack width, for the case of $L/H = 2$.

Table 3.4 Normalized crack width data based on flexibility index.

s_v (m)	$s_h = 1.5s_v$ (m)	R	β ($\times 10^{-3}$)	$\Delta l_c/L$ (%)
2.75	4.125	1266.97	1.73	0.004
2.85	4.275	1360.79	1.76	0.006
2.95	4.425	1457.96	1.79	0.007
3.05	4.575	1558.48	1.82	0.008
3.15	4.725	1662.35	1.85	0.010
3.25	4.875	1769.57	1.88	0.011
3.35	5.025	1880.14	1.90	0.012
3.45	5.175	1994.06	1.93	0.013
3.55	5.325	2111.34	1.96	0.014
3.65	5.475	2231.96	1.98	0.016
3.75	5.625	2355.94	2.01	0.017
3.85	5.775	2483.26	2.03	0.018
3.95	5.925	2613.94	2.05	0.019
4.05	6.075	2747.96	2.08	0.020
4.15	6.225	2885.34	2.10	0.021
4.25	6.375	3026.07	2.13	0.022
4.35	6.525	3170.15	2.15	0.023
4.45	6.675	3317.58	2.17	0.024
4.55	6.825	3468.36	2.19	0.025
4.65	6.975	3622.49	2.22	0.026
4.75	7.125	3779.97	2.24	0.027
4.85	7.275	3940.8	2.26	0.028
4.95	7.425	4104.98	2.28	0.029
5.05	7.575	4272.52	2.30	0.030

Figure 3.7 illustrates the relationship between flexibility index and normalized crack with. Thus for a given crack width (i.e. Element 1) and support system configuration, we are able to first predict the related flexibility index. The system flexibility index can then be used to generate the angular distortion required to produce the diagonal crack width. Again, even though Table 3.4 shows sample calculations for $I = 8000\,cm^4/m$, Figure 3.5 is valid for $I = 1000\,cm^4/m$ to $I = 125000\,cm^4/m$.

69
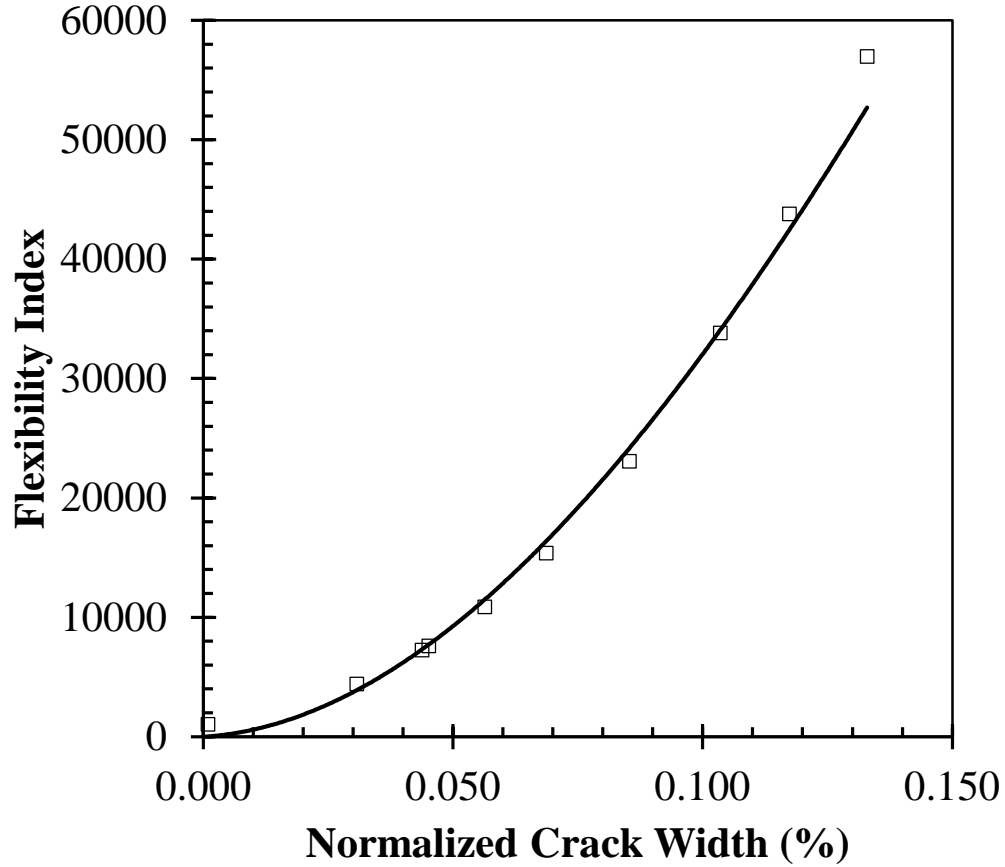
Figure 3.7 Predicting flexibility index based on crack width deformation criteria.

Figure 3.7 is a curve fitted data using a DR-Hill –Zerobackground model. The corresponding equation to obtain an excavation support system flexibility index is given by:

$$R = \frac{\theta \left(\dfrac{\Delta l_c}{L} \right)^{\eta}}{\kappa^{\eta} + \left(\dfrac{\Delta l_c}{L} \right)^{\eta}} \tag{3-4}$$

where θ, η, and κ are constants of the curve fit model and are equal to 9.397×10^7, 1.778, and 8.934 respectively. It can be observed from Figure 3.5 that no deformation occurs in the adjacent structure when the flexibility index of the system is null. This

70

agrees with Figure 3.6 since there is no deformation imposed on the structure (i.e. $\beta_{meas} = 0$ as $R \rightarrow 0$).

Figure 3.7 provides a means to link Element 1 to Element 2. This is done by first predicting the flexibility index using Figure 3.7 or Equation (3-4) at the known Element 1(i.e. acceptable crack width and subsequently the calculated normalized crack width). Next the corresponding angular distortion, β, is found using Figure 3.6 or Equation (3-3). Finally, referring back to the simplified assumption of a rigid soil-structure interaction and that plane strain condition governs, it implies that the angular distortion, β, is experienced by the infill wall sitting between points $(x_3, 0.1)$ and $(x_2, 1)$ on Figure 3.6. Given that small strain theory is valid;

$$\tan \beta_{pre} \approx \beta_{pre} = \frac{\delta_{V(\max)}}{L} \tag{3-5}$$

where β_{pre} is the predicted angular distortion obtained from the aforementioned procedure; $\delta_{V(\max)}$ is the maximum vertical settlement; and L is the length of infill wall. Finally Element 2 is obtained from Equation (3-5) as:

$$\delta_{V(\max)} = \beta_{pre} \cdot L \tag{3-6}$$

In a similar fashion, the engineer or designer may wish to predict the normalized crack width from the flexibility index, in which case Figure 3.8 should be used.

71
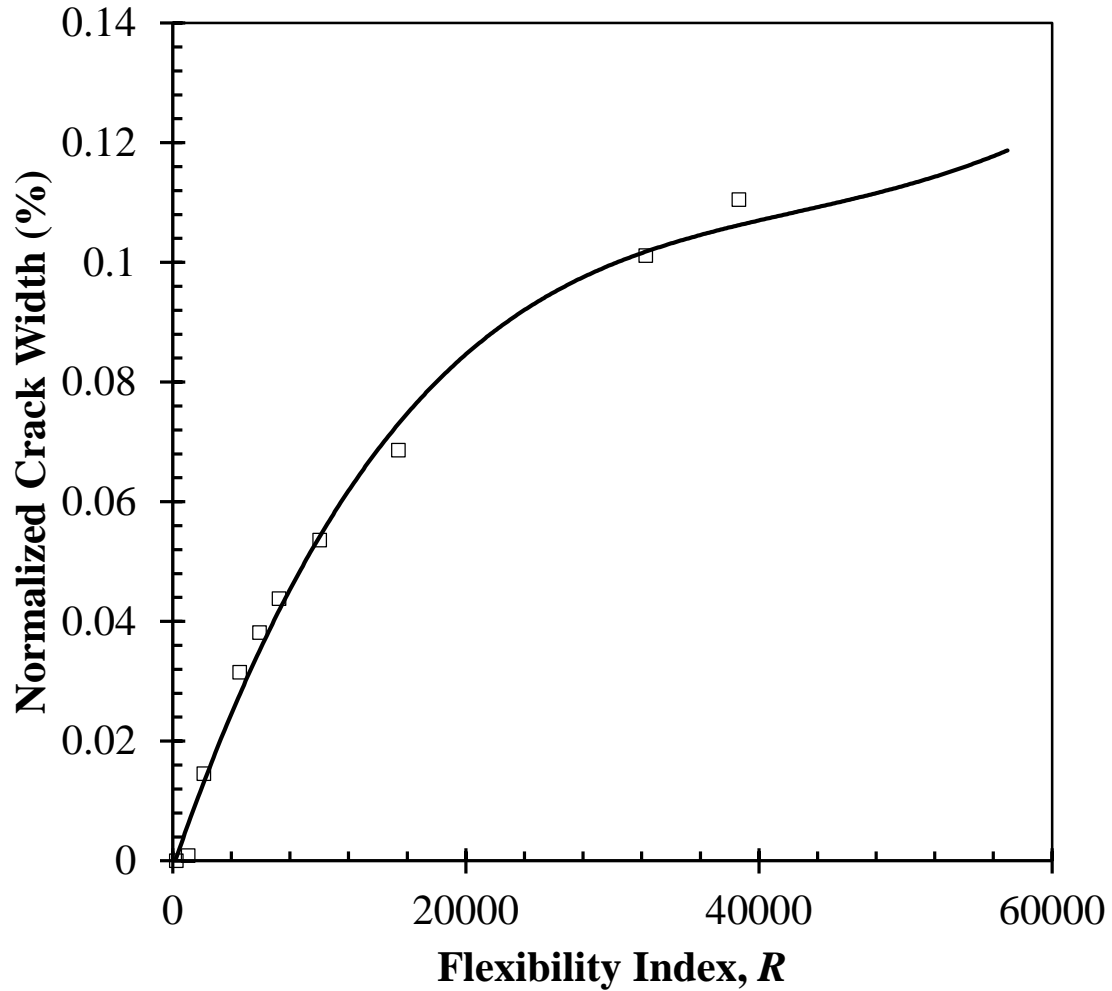
Figure 3.8 Normalized crack width versus flexibility index.

Alternatively, one may use a curve fitted DR-Hill-Zerobackground equation to obtain

normalized crack width from flexibility index and given by:

$$\frac{\Delta l_c}{L}(\%) = \frac{\theta R^{\eta}}{\kappa^{\eta} + R^{\eta}} \tag{3-7}$$

where θ, η, and κ are constants of the curve fit model and are equal to 1.3661×10^{-1},

1.2345, and 1.3718×10^{4} respectively. The importance of Figure 3.6 or Equation (3-7) is

that it will be used to recalculate the crack width that would be expected once a design

72

section is chosen. This would be demonstrated in the outline of the design process later in this chapter.

 3.2.4 Element 3 (Maximum Horizontal Displacement)

The relationship between Element 3, ($\delta_{H(\max)}$), and Element 2 ($\delta_{V(\max)}$) was established based on the relationship between the two as published in literature. Past case history data studies by researchers (Mana and Clough 1981; Ou et al., 1993; Hsieh and Ou, 1998) have shown that the maximum ground surface settlement, $\delta_{V(\max)}$, is between one half (0.5) to one (1) of the maximum wall deflection, $\delta_{H(\max)}$. Table 3.5 is an expansion of the case histories as presented by Bryson and Zapata-Medina (2012).

Table 3.5 Case history data for ground movement (after Bryson and Zapata-Medina, 2012).

Soil Type	Case	Reference	Wall Type	H [m]	He [m]	s_u [kPa]	$\delta_{H(max)}$ [mm]	$\delta_{V(max)}$ [mm]	$\delta_{H(max)}$/H [%]	$\delta_{V(max)}$/He [%]	FS_{bh}
Stiff Clay	St1	Ng (1992)	Diaph.	16.3	9.6	120	17.66	10.13	0.108	0.106	3.73
	St2	Burland and Hancock (1977)	Diaph.	30.0	18.5	190	30.00	20.00	0.100	0.108	4.46
	St3	Hsieh and Ou (1998)	Diaph.	33.0	20.0	76.5	124.76	77.76	0.378	0.389	1.24
	St4	Poh et al. (1997)	Diaph.	14.0	11.1	80	10.02	NA	0.072		2.05
	St5	Ou and Shiau (1998)	Diaph.	23.0	11.8	105	44.53	NA	0.194		3.11
	St6	Whittle et al. (1993)	Diaph.	25.6	20.2	91	53.61	45.00	0.209	0.223	1.32
	St8	Liao and Hsieh (2002)	Diaph.	27.0	15.7	77.5	81.37	NA	0.301		1.38
	St9	Becker and Haley (1990)	Diaph.	26.0	20.0	70	47.26	101.60	0.182		1.21
	St10	Ulrich (1989)	Secant	20.0	12.2	140	14.75	NA	0.074		3.62
Medium Clay	M1	Ou et al. (1998)	Diaph.	35.0	19.7	50	106.51	77.18	0.304	0.392	0.96
	M3	Finno and Roboski (2005)	Sheet	17.4	12.8	43	63.50	63.00	0.365	0.492	1.05
	M4	Hsieh and Ou (1998)	Diaph.	31.0	18.4	47.5	62.61	43.16	0.202	0.235	0.97
	M5	Miyoshi (1977)	Steel-Conc.	32.0	17.0	42	176.56	152.42	0.552	0.897	0.99
	M6	Finno et al. (1989)	Sheet	19.2	12.2	30	172.64	255.70	0.899	2.096	1.10
	M7	NGI (1962a)	Sheet	14.0	11.0	26	220.00	240.00	1.571	2.182	0.93
	M8	NGI (1962b)	Sheet	16.0	12.0	34	125.00	114.00	0.781	0.950	0.94
	M9	Clough and Buchignani (1981)	Diaph.	30.5	21.3	44	28.25	NA	0.093		0.98
	M10	Wang et al. (2005)	Diaph.	38.0	20.6	35	48.12	30.90	0.127	0.150	0.85
	M11	Peck (1969)	Sheet	14.0	8.5	27.5	228.87	210.00	1.635	2.471	1.35
Soft Clay	So1	Finno et al. (2002)	Secant	18.3	12.2	20	38.13	27.43	0.208	0.225	0.59
	So2	Goh et al. (2003)	Diaph.	31.0	16.0	10	38.55	NA	0.124		0.31
	So3	Hu et al. (2003)	Diaph.	21.0	11.5	22	15.39	7.00	0.073	0.061	0.73
	So4	Gill and Lukas (1990)	Sheet	16.8	7.0	22.7	83.27	NA	0.496		1.93
	So5	Teparaksa (1993)	Sheet	18.0	8.0	13.5	123.65	NA	0.687		0.62
	So6	Baker et al. (1987)	Diaph.	18.3	8.5	21.5	37.39	37.00	0.204	0.435	0.93
	So7	Konstantakos (2000)	Diaph.	13.7	10.3	45	3.63	NA	0.026		1.25
	So8	Clough and Buchignani (1981)	Soldier	30.5	11.0	25	107.06	NA	0.351		1.69
	So9	Kort (2002)	Sheet	19.0	8.0	20	385.38	NA	2.028		1.63
	So10	Koutsoftas et al. (2000)	Soldier	41.0	13.1	25	48.10	30.20	0.117	0.231	1.42
	So11	Clough and Denby (1977)	Diaph.	32	11	25	101.6	53.34	0.3175	0.485	1.8

In this research, the data presented by Bryson and Zapata-Medina (2012), as shown in Figure 2.7, was expanded to include more case history data. Secondly, the maximum vertical settlement was normalized with the depth of excavation while the maximum horizontal ground movement was normalized with the height of excavation support wall. This is supported by the findings of Bryson and Zapata-Medina (2007), where $\delta_{V(\max)}$ was more influenced by soil behavior and $\delta_{H(\max)}$ by the physical characteristics of the support wall. The corresponding plot is shown in Figure 3.9.
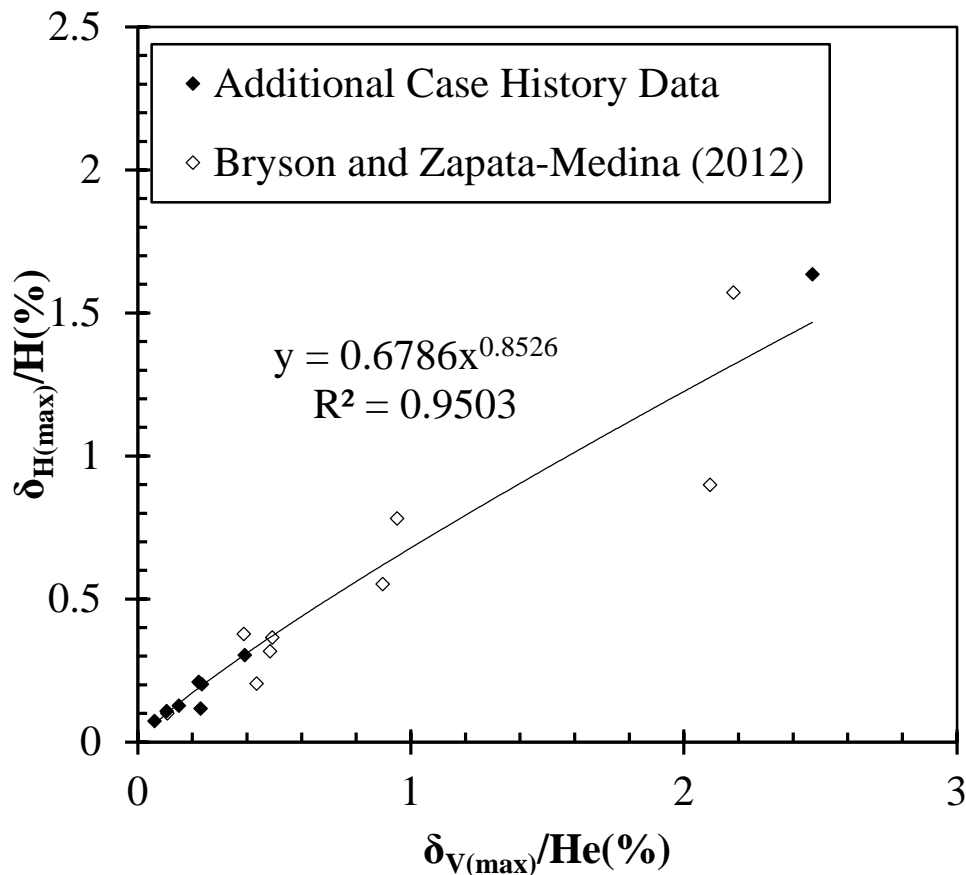
Figure 3.7- Case history data plot of normalized $\delta_{H(\max)}$ vs $\delta_{V(\max)}$

The relationship in Figure 3.9 was used as the basis for predicting maximum horizontal

75

movements. It was deemed conservative to use Figure 3.9 instead of Figure 2.8 or Equation (2-5) because the latter has not been adapted to predict excavation induced vertical deformations (Bryson and Zapata-Medina, 2012). The corresponding equation is given by:

$$\left(\frac{\delta_{H(\max)}}{H}\right)(\%) = D\left[\left(\frac{\delta_{V(\max)}}{H_e}\right)(\%)\right]^{E} \tag{3-8}$$

where $D = 0.6492$; and $E = 0.8381$

Therefore, Equation (3-8) allows Element 3 to be obtained from Element 2. This completes the determination of all the elements on Figure 3.1.

3.3   Rigidity Deficit of Excavation Support System

Up to this point, the discussion has been about predicting and relating ground deformations to the deformation criteria (i.e. diagonal crack with). The question still remains how to relate a given trial section to the excavation support system flexibility index. This would be achieved through the use of the rigidity deficit, R_{def}. This parameter gives an indication of the magnitude of moment of inertia required to meet a given deformation criteria. This quantity is also proportional to the flexibility index. Thus, the higher the deficit, the higher the expected deformation within the infill wall of an adjacent building and vice versa.

In designing an excavation support system, considerations for both the vertical and horizontal strut spacing must be as pragmatic as possible. This is to say that even though it may be theoretically achievable to design a support system that allows no cracks in an infill wall, it may not be practicable. From Figure 3.7, a support system that

allows no cracks implies a flexibility index of zero (i.e. $I \to \infty$ or $s_v = s_h = 0$). It is immediately clear that such a situation is very unlikely to occur.

As a guidance, Das (2011) provides that for braced excavations, both vertical and horizontal struts spacing typically have a minimum value of about $2.75m$. Boone et al. (1998) also suggested that the general vertical strut spacing for braced excavations is usually between $2.4m$ to $5.8m$. Nonetheless, it is up to the designer to make appropriate considerations (such as to accommodate excavation equipment) when choosing the spacing.

3.3.1 Development of Rigidity Deficit

From the above discussion and guidance given on the values of s_h and s_v, an expression was developed to predict the rigidity deficit given; soil parameters; excavation geometry; flexibility index obtained from Figure 3.7; and excavation support material properties. Re-arranging the terms in Equation (2-2) yields the rigidity deficit as:

$$R_{def} = \left(\frac{s_h}{s_v \cdot I} \right) = \left[\left(\frac{1}{s_v^2} \right) \cdot R \cdot \frac{E}{E_s} \cdot \frac{s_u}{\gamma_s \cdot H \cdot H_e} \right] \qquad (3\text{-}9)$$

where all the parameters have been defined previously. Using the values on Table 3.1 and varying the values of the flexibility index at a constant vertical strut spacing, rigidity deficit values were generated (see Appendix E). Figure 3.10 shows the plot of R_{def} versus R. It can be observed from the plot that the trend of R_{def} is defined based on the value of s_V. A line was fit to the plots and the corresponding equations are shown on the various lines. A straight line of the form shown below describes the relationship.

77

$$R_{def} = m \cdot R \tag{3-10}$$

where m is the slope of the straight line. The values of m at various vertical strut spacing, s_v, are shown on Table 3.6.

Table 3.6 Summary of slopes of straight line by vertical strut spacing.

s_v (m)	m
0.5	447.67
1	111.92
2	27.98
3	12.435
4	6.9949
5	4.4767
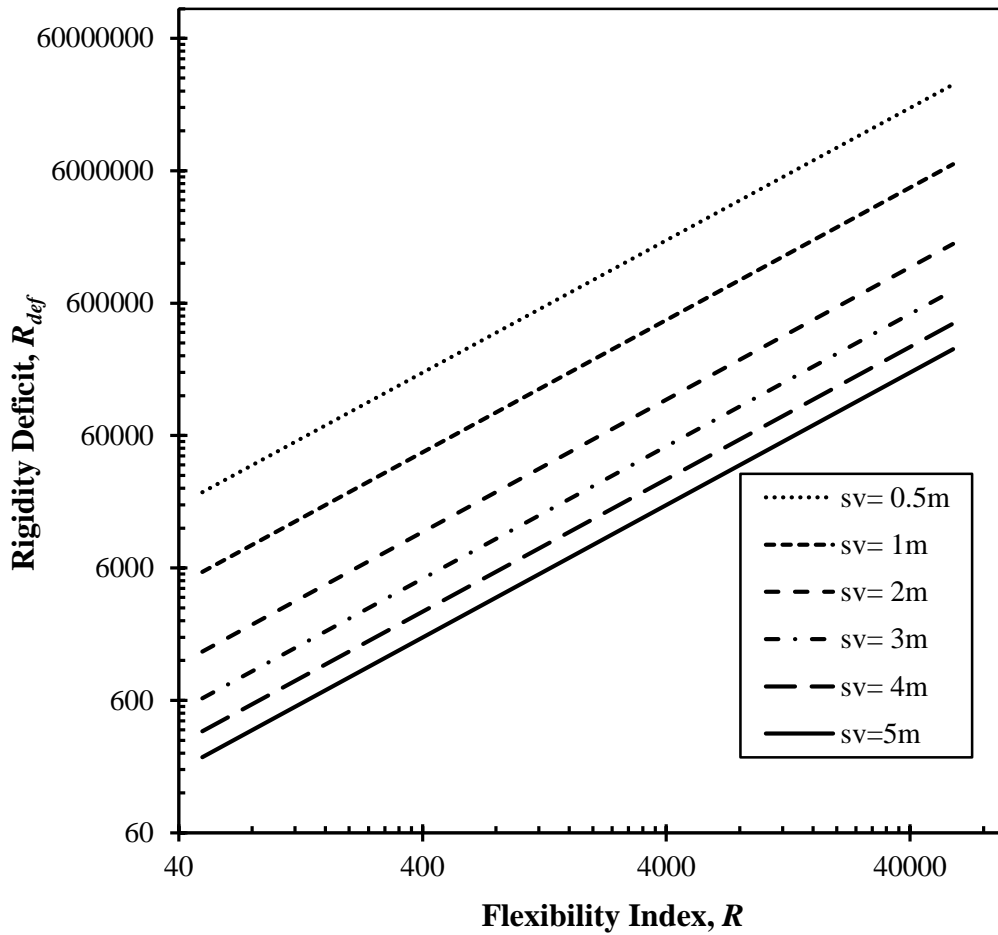
Figure 3.10 Rigidity deficit versus flexibility index.

From the observed trend, an expression can be developed that allows the explicit input of s_V. To do this, the slopes as shown on Table 3.6 are plotted against the vertical strut spacing and then a trend line is fitted through the data. Figure 3.11 shows the plot of slope versus vertical strut spacing.

The plot shows Slope, m on the y-axis (logarithmic scale from 1 to 1000) versus Vertical Strut Spacing (m) on the x-axis (0 to 6). The fitted trend line is labeled $y = 111.92x^{-2}$.
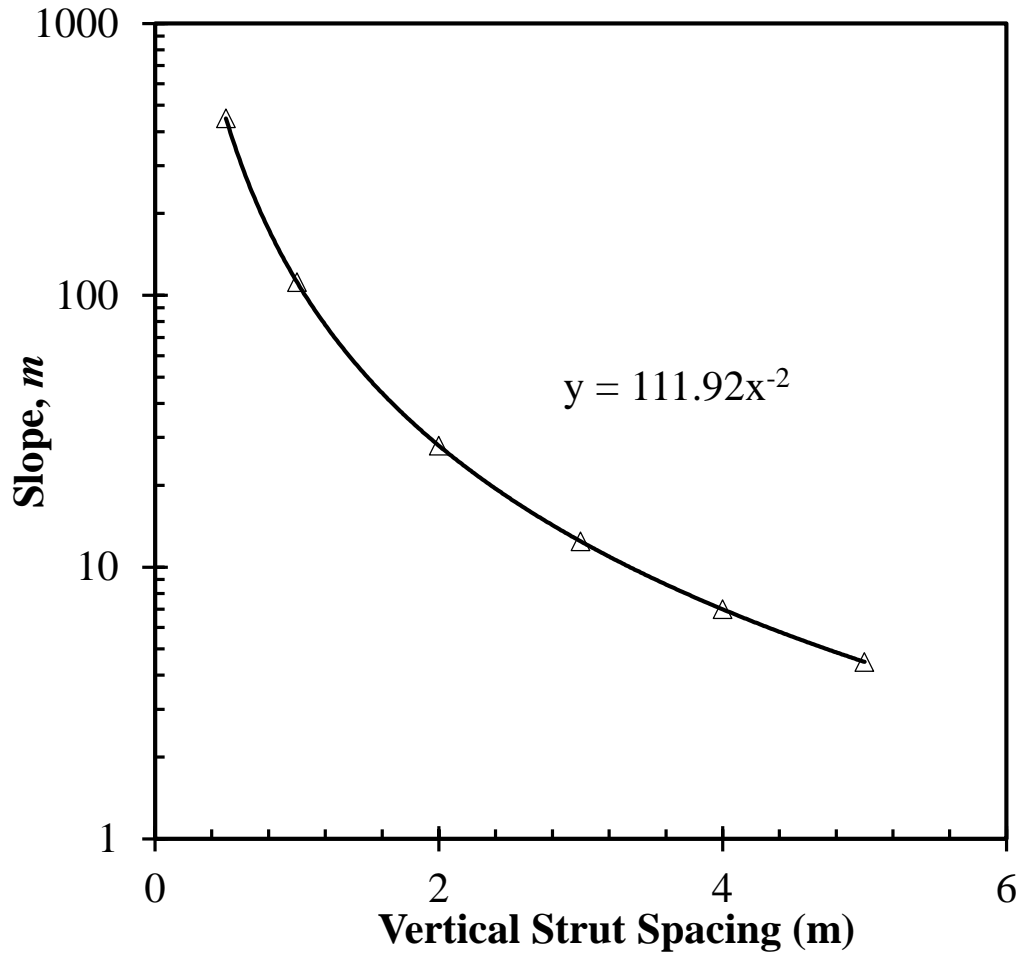
Figure 3.11 Slope versus vertical strut spacing.

From Figure 3.11, the resulting relationship is given by:

$$R_{def} = 111.92 \frac{R}{s_v^2} \tag{3-11}$$

79

It can be observed that slope decreases with increasing vertical strut spacing. This can be explained using Figure 3.8. Observe from Figure 3.8 that for a given flexibility index, the rigidity deficit increases with decreasing vertical strut spacing. Remembering that flexibility index is a dimensionless parameter, a higher vertical strut spacing implies a greater magnitude in acceptable crack width (i.e. a higher flexibility index). Hence, little rigidity would be required be required. Conversely, a low vertical strut spacing implies little acceptable crack width (i.e. design requires a very rigid system), Therefore, a higher rigidity deficit would be required to meet such criterion.

From a dimensional analysis point of view, the slope can be viewed as the ratio of rigidity deficit to flexibility index. All things being equal, a higher vertical strut spacing implies a higher flexibility index (i.e. flexible system). Therefore, the lesser the moment of inertia of the support wall required. A small vertical spacing implies a lower flexibility index (i.e. a rigid support system). Hence, a high moment of inertia of the support wall would be required.

3.3.2 Obtaining a Section from Rigidity Deficit

At this stage the only item left to be determined is a section that will meet the flexibility index requirements. To summarize, the following are known thus far; flexibility index; flexibility deficit; soil properties; factor of safety against basal heave; depth of embedment; excavation geometry; infill wall properties and geometry; excavation support wall material properties; and both horizontal and vertical strut spacing. Inspecting Equation (3-9), one can easily derive an expression for the required moments of inertia of the excavation support system as:

80

$$I_{rqd} = \left(\frac{s_h}{s_v \cdot R_{def}} \right) \qquad\qquad (3\text{-}12)$$

Therefore, the engineer or designer just has to choose a section with a moments of inertia greater than or equal to required moments of inertia of the excavation support system we wish to design. Once a section is chosen, standard methods (such as the one described in Fang, 1990) will be used in sizing the struts and wales. This approach will be illustrated later in this section.

3.4   Preliminary Costing Chart

One of the objectives presented in Chapter 1 was to develop a preliminary cost chart. This a seminal contribution in pushing the frontiers of excavation support systems design by incorporating cost tabs in the design process. As earlier stated, not much, if any, exists in current literature regarding this approach. Hence this study will greatly add to existing knowledge base.

To achieve this, construction cost data and other economic parameters would be heavily relied upon. All of the information are outside the direct control of this thesis and therefore a parsimonious approach will be warranted. Based on bare costs from RSMeans Building Construction Cost Data 2014 for sheet piles, a simplified assumption that cost increases with increasing unit weight of excavation support wall was made. This assumption is supported by the data in Table 3.8 (RSMeans, 2014). It should be noted that the term "Preliminary Cost" refers solely to the sum of material and installation costs (sometimes referred to as total cost). Due to the complicated nature of project bill of quantities, it is nearly impossible to come up with a cost index that caters for every

81

specific project. Therefore, the preliminary cost chart is only to be used as a starting point.

Table 3.7 RSMeans bare costs for 2014 for three sheet pile systems based on excavation depth and unit weight.

System	Unit	Daily output	Labor hrs	Material	Labor	Equipment	Total per sf
25' Excavation, 38psf left in place	sf	1000	0.064	31.5	2.94	3.82	38.26
Drive, extract & salvage	sf	553	0.116	10.05	5.3	6.9	22.25
20' Excavation, 27psf left in place	sf	960	0.067	21.5	3.07	3.98	28.55
Drive, extract & salvage	sf	485	0.132	7.35	6.05	7.85	21.25
15' Excavation, 22 psf left in place	sf	983	0.065	16.95	3	3.89	23.84
Drive, extract & salvage	sf	545	0.117	5.65	5.4	7	18.05

The table header "2014 Bare Costs" spans the columns Material, Labor, Equipment, Total per sf.

The linearity relationship is shown in Figure 3.12

Next step was to normalize the total cost by the GDP estimated using purchasing power parity (PPP) for the U.S. The value of $17,418.9 in billions for the year 2014 is provided by the International Monetary Fund, 2014. This value is corroborated by similar value from the U.S Department of Commerce Bureau of Economic Analysis, 2014.

The purpose of the normalization to GDP (PPP) is not only to tie the preliminary cost to an economic index but, also to make the cost dimensionless. This allows an analysis of preliminary cost in the broader context of the value of all final goods and

82

services produced within the U.S within the fiscal year of 2014. A detailed economic analysis was beyond the scope of this thesis.
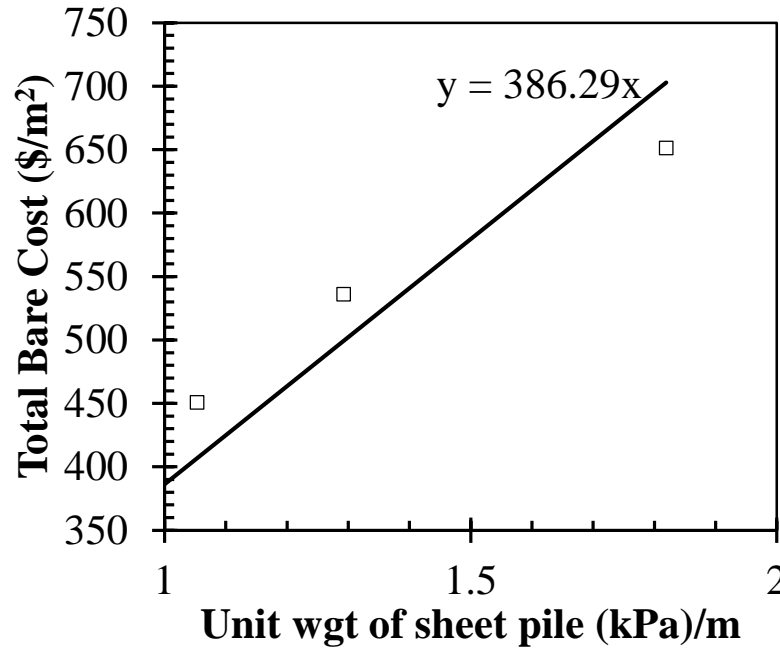
Figure 3.12 Total bare costs vs unit weight of sheet pile.

The data provided by RSMeans is only limited to three unit weights (i.e. 22 psf, 27 psf, and 38 psf per unit length of sheet pile). As can be seen from Figure 3.10, the total cost increases with increasing unit weight. Following through with the assumption of proportionality, a second order polynomial was used to fit the data points. This was achieved by optimizing the constants of the polynomial using the "Solver" function in Excel. The output of the Solver was a straight line graph. Once an expression between the unit weight of the sheet pile and the normalized cost was obtained, it was possible to predict normalized cost values of any section given the unit weight. Table 3.8 is a side-by-side comparison of bare cost values and optimized predicted values.

83

Table 3.8 RSMeans 2014 bare cost vs predicted cost.

Unit wgt (lb/sf)	Unit wgt (kPa)	Total cost/m^2	Normalized bare cost/m^2	Predicted normalized cost /m^2
0	0.00	0.00	0.000	0.000
22	1.05	450.90	0.026	0.026
27	1.29	536.04	0.031	0.032
38	1.82	651.32	0.037	0.044

It can be seen from Table 3.8 that the predicted values are very close to the actual
RSMeans cost data values. The resulting plot between normalized total bare cost and unit
weight is shown in Figure 3.13.
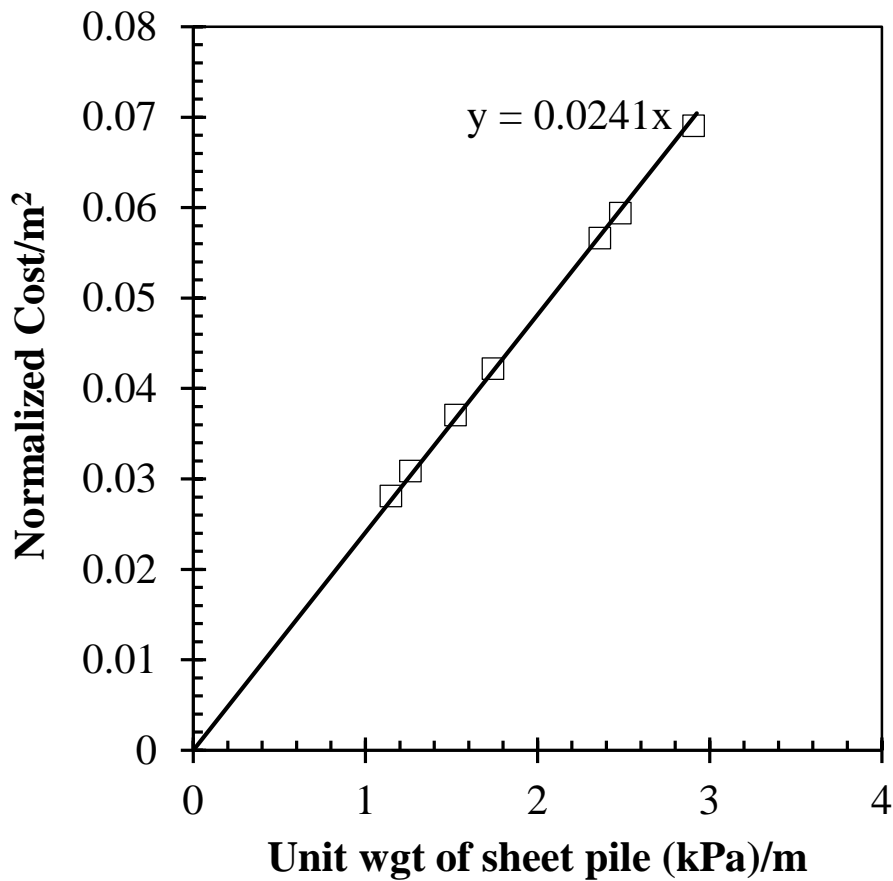
Figure 3.13 Preliminary Cost Chart.

The corresponding linear equation to predict normalized cost is given by:

$$NC = m\omega \tag{3-13}$$

where NC is normalized cost per square meter; ω is unit weight of sheet pile in psf; and the slope, m, is equal to 0.0241.

Figure 3.13 provides a very useful tool for preliminary cost assessment. It is observed that there are some discrepancies in the correlation between moments of inertia and the unit weight of sheet pile.

For instance section A12-770 has $I = 21430\,cm^4/m$ and $\omega = 19.31\,psf\,(0.92kPa)$ while AZ 12 has $I = 18140\,cm^4/m$ and $\omega = 20.22\,psf\,(0.97kPa)$, it can be seen that this is contrary to the general trend of direct proportionality between the two. Hence, if cost is of prime concern then Figure 3.13 indicates to the engineer/designer to explore other sections that will fulfil the same relative flexibility requirement but cheaper.

3.5   Inverse Method for Designing Excavation Support Systems

The procedure that is proposed in this subsection allows the designer to choose the various sections for the components (i.e. wall, struts, and wales) of the excavation support system at an acceptable deformation to adjacent buildings, and will meet both limits equilibrium and preliminary cost requirements. The following steps will be necessary to the achievement of the above stated goals:

1. *Define acceptable crack width in adjacent building, Δl_c*: this is done using the deformation criteria proposed by Burland et.al, (1977) (Table 2.4)

85

2. *Define infill wall dimension and calculate the normalized crack width*: Define the dimensions of the wall anticipated to be affected by the deep excavation (L is length of wall; H is height of wall). Using the chosen crack width and the affected wall dimension, calculate the normalized crack width, given by the ratio $\Delta l_c / L_{wall}$ in percentage.

3. *Calculate the Flexibility Index, R*: calculate the value of the flexibility index, that value is related to the normalized crack width by reading the flexibility index from Figure 3.7. Alternatively, one may use Equation (3-4).

4. *Choose a trial horizontal and vertical strut spacing*: as a guidance Das (2011) suggest that both horizontal, s_h and vertical strut spacing, s_v, are about 2.75m for braced excavations. Boone et al. (1998) also suggests s_v values are generally between 2.4 to 5.8m. In reality, it up to the designer to give due considerations for the size of the construction equipment and processes that may control both horizontal, s_h, and s_v.

5. *Calculate the flexibility deficit, R$_{def}$:* the flexibility deficit is a measure of the required stiffness of the system based on the acceptable crack width criteria chosen in *Step 1*. The value is determined using Equation (3-11).

6. *Calculate required moments of inertia of support wall, I_{rqd}*: use Equation (3-12) to calculate the required moments of inertia of the excavation support wall that will achieve the system flexibility index.

7. *Size wall*: choose a design sheet pile section such that the moment of inertia of sheet pile, I_{des}, is greater or equal to required moments of inertia, I_{rqd} (i.e.

86

$I_{rqd} \leq I_{des}$). In case of reinforced concrete, the Young's modulus of elasticity can be taken to be 27.6 GPa for design purposes. The I_{rqd} per meter length of wall is purely a function of the thickness of the wall, t, and given by:

$$I_{rqd} = \frac{t^3}{12} \left(m^4 \right)$$ (3-14)

8. *Preliminary cost check*: evaluate a preliminary cost of project based on the unit weight of the steel sheet pile section using Equation (3-13) or Figure 3.13. The importance of this check is that it offers the designer an opportunity to explore further options that may be cheaper, yet provide the same strength requirements as the initial trial section. On the other hand, if cost is the driving factor then the designer is obliged to reduce cost by choosing a design support system that trades rigidity for cheaper cost. This is achieved through increasing the s_h / s_v ratio. This will increase the rigidity deficit which will subsequently reduce the I_{rqd} and eventually reduce the preliminary cost.

9. *Re-calculate system flexibility deficit using the chosen section*: use I_{des} from step 7 to calculate the new rigidity deficit by making R_{def} the subject of Equation (3-12) so that:

$$R_{defdes} = \left(\frac{s_h}{s_v \cdot I_{des}} \right)$$ (3-15)

10. *Re-calculate the flexibility index using R_{defdes}*: make R the subject of Equation (3-11) and calculate its new value based on the new rigidity deficit as:

87

$$R_{des} = \left(\frac{R_{defdes}}{111.92} \right) \cdot s_v^2 \tag{3-16}$$

11. *Calculate anticipated crack width using R_{des}*: based on the new flexibility index, use Equation (3-7) to calculate the normalized crack width and subsequently the crack width. The crack width should be less than that chosen in *Step 1*, otherwise a bigger section is warranted.

12. *Predict the ground movements*: use Figure 3.6 or Equation (3-3) to determine the angular distortion that will be generated from the modified support system. Next, use Equation (3-6) to determine $\delta_{V(\max)}$. Finally, use Figure 3.9 or Equation (3-8) to determine $\delta_{H(\max)}$.

13. *Determine number of strut levels*: the number depends on the depth of the excavation and the average vertical strut spacing (with guidance given earlier in the chapter and in S*tep 4*). Furthermore, consideration should be given to the depth of the first strut. This depth should not be more than the depth of tensile crack given by:

$$z_c = \frac{2s_u}{\gamma_s} \tag{3-17}$$

14. *Determine the maximum moments in the wall*: using the elastic section modulus, S_{des}, of the design section, we can calculate the maximum bending moments in the wall using ANSI/AISC 360-10. Assuming a minimum yield stress of F_y, (and for this research using A36 steel, $F_y = 248.3 MPa$), the maximum moments is given by:

88

$$M_{\max} = S_{des} \cdot F_y \qquad (3\text{-}18)$$

Figure 3.14 illustrates the moment distribution.

Wall Moment Diagram
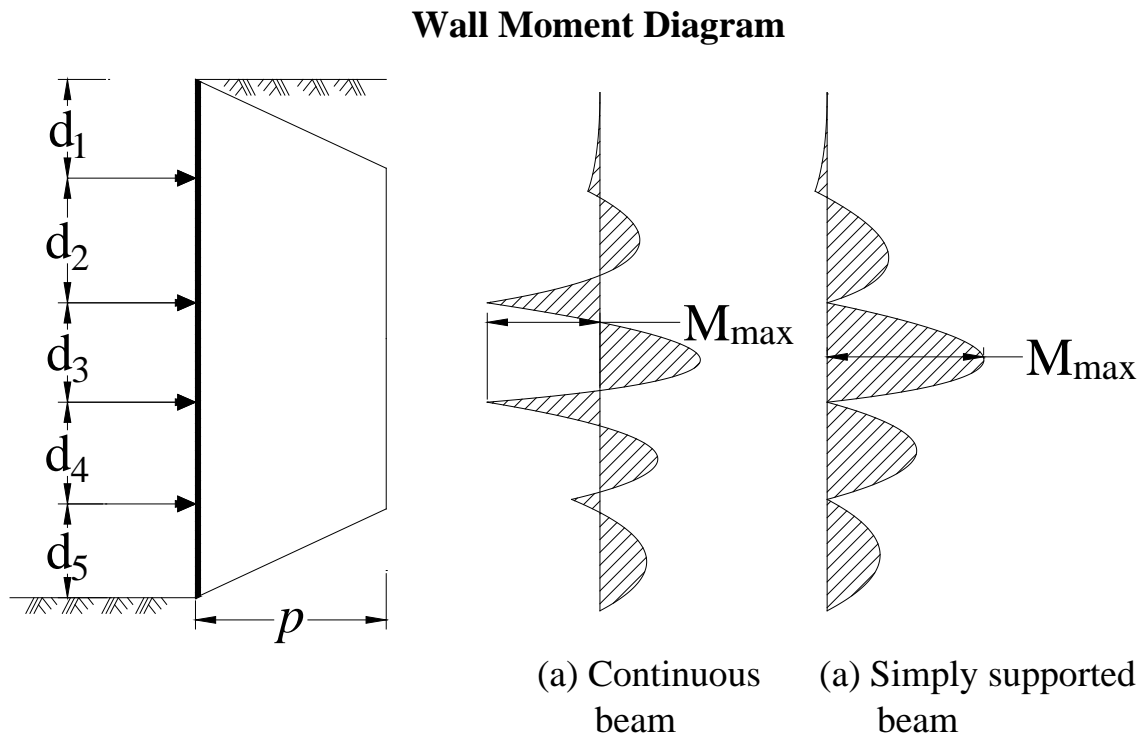
Figure 3.14 Wall moment distribution (after Fang, 1991).

15. Calculate the uniform loading: from Figure 3.14, the uniform loading that will produce the maximum bending moments in the wall is given by the expression:

$$p = \frac{8M_{\max}}{s_v^2} \qquad \text{for simple spans} \qquad (3\text{-}19)$$

$$p = \frac{10M_{\max}}{s_v^2} \qquad \text{for three (3) or more spans} \qquad (3\text{-}20)$$

89

For this research, a span refers to the distance between any two struts. It should be noted that continuous spans refer to arrangements with 3 or more spans and this approach assumes an average uniform loading along the excavation support wall.

16. *Calculate required wale section modulus, S_{rqd} ,:* the uniform load distribution and actual load distribution is illustrated in Figure 3.15. The uniform load distribution is used in the calculation of the moment induced in the wales.

(a)   **(b)**
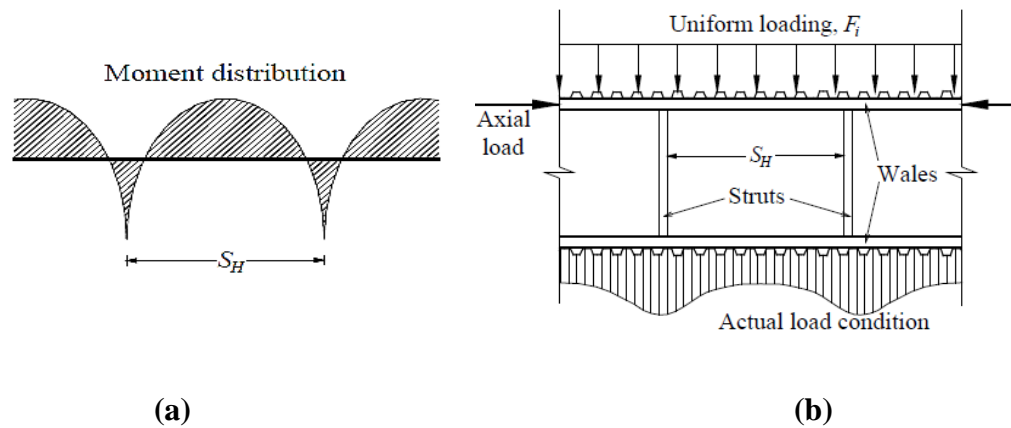
Figure 3.15 Calculation of wale section modulus (a) moment distribution resulting from uniform loading (b) deep excavation as seen in plan (Fang, 1991).

The moment in the wale is given by:

$$M_{wale} = \frac{ps_h^2}{10} \text{ for three (3) spans} \tag{3-21}$$

$$M_{wale} = \frac{ps_h^2}{12} \text{ for continuous spans} \tag{3-22}$$

Equation (3-21) is used when there four struts running longitudinally along the excavation (i.e. four horizontal struts with three spacing between them). Equation (3.22)

is used when there are more than four horizontally spaced struts running longitudinally to the excavation.

Thus, the resulting required section modulus of the wale is given by:

$$S_{rqd} = \frac{M_{wale}}{F_y} \qquad (3\text{-}23)$$

17. *Size the wale*: choose an H or W-section with section modulus, S_{des}, such that;

$$S_{rqd} \le S_{des} \qquad (3\text{-}24)$$

18. *Calculate strut loads:* using the uniform loading calculated in step 15 and the average vertical strut spacing of s_v, the design strut load is given by:

$$P_u = p \cdot s_v \qquad (3\text{-}25)$$

19. *Size strut*: using load and resistance factor design (LRFD) for steel hollow structural sections (HSS) as presented by the Manual of Steel Construction (AISC, 2001).

  i.   *Calculate required cross-sectional area of section given by:*

$$A_{rqd} = P_u / F_y \qquad (3\text{-}26)$$

  ii. *Size round HSS*: choose a circular HSS with gross cross-sectional area, A_g, such that: $A_g \ge A_{rqd}$

  iii. *Determine effective length factor, K*: assuming a hinge-hinge connection as end condition of strut, *K=1*. This is recommended by researchers (Fang, 1991; Ou, 2006).

91

iv. *Calculate design compressive strength*: Table 4-7 of AISC (2001) provide the following steps for calculating the design compressive strength of the trial section:

a. *Design compressive strength* $= \phi_c P_n$ (3-27)

where ϕ_c the load resistance factor is equal to 0.85, and P_n is the nominal axial strength of the circular HSS and given by the expression:

$$P_n = F_{cr} A_g \tag{3-28}$$

where F_{cr} is the critical stress for column buckling.

b. *Determine the critical column buckling stress,* F_{cr} : this is computed from the following equations:

if $\lambda_c \sqrt{Q} \le 1.5$, *then* $F_{cr} = Q\left(0.658^{Q\lambda_c^2}\right)F_y$ (3-29)

else $F_{cr} = \left[\dfrac{0.877}{\lambda_c^2}\right]F_y$ (3-30)

where λ_c is the column slenderness and given by the expression:

$$\lambda_c = \frac{Kl}{r\pi}\sqrt{\frac{F_y}{E}} \tag{3-31}$$

r is the radius of gyration, *l* is the unsupported length of member, *E* is the elasticity modulus of the material and *Q* is the effective area factor.

c. *Determine effective area factor*:

if $\lambda \le 0.114E/F_y$, *then* $Q = 1$ (3-32)

else if $0.114E/F_y < \lambda < 0.448E/F_y$, *then* $Q = \dfrac{2}{3} + \dfrac{0.0379E}{F_y\left(D_{pipe}/t_{pipe}\right)}$ (3-33)

92

where λ is the wall slenderness ratio and equal to D_{pipe}/t_{pipe} (where D_{pipe} and t_{pipe} are the outside diameter and wall thickness of the circular HSS respectively).

d. *Check adequacy of section*: check that the design compressive strength is greater or equal to the ultimate axial load (i.e. $\phi_c P_n \geq P_u$).

The aforementioned steps leading to the design of an excavation support system which fulfills both limits equilibrium requirements and limited ground distortions, from induced deformation in adjacent building standpoint, is summarized in the following flowchart (Figure 3.16).
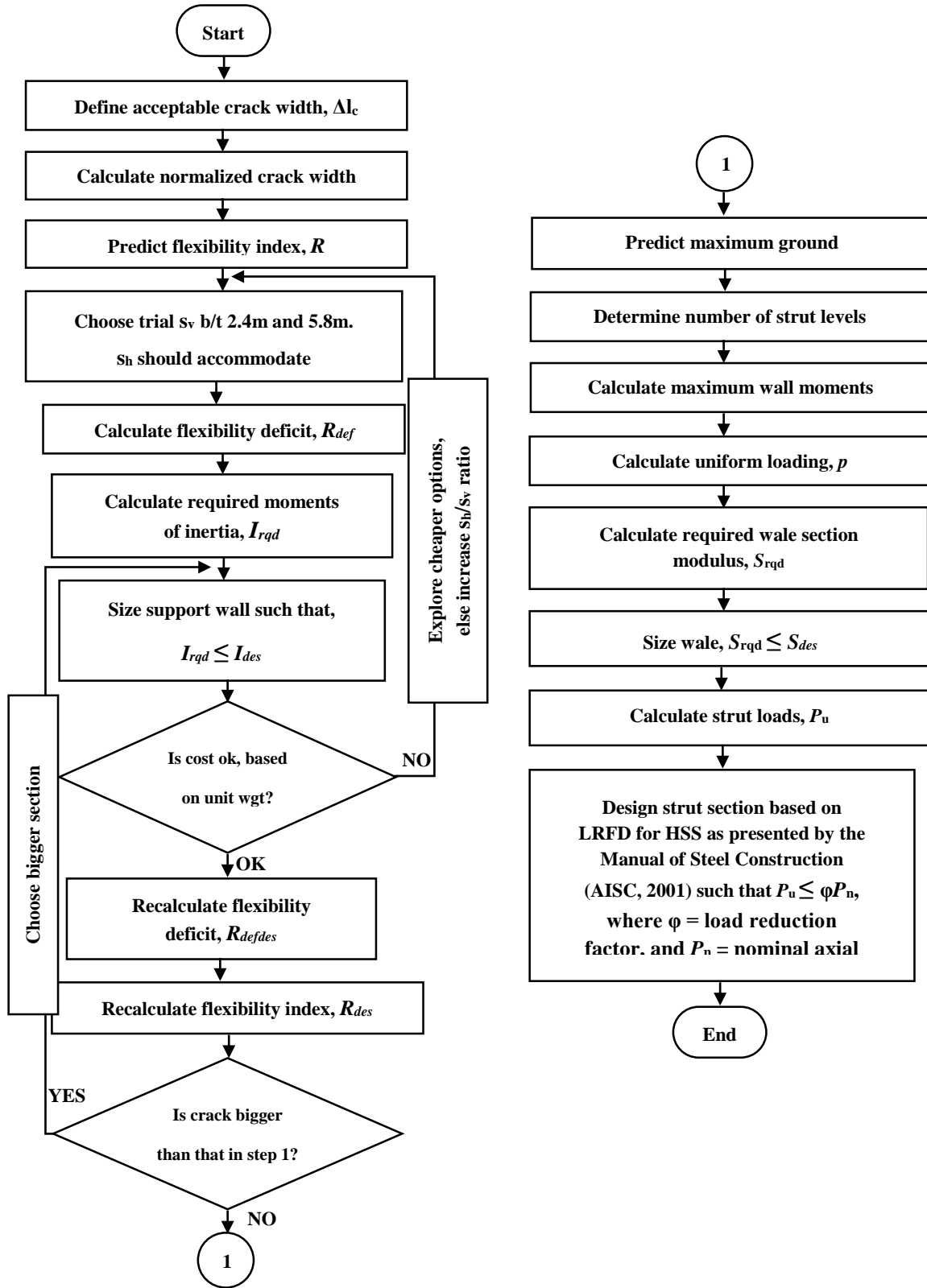
Figure 3.16 Inverse Method for Deep Excavation Support System Design.

3.5.1 Sample Design to limit cracking in adjacent wall to 1mm (Very Slight Damage)

This section will be used to demonstrate how to use the proposed approach to design an excavation support system that limits deformations in adjacent buildings caused by excavation-induced ground settlement.

3.5.1.1 Input Parameters

Excavation Geometry: Depth, H_e = 12.2 m, Width, B = 25 m, Length of excavation is very long (i.e. plane strain condition holds)

Soil Properties:

Use values on Table 3.1

Affected Adjacent Wall Properties

Length, *L = 12 m*, Height, *H=6 m*, *E/G=2.6*, Critical diagonal strain, $\varepsilon_{crit} = 0.00109$

Horizontal tensile strain, $\varepsilon_h = 0.0005$

3.2.1.2 Design Process

Step 1: Acceptable damage is very slight, $\Delta l_c \leq 1mm$

Step 2: Normalized crack width (%), $\dfrac{\Delta l_c}{L_{wall}} = \dfrac{1}{12 \times 10^3} \cdot 100 = 0.008$

Step 3: From Figure 3.7 or Equation (3-4), $R = 385.75$ *Step 4*: Using the guidance, let average vertical strut spacing, $s_v = 2.44m$. Assume excavation equipment to be used is Caterpillar 345CL Hydraulic with a width of 3.5m and allowing 1.5m maneuverability, the horizontal strut spacing, $s_h = 5m$.

95

Step 5: Flexibility deficit using Equation (3-11):

$$R_{def} = 7251.53$$

Step 6: Required moments of inertia of support wall using Equation (3-12):

$$I_{rqd} = 28258.61 \, cm^4/m$$

where $\dfrac{s_h}{s_v} = \dfrac{5}{2.44} = 2.05$

Step 7: Size wall

Assuming A36 steel, choose section SCZ 23 with the following properties:

$$I_{des} = 28900 \, cm^4/m, \quad \omega = 23.35 \, psf, \quad S_{des} = 1700 \, cm^3/m, \quad E = 200.1 \, kPa,$$

$$F_y = 248.3 \, kPa$$

Step 8: Preliminary cost check in $GDP(PPP)/m^2 - lb \cdot ft^2$

From Figure 3.13, $Cost_{pre\lim} = 0.027 \, GDP(PPP)/m^2$

It is assumed that cost is not controlling the design, thus cost is acceptable.

Step 9: Recalculate flexibility deficit

From Equation (3-25), the recalculated flexibility deficit, $R_{defdes} = 7090.59$. This is consistent with the approach because we have seen that the flexibility deficit is inversely proportional to the moments of inertia. Thus, an increase in moments of inertia warrants a decrease in the flexibility index and subsequently a decrease in the flexibility index (i.e. increase in rigidity).

96

Step 10: Calculate new value of flexibility index

Use Equation (3-16) to calculate new flexibility index. This will give $R_{des} = 377.18$. This is as expected because the design section is bigger than the required section, thus making the excavation support system stiffer.

Step 11: Calculate anticipated crack width

From Equation (3-7), $\frac{\Delta l_c}{L}(\%) = 0.0016$. Using a length of wall of *12 m*, $\Delta l_c = 0.19mm$.

This is acceptable since the value is less than that chosen in step 1.

Step 12: Predict ground movements

From Figure 3.6 or using Equation (3-3), angular distortion from the new support system will be $\beta = 1.352 \times 10^{-3}$. Using Equation (3-6), $\delta_{V(\max)} = 16.23mm$ and using Equation (3-8) will yield $\delta_{H(\max)} = 31.65mm$.

Step 13: Determine number of levels of struts

From Equation (3-17), depth of tensile crack $z_c = 4.64m$. To avoid excessive ground movement near the surface, the distance between consecutive struts will be as follows (i.e. from the surface down to bottom of excavation), $1m$, $3m$, $3m$, $3m$, and $2.2m$. Note that these lengths have not been optimized for effective moment distributions. The average of this arrangement is $2.44m$ for an $H_e = 12.2m$.

Step 14: Maximum Wall Moments

97

From Equation (3-18), $M_{max} = S_{des} \cdot F_y = 1700 \times 10^{-6} \times 248.3 \times 10^3 = 422 kN - m$

Step 15: Average uniform loading for more than three (3) spans:

From Equation (3-20), $p = \dfrac{10 M_{max}}{s_v^2} = \dfrac{10 \times 422}{2.44^2} = 709 \, kN/m^2$

Step 16: Required section modulus of wale

Wale moments for continuous span from Equation (3-22), $M_{wale} = 1477 \, kNm/m$ for continuous spans. Thus the resulting required section modulus of the wale is given by (Equation 3-28): $S_{rqd} = 5949 \, cm^3/m$.

Step 17: Size wale

Choose W30x132 section with $S_{des} = 6227 > S_{rqd} \Rightarrow ok$

Step 18: Ultimate strut load

From equation (3-25) and using average strut spacing, $P_u = 1730 kN/m$.

Step 19: LRFD Strut design (AISC, 2001)

    i.   Required cross-sectional area, $A_{rqd} = \dfrac{P_u}{F_y} = \dfrac{1730 \times 10^3}{248.3 \times 10^3} = 70 cm^2$

    ii.   Trial section, $CHS 193.7 \times 16.0$ with $A_g = 89.3 cm^2 > A_{rqd} \Rightarrow ok$. Other properties include $r_x = r_y = 6.31 cm$, $t_{pipe} = 16.0 mm$, $D_{pipe} = 193.7 mm$

    iii.   Effective length factor, *K=1*

        a. Design compressive strength:

98

b. $\phi_c = 0.85$

c. Wall slenderness ratio, $\lambda = \dfrac{D_{pipe}}{t_{pipe}} = \dfrac{193.7}{16} = 12.11$

$$\frac{0.114E}{F_y} = \frac{0.114 \times 200.1 \times 10^3}{248.3} = 91.87 \geq \lambda \Rightarrow Q = 1$$

d. Column critical buckling stress

$$\lambda_c = \frac{Kl}{r\pi}\sqrt{\frac{F_y}{E}} = \frac{1 \times 25 \times 10^2}{6.31 \cdot \pi}\sqrt{\frac{248.3}{200.1 \times 10^3}} = 0.044$$

$\lambda_c\sqrt{Q} = 0.044 \times \sqrt{1} = 0.044 < 1.5$, thus

$$F_{cr} = Q\left(0.658^{Q\lambda_c^2}\right)F_y = 1\left(0.658^{1 \times 0.044^2}\right) \times 248.3 \times 10^3 = 248095 \, kN/m^2$$

e. Design compressive strength

$$\phi_c P_n = 0.85 \times 247901 \times 89.3 \times 10^{-4} = 1883 kN > P_u \Rightarrow ok$$

99

CHAPTER 4

4.0   Sensitivity Analyses

4.1   Introduction

This chapter presents the sensitivity analyses of the analytical approaches and equations used in the previous chapter. The effects of varying parameters such as moments of inertia of excavation support wall, l; length-to-height ratio of infill wall, L/H; factor of safety against basal heave, FS_{bh} undrained shear strength of the soil, s_u; effect of frame structures; flexibility factor, η; was studied in order to further understand their roles in the proposed deformation based excavation support system design. Variations in both the vertical and horizontal strut spacing serve as the basis for generating excavation support system configurations. As a result, they were constantly varied throughout the sensitivity analyses. The parameter s_v was varied between 2.75m and 5.05m, while s_v/s_h was varied between 1 and 2.5.

4.2   Effect of Frame Structures

Boone (1996) noted that deformation in frame buildings was caused principally by differential settlement of the columns. The differential settlement was attributed to the high tensile resistance of frame structures. In fixed-end beams (such as in reinforced concrete frames), the deflected shape relative to settlement at one end will mimic an elongated $S-shape$ with an inflection point at the mid-span as can be seen in Figure 4.1(a). In addition, Boone (1996) noted that the deflection can be shown to be equal to $\Delta S/L$. However, the minimum radius of curvature will be half of that for a simple wall

100

modeled as a beam of equal length and equal differential settlement. Therefore, calculations using L/H ratio, radius of curvature, and central deflection must be based on the reduced length of $0.5L$.

(a)   **(b)**
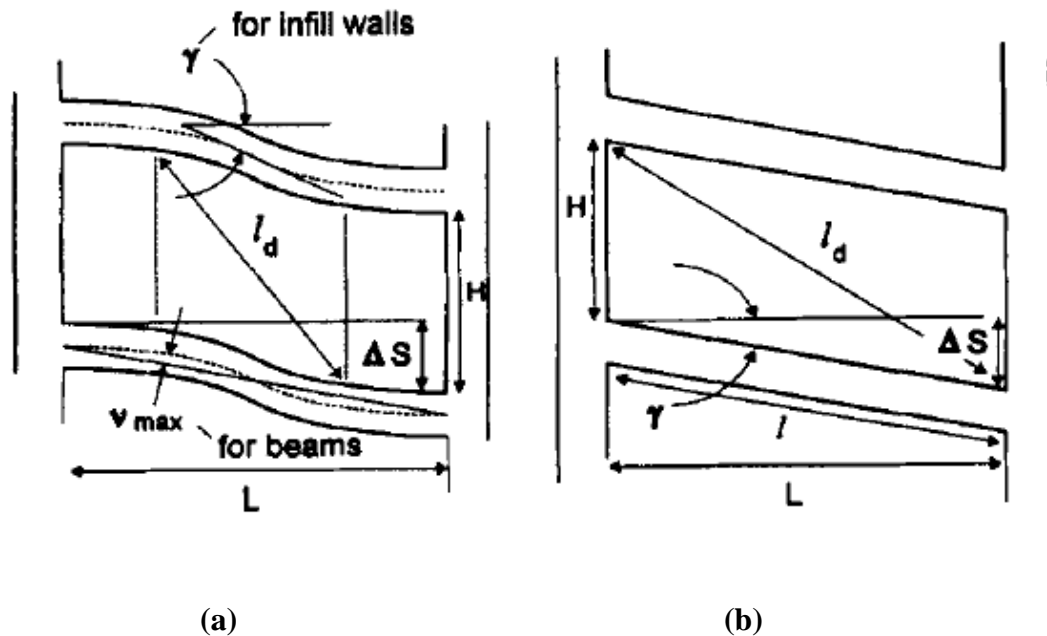
Figure 4.1 Geometry of beams and infill/panel walls (a) fixed-end beam frame; (b) simple beam frame (Boone, 1996).

The deformed shape, approximated as shown in Figure 4.1(a), is due to the fact that the walls framed by beams and columns are subjected to rotation and elongation at either end. These strains are resisted by adjacent columns and neighboring infill walls and the distortion will be governed by the nearly parallel deformation of the bounding beams. Since end rotation is restricted and the wall is forced to conform to the beam's shape, the wall itself will experience the greatest deformation between the wall quarter points with a maximum shear at the mid-span equal to $2\Delta S/L$ (i.e. without rigid body rotation), or

101

twice the angular distortion as defined by Skempton and MacDonald (1956). For simple beams and columns (i.e. steel beam and girder construction), a deformed shape resembling a rhombus, as shown in Figure 4.1(b), is likely. In which case Boone (1996) noted that the shear strain ($\tan \gamma = \Delta S/L$) will be the same as Skempton and MacDonald's definition of angular distortion (excluding rigid body rotation). In both cases, shear will be the likely predominant mode of strain deformation (Boone, 1996).

Based on the above background information, three cases (i.e. simple frame $L = 1$; hybrid of $L = 0.5$; and fixed-end $L = 0.5$) were investigated to see their effects on the diagonal crack with using Equation (2-20). Figure 4.2 shows the variance of normalized crack $(\Delta l_c/L)$ width with length-to-height ratio (L/H). The chart was created using an angular distortion of, $\beta = 0.002$; critical angular distortion, $\beta_{crit} = 0.001$; and flexibility factor, $\eta = 1$. The value of critical angular distortion is the value given by Meyerhof (1956) and corroborated by the findings of Finno and Bryson (2002). The value represents the angular distortion for onset of cracking in unreinforced load bearing walls.

It can be seen from the graphs that effect of end-condition of the frame structure is little to insignificant as the L/H ratio approaches zero. Hence, the normalized crack width (and crack width) is similar in all three cases. However, as the L/H increases beyond about 0.2, the normalized crack width is clearly distinguishable between the three cases. It is also clear from the graphs that fixed-end condition causes the maximum distortions in infill walls due to the rigidity in the connection between the walls and the bounding columns and beams. This results also agrees with the findings of Boone (1996).

102
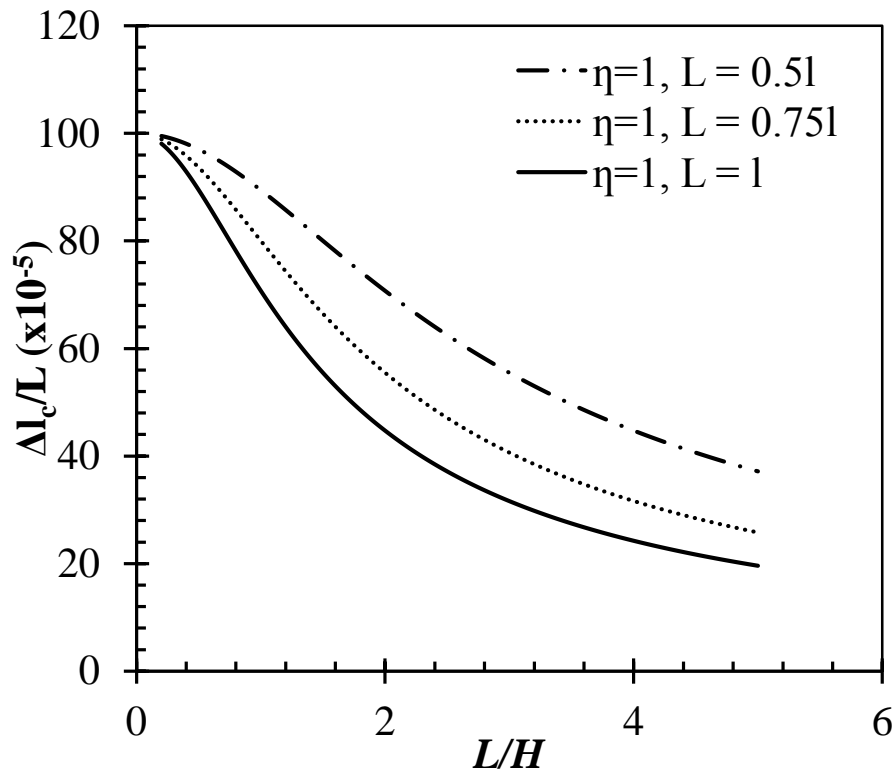
Figure 4.2 Effect of frame type on crack width.

The behavior of normalized crack width with frame types is similar when the flexibility factor is $\eta = 0.5$, as shown in Figure 4.3.

103
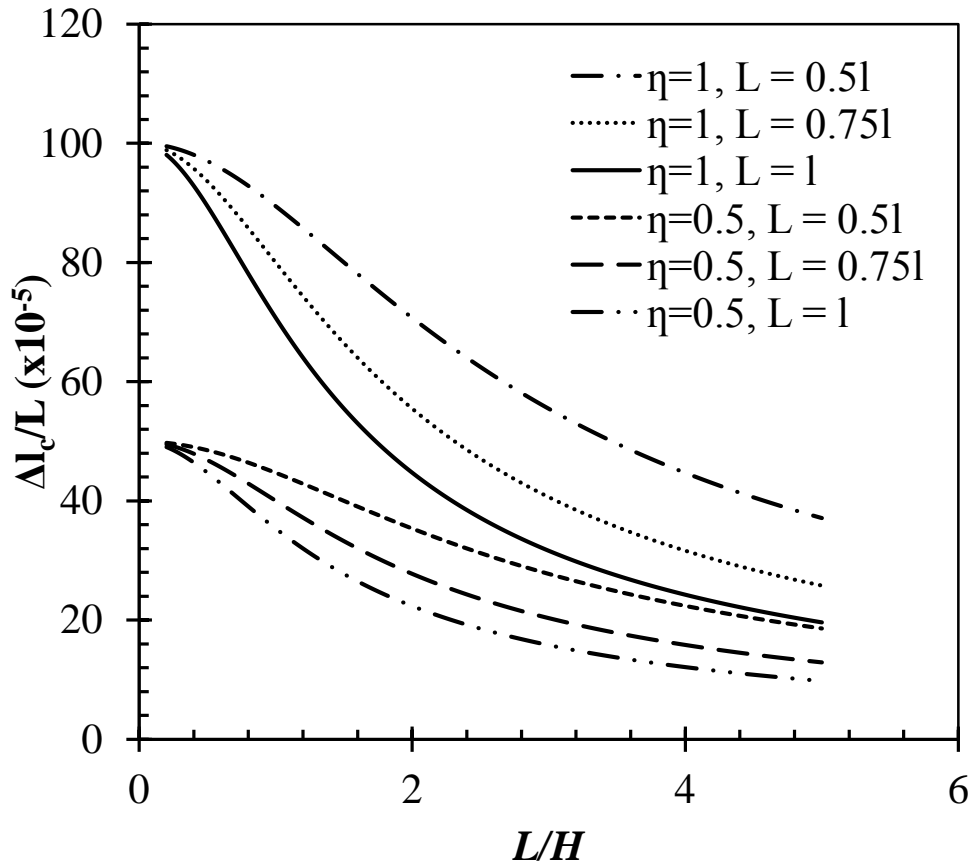
Figure 4.3 Normalized crack width versus length-to-height ratio.

4.2   Effect of Flexibility Factor

As indicated earlier, Dulacska (1992) proposed the concept of flexibility factor, η, ranging from 0.5 to 1.0. In the proposed concept, $\eta = 0.5$ represents a stiff or solid wall section, while $\eta = 1.0$ represents a highly punctured or flexible wall section. This follows findings that stiffer structures are less affected by the ground distortions. Hence, the use of the flexibility factor accounts for the rigid body response of the building to excavation-induced ground distortions.

Following this, a sensitivity analysis was conducted to throw more light on the effect of the flexibility factor on the normalized crack with, and subsequently the calculated crack

104

width. Inspecting Equation (2-29), it is clear that there is a direct proportionality between calculated normalized crack width and the flexibility factor. Hence, it will be of little importance to vary only the flexibility factor. However, one may interested in exploring further the behavior of the flexibility factor on the normalized crack width in walls of varying L/H ratio.

To do this, the following parameters were held constant; a fixed-end condition, $L = 0.5l$; measured angular distortion, $\beta = 0.002$; and critical angular distortion, $\beta_{crit} = 0.001$. Nest the flexibility factor was varied from 0.5 (i.e. stiff wall section) to 1.0 (i.e. highly punctured wall section) and L/H from 0.5 to 5. By so doing, a better understanding of the role of the flexibility factor on the calculation of normalized crack width was gained. The significance of this study is that it provides an insight on intermediate building stiffnesses since not all structures can be described as either highly punctured or rid. Figure 4.4 is an illustration of the above description.

105
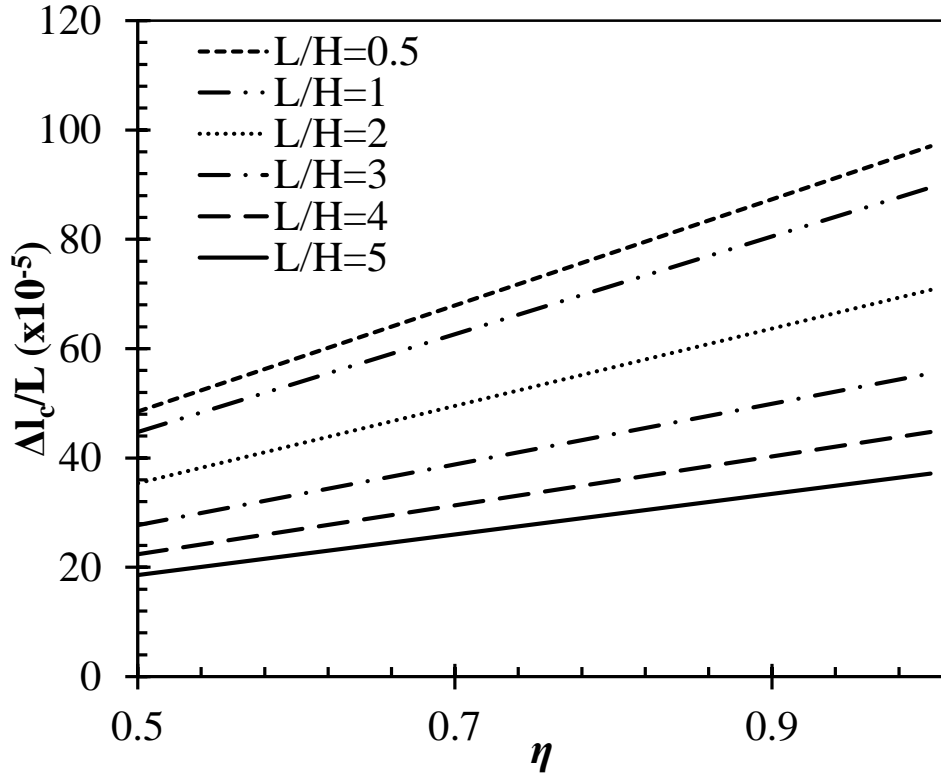
Figure 4.4 Normalized crack width with flexibility factor.

From Figures 4.2 to 4.4, it is observed that normalized crack width still has a stronger relationship across L/H ratios and the relationship with flexibility factor is seen to be directly proportional. It follows that normalized crack width increases with increasing flexibility factor and vice versa.

4.2.1   Verification of Fixed-Frame and Flexibility Factor

To ascertain the veracity of the two parameters discussed previously, Equation (2-29) was used to predict crack width from case history data. The predicted crack width values were then compared with Boone (1999) cumulative diagonal crack width data, and the predicted values using Halim and Wong (2012) method. Table 4.1 is a summary of the case history data based upon which the comparison was made.

106

Table 4.1 Summary of 13 crack width case history data (after Boone, 1996).

Case	L (mm)	H (mm)	L/H	v_{max} (mm)	Measured Crack Width (mm)
1. Littlejohn (1974) struct. 1, 0.6r	15200	1220	12.46	1.00	0.18
2. Littlejohn (1974) struct. 1, 1.1r	15200	1220	12.46	6.00	0.92
3. Littlejohn (1974) struct. 1, 1.6r	15200	1220	12.46	10.50	1.50
4. Littlejohn (1974) struct. 1, 2.1r	15200	1220	12.46	17.00	13.60
5. Golder Assoc. (1994) files	17300	2500	6.92	26.00	12.00
6. Peck et al. (1956)	3660	6000	0.61	3.20	6.00
7. Wilson et al. (1984) block B rear C	18000	6000	3.00	55.00	40.00
8. MacLeod/Paul (1984) Block 20	8500	12600	0.67	3.50	2.00
9. MacLeod/Paul (1984) Block 21	22000	13400	1.64	1.50	22.00
10. MacLeod/Paul (1984) Block 7	11000	7800	1.41	8.00	7.00
11. Driscoll (1983) gable wall	13000	5400	2.41	5.00	2.50
12. Boscardin et al. (1979), C	10700	12500	0.86	6.40	6.00
13. Boscardin et al. (1979), D	6000	13500	0.44	18.80	25.00

The choice of the critical angular distortion in Equation (2-20) (i.e. Dulacska, 1996), once again, was based on the value presented by Meyerhof (1956) and is equal to $1/1000$. Further credence to this value was provided by the work of Finno and Bryson (2002) when they provided $\beta = 1/940$ from their research. The frame condition was assumed to be a fixed-end condition (i.e. $L = 0.5l$) and this is what Boone (1996) also used, and the flexibility factor was assumed to be $\eta = 0.5$ (i.e. the wall was assumed to be highly punctured). Table 4.2 provides the summary comparison of the three methods used in predicting the crack width. It should be noted that the measured crack widths may not be

107

exact. It could be the average in some cases and the minimum in others. For example, for crack widths greater than 25mm, 25mm was used for the purposes of this study. And in cases where a range of values were given, the average value was used. Further details on the case history data can be found in Boone (1996).

Table 4.2 Summary of predicted crack widths and measured crack widths. All values in millimeters.

Case	Halim & Wong (2012), c	Boone et al. (1999), C_p	Dulacska (1992)	Measured Crack Width
1. Littlejohn (1974) struct. 1, 0.6r	0.32	0.38	0.89	0.18
2. Littlejohn (1974) struct. 1, 1.1r	1.92	0.77	0.70	0.92
3. Littlejohn (1974) struct. 1, 1.6r	3.36	1.15	2.12	1.50
4. Littlejohn (1974) struct. 1, 2.1r	5.44	2.69	4.18	13.60
5.Golder Assoc. (1994) files	14.87	3.81	12.04	12.00
6. Peck et al. (1956)	10.93	10.71	4.37	6.00
7. Wilson et al. (1984) block B rear C	69.57	26.17	56.02	40.00
8. MacLeod/Paul (1984) Block 20	11.61	14.58	2.61	2.00
9. MacLeod/Paul (1984) Block 21	3.12	1.40	6.18	22.00
10. MacLeod/Paul (1984) Block 7	18.51	10.54	8.58	7.00
11. Driscoll (1983) gable wall	2.24	7.67	2.24	2.50
12.Boscardin et al. (1979), C	19.45	19.04	6.85	6.00
13. Boscardin et al. (1979), D	68.72	99.57	33.78	25.00

Figure 4.5 shows the performance of the Dulacska (1992) method compared to the measure crack widths.
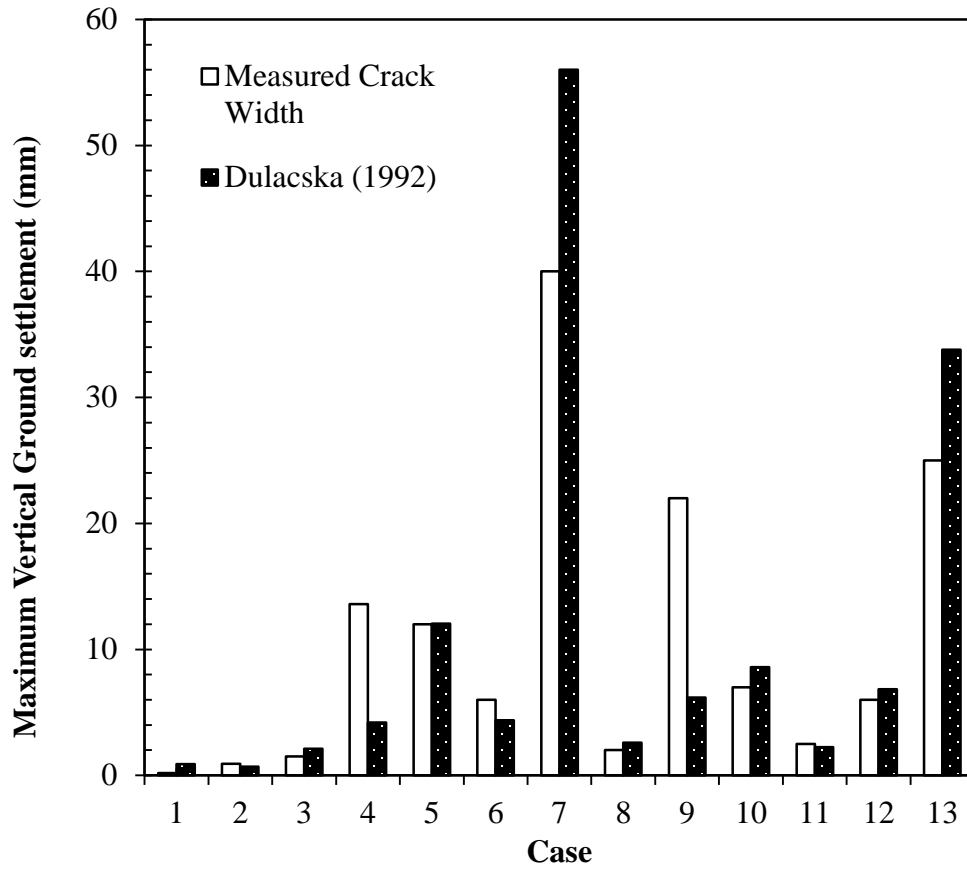
Figure 4.5 Comparison of Dulacska (1992) predictions with measured data.

Figure 4.5 shows that the Dulacska (1992) method predicted very well generally. The method over-predicted by more than 8mm in two instances (i.e. Cases 7 and 13). Similarly, the method under-predicted by more than 9mm in two instances (i.e. Cases 4 and 9). Besides the four cases, the method predicted diagonal crack width values that were within no more than 1.7mm from actual crack widths. Hence, the Dulacska (1992) is fairly accurate.

Figure 4.6 illustrates the performance of the Boone (1996) data, Dulacska (1992) predicted values, and Halim and Wong (2012) predicted values.

109
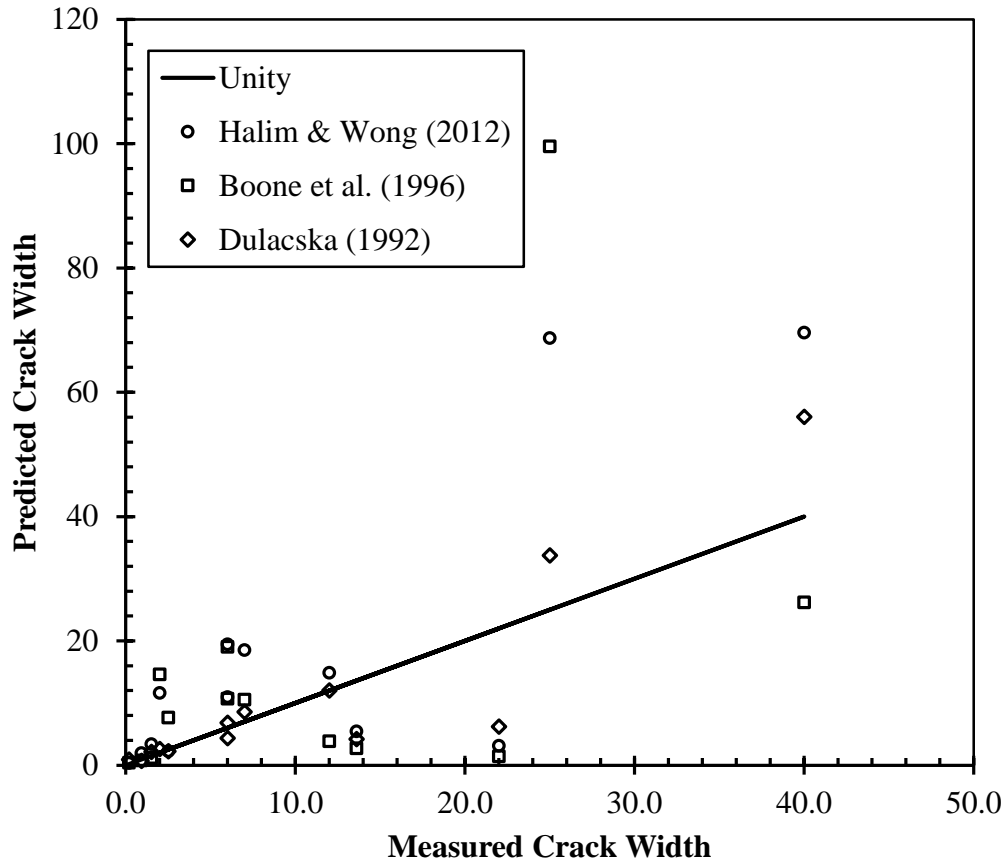
Figure 4.6 Comparison of crack width data and prediction methods.

The unity line (i.e. $45°$ line) is created by plotting the measured crack width against itself. This was used as the basis for graphically comparing the predictive power of the three equations. Thus, the closer the predicted value to the line of unity, the stronger the predictive performance of the corresponding method. Generally, the Dulacska (1992) method provided a good a prediction as the other two. Out of the 13 cases, the Dulacska approach predicted closer to the measured value in 7 instances than the other two methods. While both the Boone (1996) data and Halim and Wong (2012) method out-predicted the other two in 3 instances each. In Case 13, both the data provided by Boone (1996) and the predicted value using the Halim and Wong (2012) method performed

110

poorly, as can be seen from Figure 4.6. In Case 7, both the Dulacska (1992) and Halim and Wong (2012) predictions as well as the Boone (1996) performed poorly. The Boone (1996) data was the only under-prediction, while the other predicted methods over-predicted by at least 16mm. Table 4.3 is a summary of the absolute difference between the measured crack widths and Boone (1996) data, predicted values using Halim and Wong (2012) and Dulacska (1992) methods. Enclosed values implies the most accurate value of the three.

Table 4.3 Summary comparison of deviation from measured values.

Case	Halim & Wong (2012), c	Boone et al. (1996), C_p	Dulacska (1992)
1. Littlejohn (1974) struct. 1, 0.6r	0.14	0.20	0.71
2. Littlejohn (1974) struct. 1, 1.1r	1.00	0.15	0.22
3. Littlejohn (1974) struct. 1, 1.6r	1.86	0.35	0.62
4. Littlejohn (1974) struct. 1, 2.1r	8.16	10.91	9.42
5.Golder Assoc. (1994) files	2.87	8.19	0.04
6. Peck et al. (1956)	4.93	4.71	1.63
7. Wilson et al. (1984) block B rear C	29.57	13.83	16.02
8. MacLeod/Paul (1984) Block 20	9.61	12.58	0.61
9. MacLeod/Paul (1984) Block 21	18.88	20.60	15.82
10. MacLeod/Paul (1984) Block 7	11.51	3.54	1.58
11. Driscoll (1983) gable wall	0.26	5.17	0.80
12.Boscardin et al. (1979), C	13.45	13.04	0.85
13. Boscardin et al. (1979), D	43.72	74.57	8.78

The predictions by the different approaches compared side-by-side with the measured crack widths are illustrated on Figure 4.7. This allows a quick estimation of how close the method predicted in relation to the actual measured value.
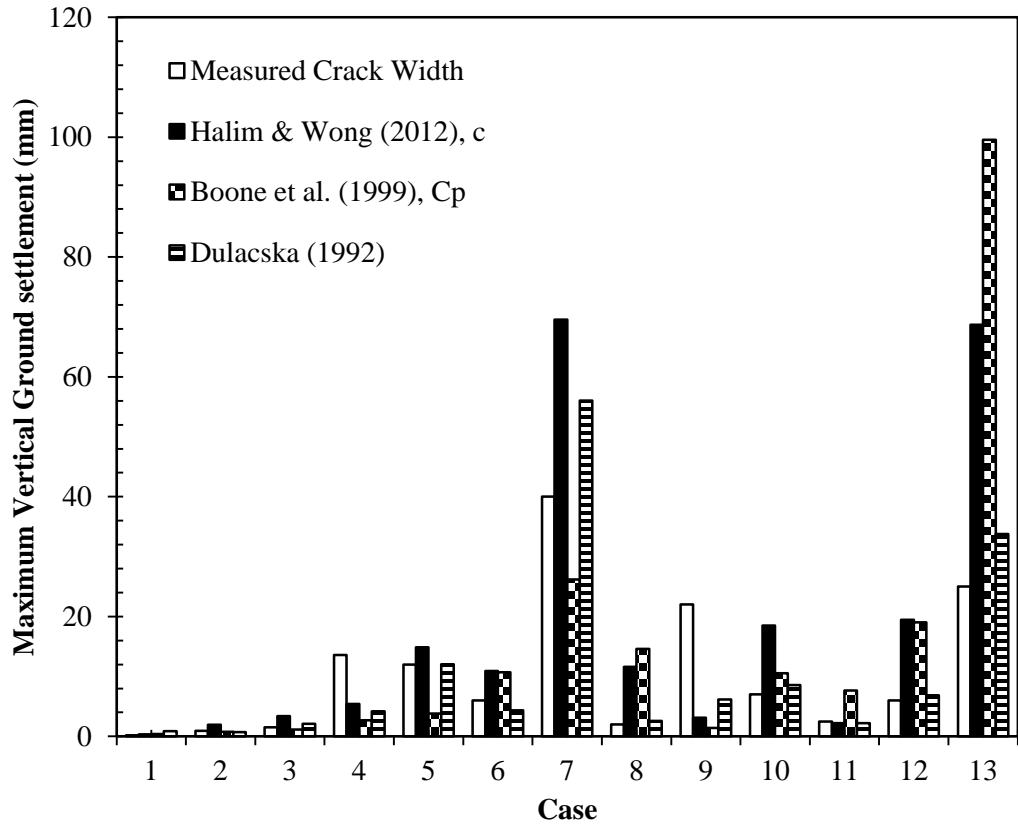
Figure 4.7 Crack width prediction accuracy of three methods (Dulacska, 1992; Boone, 1999; Halim & Wong, 2012).

4.3   Effect of Length-to-Height Ratio of Infill Wall

It has been shown already that the calculation of the critical angular distortion, β_{crit}, depends on the value of the length-to-height ratio, L/H, of the infill wall, as well as the calculation of the diagonal crack with, Δl_c [Equations 2-(15-19)], and Equations 2-(28-29) respectively.

Hence, it may be of interest to find out how this relationship will affect the flexibility index, R, and the normalized crack width. Figures 3.5 and 3.6 were developed for the case of $L/H = 2$. For the purposes of this investigation, the approach and

112

relationship will remain the same all other values nonetheless, the following would remain constant $s_h/s_v = 2$; soil properties given as shown Table 3.1; factor of safety against basal heave, $FS_{bh} = 1.5$; the wall moments of inertia $I = 1000\,cm_4/m$ (this is arbitrary and for simplicity); s_v will vary from $2.75m$ to $5.05m$; and vary only the L/H ratio of the infill wall. The results are summarized as follows:

Table 4.4 Values of normalized crack width for varying L/H ratio.

	Δl_c/L (%)							
R	**L/H=0.25**	**L/H=0.5**	**L/H=1**	**L/H=1.5**	**L/H=2**	**L/H=3**	**L/H=4**	**L/H=5**
13514.35	0.18	0.17	0.12	0.09	0.06	0.03	0.00	0.00
14515.08	0.19	0.17	0.13	0.09	0.07	0.03	0.00	0.00
15551.55	0.19	0.18	0.13	0.10	0.07	0.03	0.00	0.00
16623.77	0.20	0.18	0.14	0.10	0.07	0.03	0.01	0.00
17731.72	0.20	0.19	0.14	0.10	0.07	0.03	0.01	0.00
18875.41	0.21	0.19	0.15	0.11	0.08	0.04	0.01	0.00
20054.85	0.22	0.20	0.15	0.11	0.08	0.04	0.01	0.00
21270.02	0.22	0.20	0.15	0.11	0.08	0.04	0.01	0.00
22520.94	0.23	0.21	0.16	0.12	0.08	0.04	0.01	0.00
23807.59	0.23	0.21	0.16	0.12	0.09	0.04	0.01	0.00
25129.99	0.24	0.22	0.16	0.12	0.09	0.05	0.02	0.00
26488.12	0.24	0.22	0.17	0.12	0.09	0.05	0.02	0.00
27882.00	0.25	0.23	0.17	0.13	0.09	0.05	0.02	0.00
29311.62	0.25	0.23	0.18	0.13	0.10	0.05	0.02	0.00
30776.97	0.26	0.24	0.18	0.13	0.10	0.05	0.02	0.00
32278.07	0.26	0.24	0.18	0.14	0.10	0.05	0.02	0.00
33814.91	0.27	0.24	0.19	0.14	0.10	0.06	0.02	0.00
35387.49	0.27	0.25	0.19	0.14	0.11	0.06	0.02	0.00
36995.81	0.28	0.25	0.20	0.15	0.11	0.06	0.03	0.00
38639.87	0.28	0.26	0.20	0.15	0.11	0.06	0.03	0.00
40319.67	0.29	0.26	0.20	0.15	0.11	0.06	0.03	0.00
42035.21	0.29	0.27	0.21	0.15	0.12	0.06	0.03	0.00
43786.49	0.30	0.27	0.21	0.16	0.12	0.07	0.03	0.00
45573.51	0.30	0.28	0.21	0.16	0.12	0.07	0.03	0.01

113

Following the procedure as for the creation of Figure 3.5, plots of the normalized crack width versus the flexibility index at various L/H ratios were developed, as shown in Figure 4.8. In Figure 4.8, there is a general proportional relationship between normalized crack width and the flexibility index. This is to be expected since a stiffer excavation support system will provide a lesser flexibility index and vice versa. Furthermore, it can be observed that as the L/H ratio increases, the normalized crack width decreases. It should be noted that Equation (2-29) is setup in such a way that, crack width is only recorded when angular distortions are greater than the critical angular distortion. This explains why for $L/H = 5$ there is no observable crack width until the flexibility index is about 37,000. The interpretation is that, for this current excavation support system, one should only expect infill wall openings, due to cracks, when the flexibility factor is about 37,000 or more in an infill wall with a dimension ratio $L/H = 5$.

114
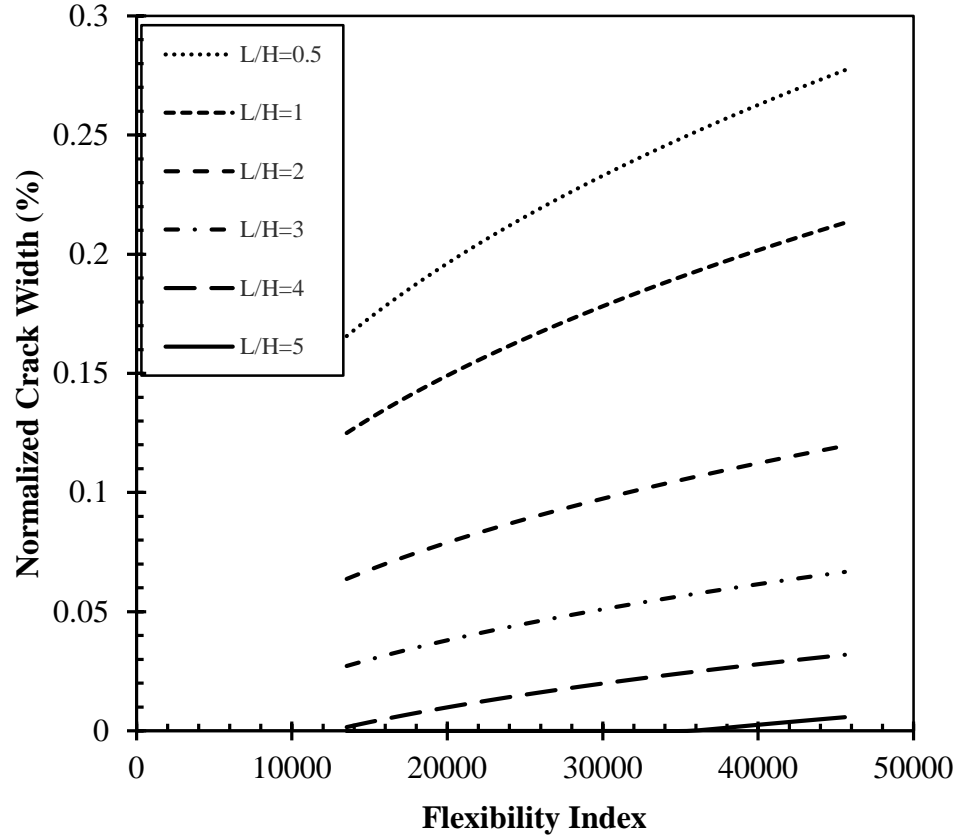
Figure 4.8 Effect of L/H ratio on normalized crack width in infill wall.

4.4   Effect of Factor of Safety against Basal Heave

The factor of safety equation provided by Ukritchon et al., (2003) , as a modification of the Terzaghi (1943) factor of safety, is related to the flexibility index equation by the depth of embedment term, D. This can be seen reflected in the height of the excavation support wall, $H_{wall} = H_e + D$, common to both expressions. The factor of safety against basal heave, FS_{bh}, determines the depth of embedment (assuming all other parameters remain the same).

Hence, the accuracy of the proposed method depend on a deeper understanding of the effect of the factor of safety against basal heave on the process. Maintaining all other

115

parameters in the previous subsection as well as $L/H = 1$, the value of FS_{bh} was varied

from 1.5 to 2.1. Table 4.5 is a summary of the depth of embedment with changing FS_{bh}.

Table 4.5 Effect of factor of safety against basal heave on excavation support system configuration.

FS_{bh}	H_e (m)	D (m)	H_{wall} (m)
1.5	12.20	15.06	27.26
1.7	12.20	22.76	34.96
1.9	12.20	30.46	42.66
2.0	12.20	34.31	46.51
2.1	12.20	38.16	50.36

The plot of normalized crack width versus flexibility index is shown on Figure 4.9. Generally, crack width increases with increasing flexibility index and the reason remain as previously explained. Secondly, it can be seen that crack width increases with decreasing factor of safety against basal heave, for a given flexibility index value. Furthermore, it can be observed that when the depth of embedment is more than 4 times the excavation depth, no damage is recorded. Again, this is due to the fact that the configuration yields angular distortions lesser than the critical value. This only holds for this configuration, since similar flexibility index values can be obtained in different configurations.

116
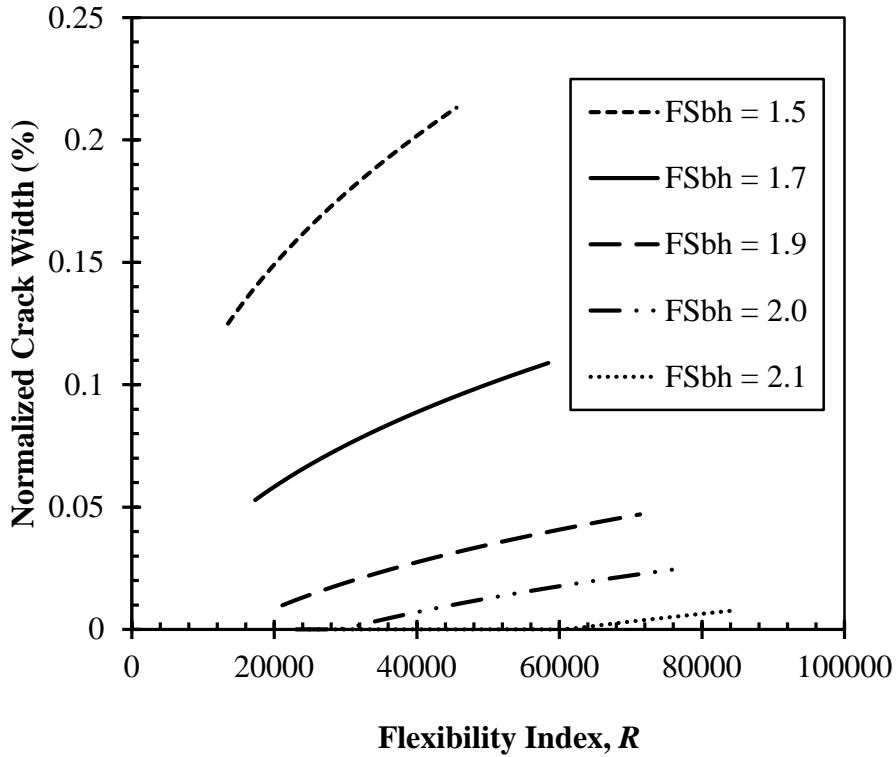
Figure 4.9 Influence of factor of safety on the stiffness of excavation support systems.

4.5   Effect of Undrained Shear Strength

The undrained shear strength, as seen in previous chapters, is used in calculations involving the factor of safety against basal heave and the flexibility index. Throughout the study, the value of the undrained shear strength, s_u, has been limited to $42kPa$ (i.e. medium clay). Thus, the perpendicular settlement profile was predicted using the medium clay chart on Figure 2.5. Keeping the convention of the definition of medium clay in this thesis (i.e. $25kPa < s_u < 50kPa$); reverting the value of FS_{bh} to 1.5; as well as all other parameters used in the previous subsection constant, the value of s_u was varied to see

117

the effect on the excavation-induced deformation in an adjacent infill wall. Table 4.6

summarizes the excavation configurations by varying S_u.

Table 4.6 Effect of undrained shear strength on excavation support system configuration.

S_u (kPa)	Υ_{eq} (kN/m³)	H_e (m)	B (m)	D (m)	H_{wall} (m)
30	18.10	12.20	25	38.16	50.36
35	18.10	12.20	25	26.61	38.81
40	18.10	12.20	25	17.94	30.14
45	18.10	12.20	25	11.21	23.41

Figure 4.10 shows a plot of the normalized crack width versus the flexibility index.

Again, it was observed that the pattern between normalized crack width and flexibility

index was repeated.

118
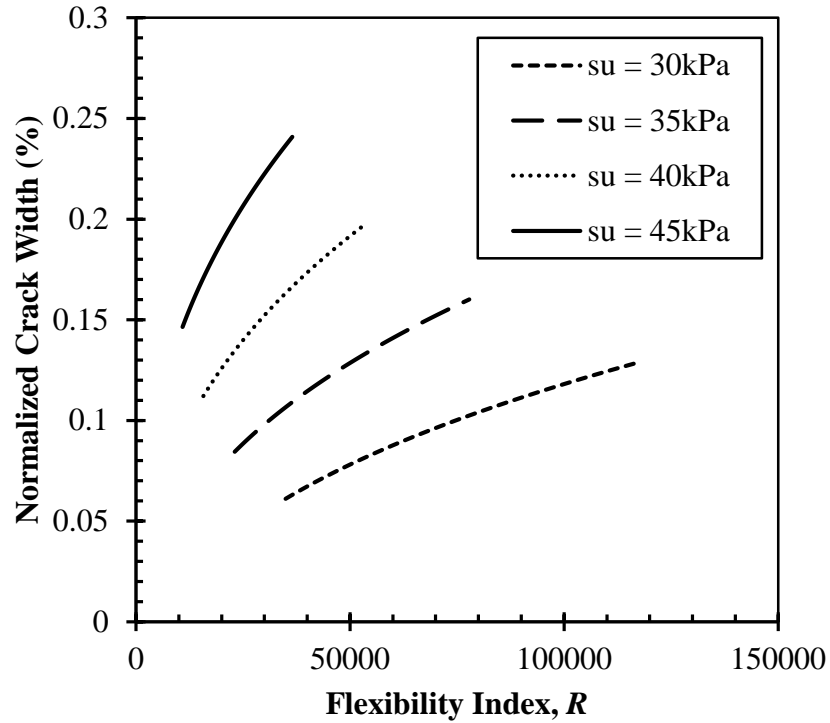
Figure 4.10 Influence of undrained shear strength on the deformation resisting potential excavation support systems.

From Figure 4.10, normalized crack width increases with increasing undrained shear strength, for a given flexibility index. This result may be counterintuitive, as relatively soft clays are generally associated with excessive consolidation and sometimes undergo settlements in excess of the horizontal wall displacements (Goldberg, 1976). However, recent works by Son and Cording (2005; 2011) have shown that indeed this relationship is more probable. They conclude that a building founded on stiffer soil type may be more susceptible to building damage as a result of excavation-induced ground movement, compared to a softer soil given the same magnitude of ground settlement. They posit that the lower deformation experienced in the relatively softer soil is due to the tendency of the structure to modify the ground settlement profile, thus undergoing less distortion.

119

4.6   Effect of Moments of Inertia of Support Wall

A quick inspection of Equation (2-3) reveals an inverse relationship between flexibility index and the moments of inertia of the excavation support wall system. To explore this relationship further, all parameters from the previous subsection was maintained but varied only the moments of inertia, I, of the wall. Figure 4.11 is an illustration of this relationship.
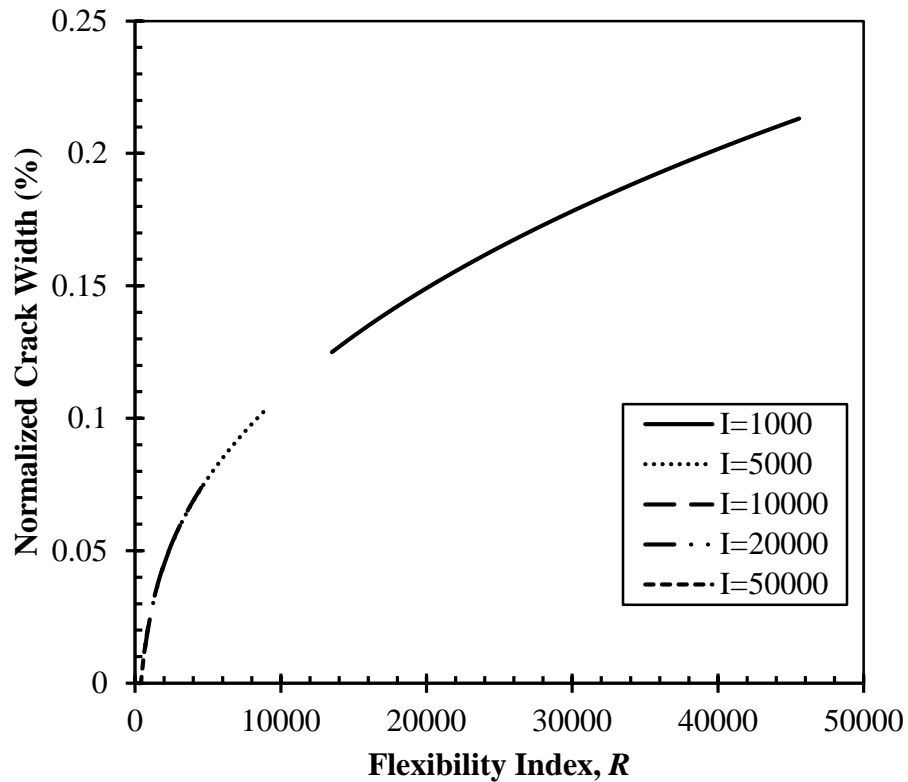
Figure 4.11 Influence of excavation support wall moments of inertia on system flexibility.

Figure 4.11 illustrates the direct relationship between normalized crack width and flexibility index. Despite the fact that the above relationship is for the case where $s_h/s_v = 2$, similar relationship would be displayed with any s_h/s_v ratio. Furthermore, the

120

graph demonstrates that irrespective of the moments of inertia of the wall, there is a well-defined relationship between normalized crack width and flexibility index. A similar relationship is also demonstrated irrespective of L/H ratio of the infill wall, as shown in Figure 4.12.
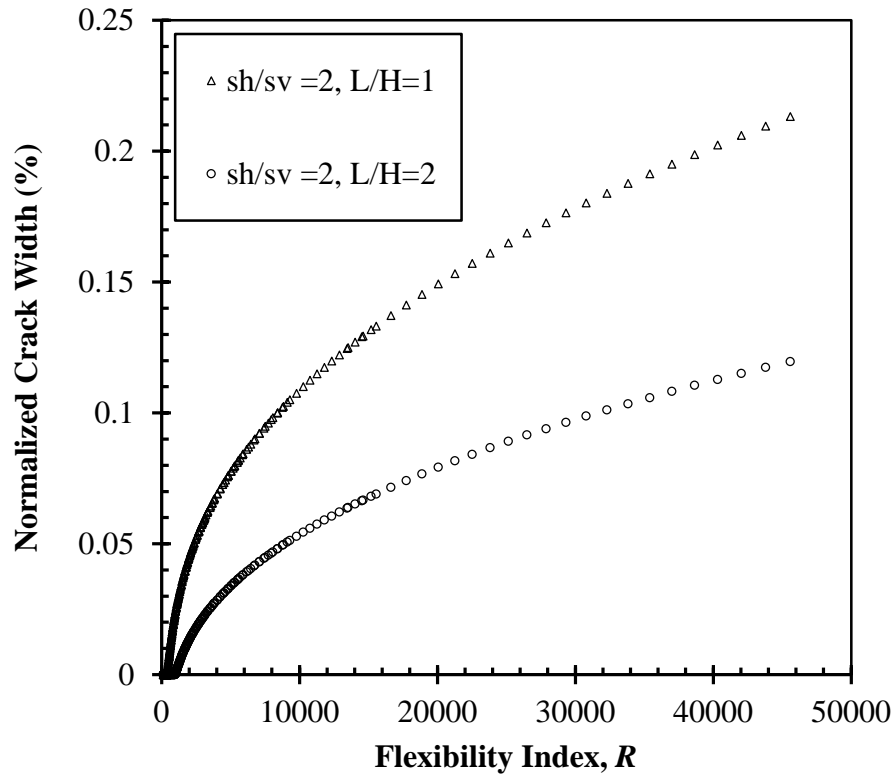
Figure 4.12 Influence of moments of inertia of excavation support wall on normalized crack widths in buildings with different L/H ratios.

121

CHAPTER 5

5.0   Method Validation

5.1   Introduction

This chapter describes the validation process for the proposed inverse excavation support system design. A two dimensional (2D) model was developed in Plaxis and the resulting ground settlements obtained from the analyses were compared with predicted ground movements. This was the only viable means of verification for the proposed method because no case histories exist were found in current literature to be used for the same purpose. Furthermore, Plaxis has used frequently for analyzing both 2D and 3D excavation support systems in past studies by other researchers (Finno and Roboski, 2005; Finno et al., 2007, Bryson and Zapata-Medina, 2012). Finally, it is noted that 2D Plaxis is used solely for the purposes of showing the general trend in ground distortions with respect to the excavation support system flexibility index.

5.2   2D Finite Element Model

The FE modeling software used to simulate a 2D cross-lot deep excavation was "Plaxis 2D AE.02". The software was used to analyze a simplified version of the Chicago Avenue and State Street excavation (Finno et al., 2002). The simplified geometry of the excavation consists of width-of-cut $B = 25m$; depth, $H_e = 12.2m$; and extends in the longitudinal direction for a very large distance (such that plane strain mode is applicable). The sides of the excavation supported by a sheet pile wall was approximately $30m$ long;

wales; and horizontal struts which are spaced 5*m* apart forming a cross lot. No surcharge as imposed on the surface along the excavation.

Figure 5.1 is a schematic of the 2D model. The soil was uniform throughout the depth.
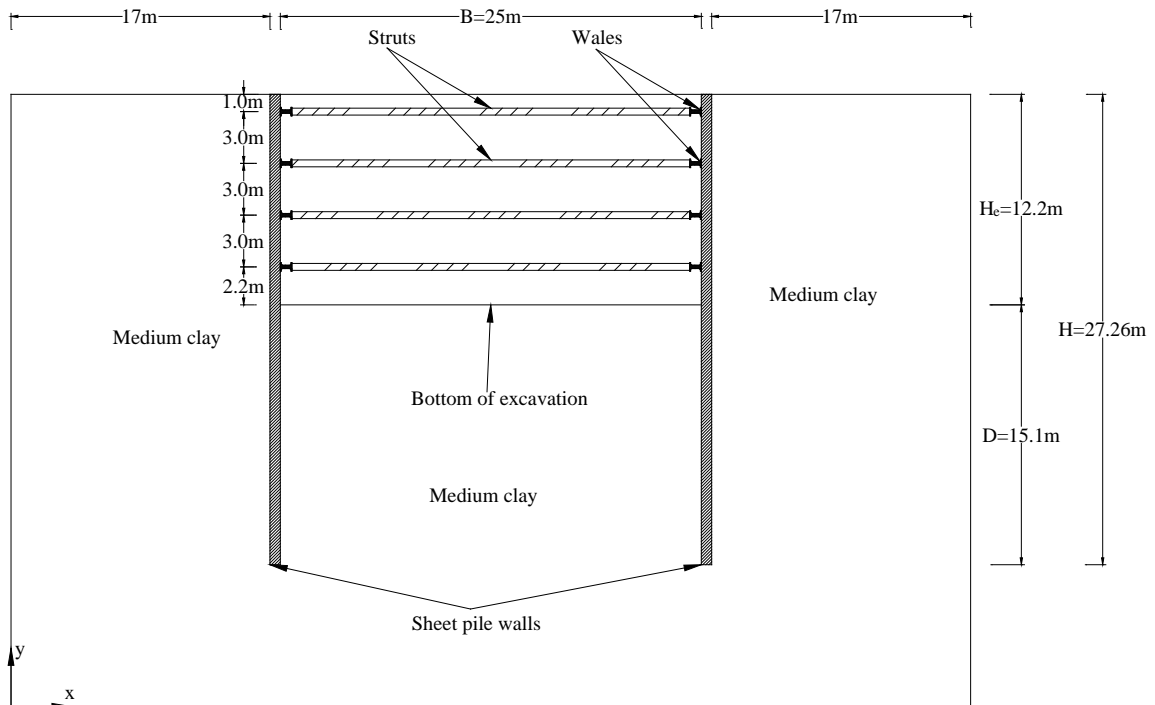
Figure 5.1 Geometry model of deep excavation.

It should be noted that Plaxis 2D only considers one half of the (in this case the left side) excavation support system due to the symmetry in the geometry. From Figure 5.1, the excavation process was simulated in five excavation stages. Within the model, the interaction between the sheet pile wall and the soil was modelled at both sides by means of interfaces (that were either positive or negative). Interfaces allow for the specification of a reduced wall friction compared to the friction in the soil. Finally, the strut was modelled as a spring element for which the normal stiffness is a required input parameter.

123

5.2.1   Soil Parameters and Model

For a simplicity, a uniform soil type was assumed throughout the stratum. However, the assumption of simplicity did not suppress the need to use soil properties that simulate in situ conditions. The Hardening Soil constitutive model (HSM) was used for the soil model. The HSM is an elasto-plastic multi-yield surface model. In comparison to the Mohr-Coulomb model (MC) and other similar perfectly linear models, which assumes a linear elastic perfectly-plastic behavior, the HSM is an advanced model for the simulation of real soil behavior. The model achieves improved accuracy in soil stiffness by using three different input stiffnesses: namely the triaxial loading stiffness, E_{50} ; the triaxial unloading stiffness, E_{ur} ; and the oedometer loading stiffness, E_{oed} . The Hardening Soil Model also takes into account the stress-dependency of the stiffness moduli. The implication of this is that all the stiffnesses increases with increasing pressure. Usually, a reference stress of $1\ bar$ or $100kPa$ is used and is related to all three stiffnesses. Despite its advantages, it does suffer some limitations that are missing in the model but present in real soils. For one, it does not account for softening due to soil dilatancy and de-bonding effects. This arises from the fact that the model does not model both hysteretic and cyclic loading, owing to its isotropic hardening nature. Furthermore, the model does not distinguish between large stiffness at small strains and reduced stiffness at engineering strains. This leaves room for error, as the user has to select the stiffness parameters in accordance with the dominant strain. Lastly, it leads to longer calculation times. Additional details of the hardening soil model (HSM) is beyond the

124

scope of this thesis. The interested reader may find the details of the mathematical formulations of the HSM in Schanz et al. (1999).

Table 5.1 is a summary of the Hardening Soil model parameters used in the 2D FE model.

Table 5.1 Hardening Soil Parameters of 2D FE Modeling.

Parameter	Unit	Undrained Medium clay
γ_{unsat}	kN/m^3	18.1
γ_{sat}	kN/m^3	18.1
$k_x = k_z$	m/day	0.00015
k_y	m/day	0.00009
$E_{50}{}^{ref}$	kN/m^2	6550
$E_{oed}{}^{ref}$	kN/m^2	4000
$E_{ur}{}^{ref}$	kN/m^2	19650
c^{ref}	kN/m^2	0
φ	$^\circ$	29
ψ	$^\circ$	0
υ_{ur}	-	0.2
p^{ref}	kN/m^2	100
m	-	1
$K_0{}^{nc}$	-	0.55
c_{inc}	kN/m^3	0
y_{ref}	m	0
C_k	-	1E+15
R_f	-	0.95
$T\ strength$	kN/m^2	0
R_{interf}	-	1
$\delta\text{-}inter$	m	0

where c is cohesion; φ is angle of internal friction; ψ is angle of dilatancy; γ_{unsat} is unsaturated unit weight of soil; γ_{sat} is saturated unit weight of soil; k is hydraulic conductivity in the denoted direction; E_{50}^{ref} is secant stiffness in standard drained trial test; E_{oed}^{ref} is tangent stiffness for primary oedometer loading; E_{ur}^{ref} is unloading/reloading stiffness with a default value, $E_{ur}^{ref} = 3E_{50}^{ref}$; υ_{ur} is Poisson's ratio for unloading/reloading with default value of 0.2; p^{ref} is reference stress for stiffnesses with default value of $100kPa$; m is the power for stress-level dependency of stiffness; K_0^{nc} is the K_0-value for normal consolidation with default $K_0^{nc} = 1 - \sin\varphi$; c_{inc} is cohesion increment; y_{ref} is reference level; R_f is interface strength with $R_f = 1$ for a rigid interface (i.e. an interface with the same strength as the associated soil layer) and $R_f < 1$ for a flexible interface (i.e. an interface of less strength than associated soil layer); and *T strength* is tensile strength with default value of 0.

5.2.2   Steps involved in creating model

Below is the summary of the steps involved in creating the model in 2D Plaxis. Detailed step-by-step can be found in "2D-1 Tutorial" manual from the software manufacturer website.

1. Setup general settings. Set model dimensions; plane strain condition; and units, as shown in Figure 5.2.

126
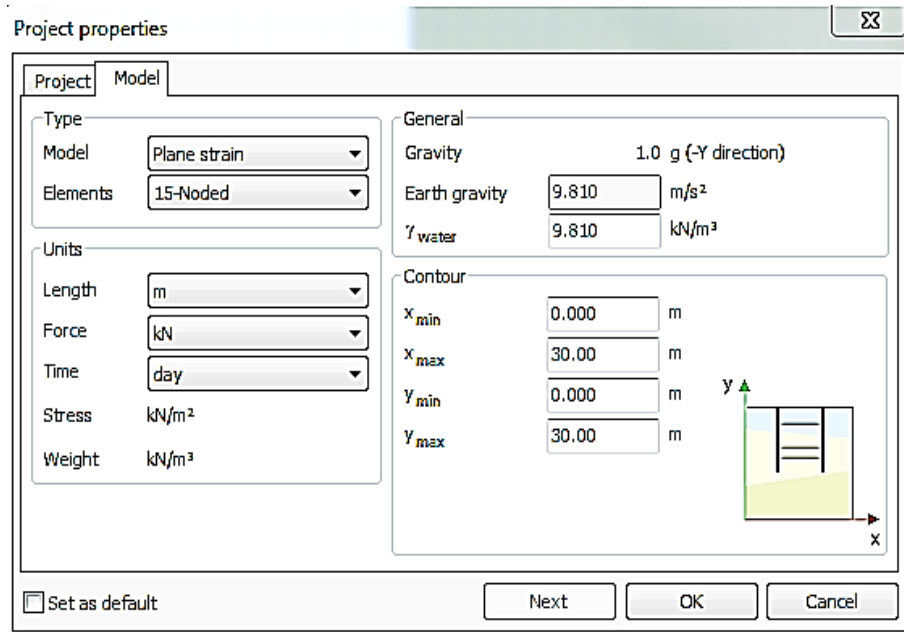
Figure 5.2 General settings in 2D Plaxis.

2. Define soil stratigraphy. Create a borehole log and define necessary parameters, as shown in Figure 5.3.
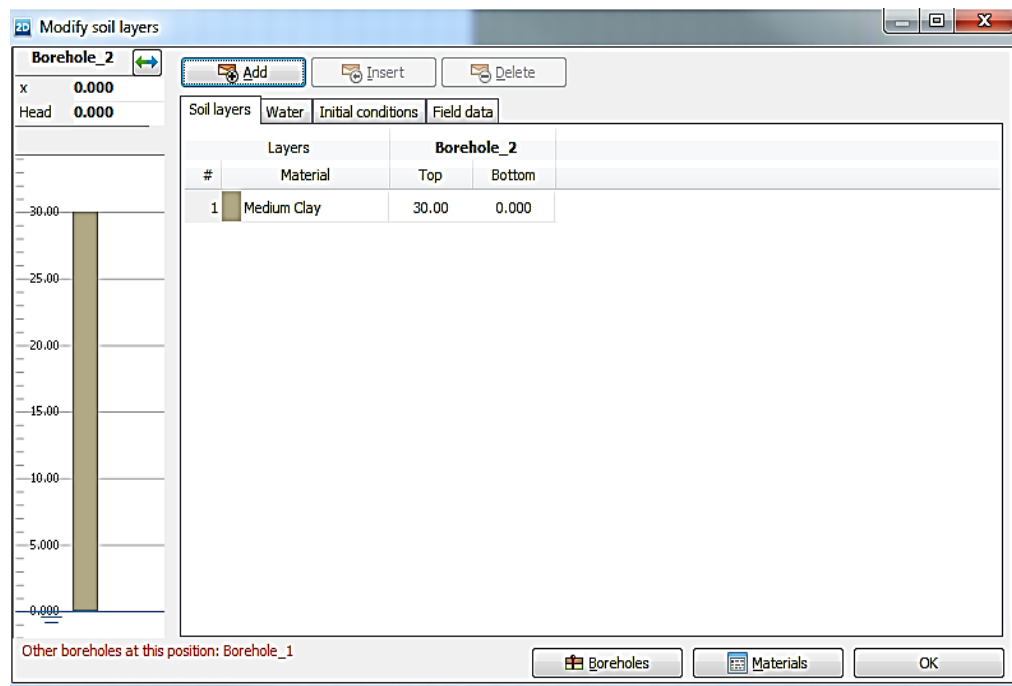
Figure 5.3 Definition of stratigraphy.

127

3. Define structural elements. In this study, the relevant elements are plate (i.e. excavation wall which will be sheet pile); and struts (i.e. anchors). In this study, the properties of sections designed using the inverse support system design are used. This provides the basis for comparison of results. A generated mesh of the excavation support configuration prior to excavation as shown Figure 5.4.
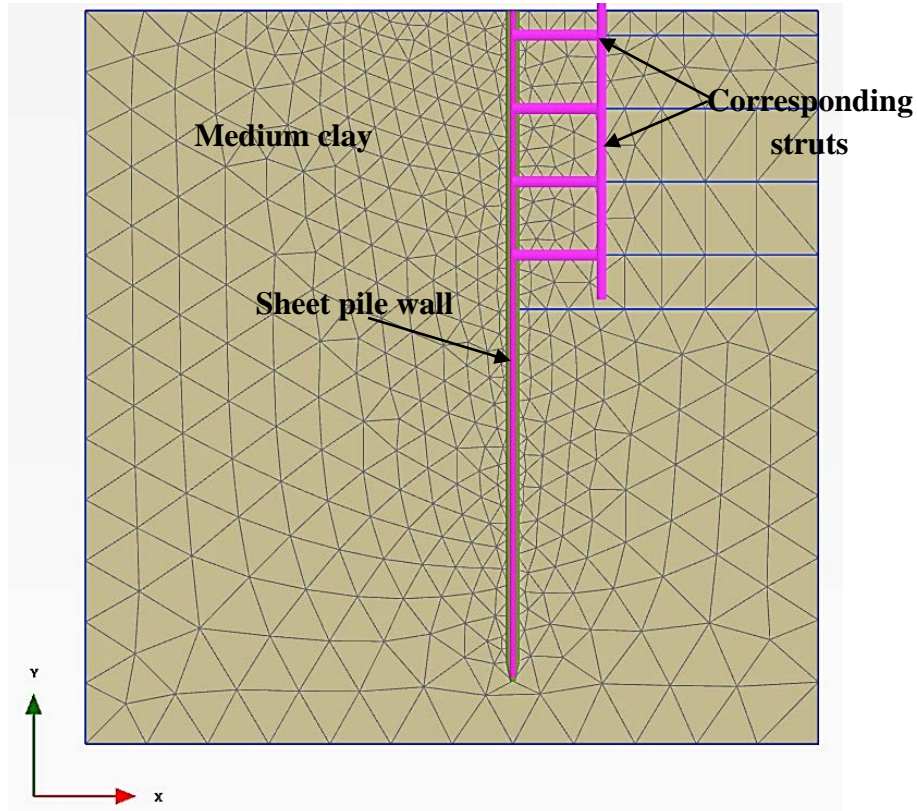
Figure 5.4 Left side of excavation model showing mesh prior to excavation.

4. Calculations. Plaxis 2D works similarly to practical construction, which means it first installs the excavation support wall and then uses stages of excavation and installation of struts until the final depth. Figure 5.5 shows the excavation to the final depth, as well as the installed four levels of struts.

128
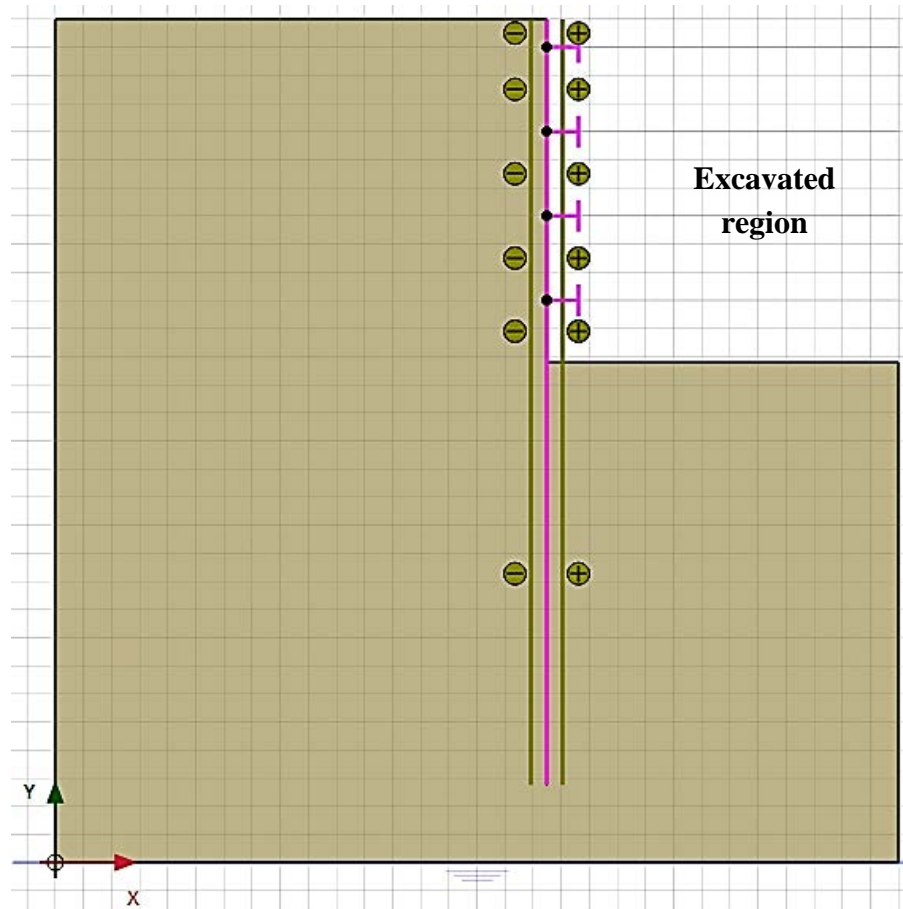
Figure 5.5 2D Plaxis model showing excavation to final depth, and four levels of struts installed.

Next was to perform calculation on the staged excavation. Finally, the results can be viewed in the 2D Plaxis software. Since the interest of this research is in the excavation-induced ground movements or settlement and the effect on adjacent building (and in particular crack width), a closer attention was paid to the maximum lateral wall movements and the maximum vertical ground movements. Figures 5.6 and 5.7 provides a snapshot of the output of the model (i.e. maximum lateral movement and maximum vertical settlement respectively).

129
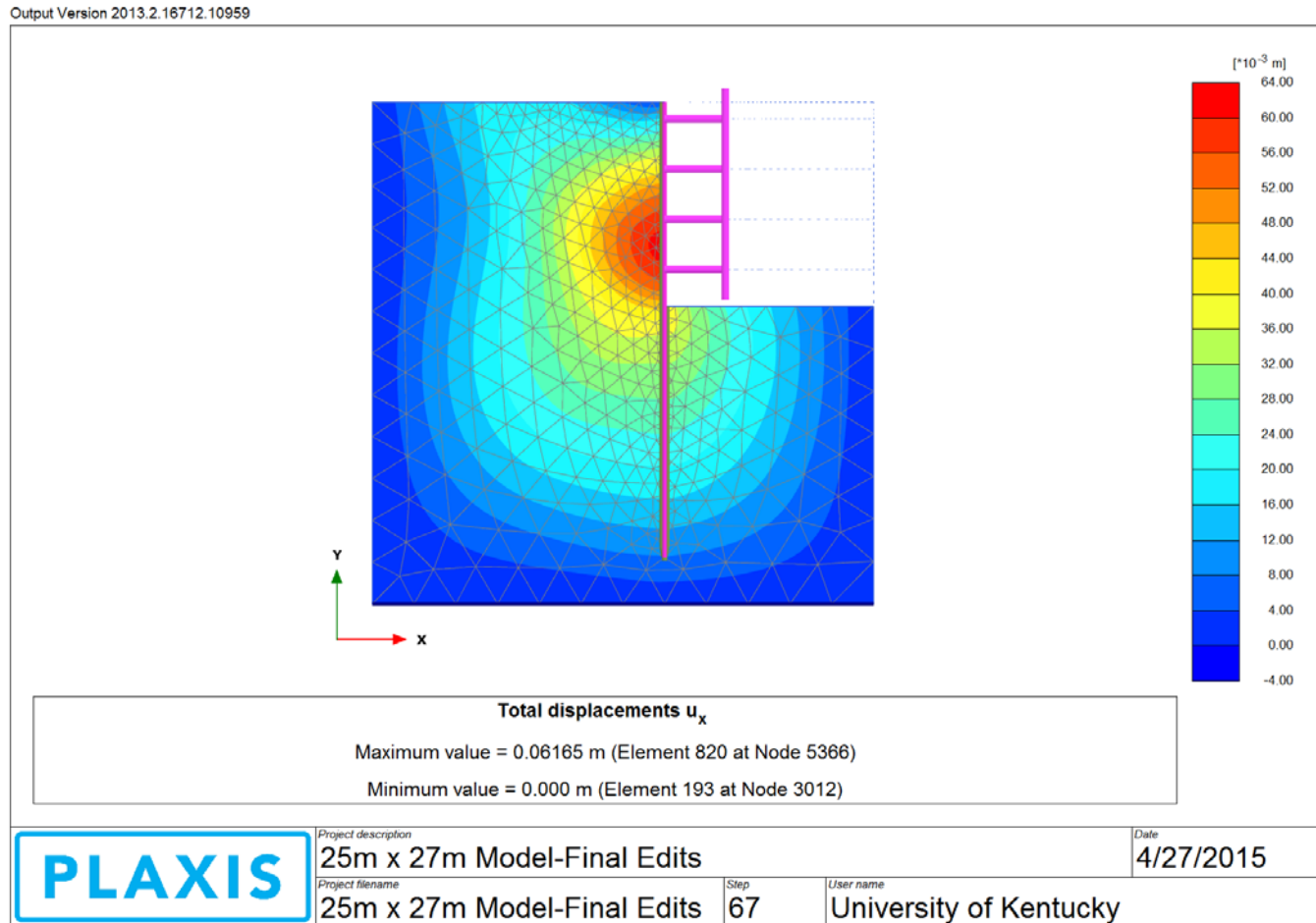
Figure 5.6 Output results showing maximum lateral wall movements.

$[*10^{-3}$ m$]$

	40.00
	35.00
	30.00
	25.00
	20.00
	15.00
	10.00
	5.00
	0.00
	-5.00
	-10.00
	-15.00
	-20.00
	-25.00
	-30.00
	-35.00
	-40.00
	-45.00
	-50.00
	-55.00
	-60.00
	-65.00

Total displacements u_y

Maximum value = 0.03508 m (Element 198 at Node 3948)

Minimum value = -0.06075 m (Element 741 at Node 4858)

PLAXIS	Project description 25m x 27m Model-Final Edits			Date 4/27/2015
	Project filename 25m x 27m Model-Final Edits	Step 67	User name University of Kentucky	

Figure 5.7 Output results showing maximum vertical ground movements.

5.3   Prediction from Proposed Inverse Excavation Support System Design

The proposed deformation-based method was used to design all the various components of the excavation support system in accordance with the procedure detailed in Chapter 3.

Five crack width situations were considered as follows:

Table 5.2 Acceptable crack widths to guide the design of excavation support system.

Case	Acceptable crack width, Δl_c (mm)	Degree of damage
1	0.5	Very slight
2	1	Very slight to Slight
3	2	Slight
4	3	Slight
5	5	Slight to Moderate

Assuming $L/H = 2$, and $L = 12m$, the forward calculation will lead to obtaining normalized crack width, $\Delta l_c / L$; Flexibility Index, R; rigidity deficit, R_{def}; and required moments of inertia of the wall, I_{rqd}.

It should be noted that the various guidelines provided in the development of the method were strictly adhered when choosing the value for the horizontal strut spacing, s_h. The value was based on the width of an excavation equipment (e.g. Caterpillar 345C L Hydraulic Excavator, which is about 3.5m wide) plus 1.5m additional space for maneuverability. The value of the vertical strut spacing, s_v, is based on the average strut

132

spacing from Figure 5.1. The summary for the five cases for the forward calculations to determine the required parameters are as follows:

Table 5.3 Forward calculations yielding required parameters.

Case	Δl_c (mm)	L (m)	$\Delta l_c/L$ (%)	R	s_v (m)	R_{def}	s_h (m)	s_h/s_v	I_{rqd} (cm⁴/m)
1	0.5	12.0	0.004	111.80	2.44	2114.9	5.0	2.05	96890.25
2	1	12.0	0.008	377.18	2.44	7251.5	5.0	2.05	28258.61
3	2	12.0	0.017	1127.26	2.44	24863.1	5.0	2.05	8241.85
4	3	12.0	0.025	1895.76	2.44	51118.8	5.0	2.05	4008.67
5	5	12.0	0.042	4274.76	2.44	126746.1	5.0	2.05	1616.76

Next, a sheet pile wall section was sized based on the required moments of inertia. Afterwards, a back calculation was performed to ensure that the chosen section is adequate. Adequacy of a design section can be defined in a number of ways. A section is said to be adequate if all of the following are true: i) the section has a moments of inertia greater or equal to the required; ii) the section has an acceptable cost based on the unit weight; iii) the section has a lesser rigidity deficit than required; and iv) the section will lead to lesser cracks within an adjacent building.

Using the above definitions of adequacy, design wall sections were chosen and checked against all four definitions using the proposed inverse method. Table 5.4 summarizes the outcome of checks. Additional their respective normalized costs were calculated.

Table 5.4 Recalculated values based on design sections.

Case	Δl_c (mm)	Section type	I_{des} (cm^4/m)	Unit wgt (psf)	NC per m^2	R_{defdes}	R_{des}	$\Delta l_c/L$ (%)	Design Δl_c (mm)
1	0.5	AZ 39-700	97500	38.59	0.045	2101.7	111.8	0.0004	0.04
2	1	SCZ 23	28900	23.35	0.027	7090.6	377.2	0.002	0.19
3	2	GU 6N	9670	14.336	0.017	21191.1	1127.3	0.006	0.72
4	3	CZ 67	5750	13.72	0.016	35637.9	1895.8	0.011	1.31
5	5	SKS 11	2550	11.26	0.013	80360.0	4274.8	0.026	3.14

where NC refers to the normalized cost.

It can be seen from Table 5.3 and Table 5.4 that the chosen sections meet all the four conditions of adequacy and therefore will result in an excavation support system which limits the distortions in adjacent buildings. In Table 5.4, the preliminary normalized cost from the unit weight of the sections was computed. This check offers the designer the option of exploring cheaper sections that will meet all the four adequacy conditions. But for purposes of this research, it was assumed that cost is not the controlling factor.

134

Figure 5.8 shows the plot of normalized cost versus moments of inertia of the excavation support wall. There seem to be a general pattern between the two, where normalized cost increases with increasing moments of inertia. As earlier indicated, there is a general direct proportionality between moments of inertia and the unit weight of steel sheet pile.
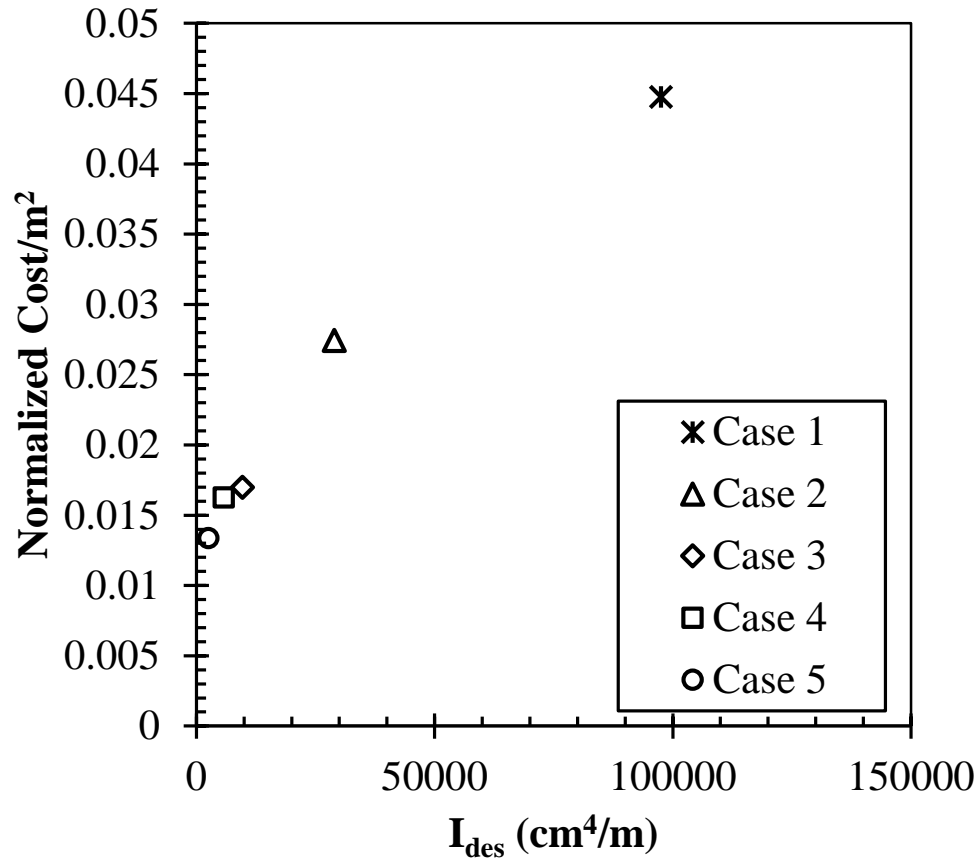
Figure 5.8 Distribution of normalized cost with design moments of inertia.

Alternatively, one may be interested in finding the relationship between expected deformation and its associated preliminary cost. This can prove very useful because it allows the designer/engineer to track cost and deformation simultaneously. In other words, it can be viewed as cost-benefit analysis tool and can be used as a guide in making business decisions. Figure 5.9 is a graph of normalized cost versus normalized crack

135

width. From the graph, there seem to be a general decline of cost with increasing normalized crack width. This is reasonable since the general trend between moments of inertia and unit weight of sheet pile walls is proportional. Thus, as system flexibility index increases, normalized cost decreases.
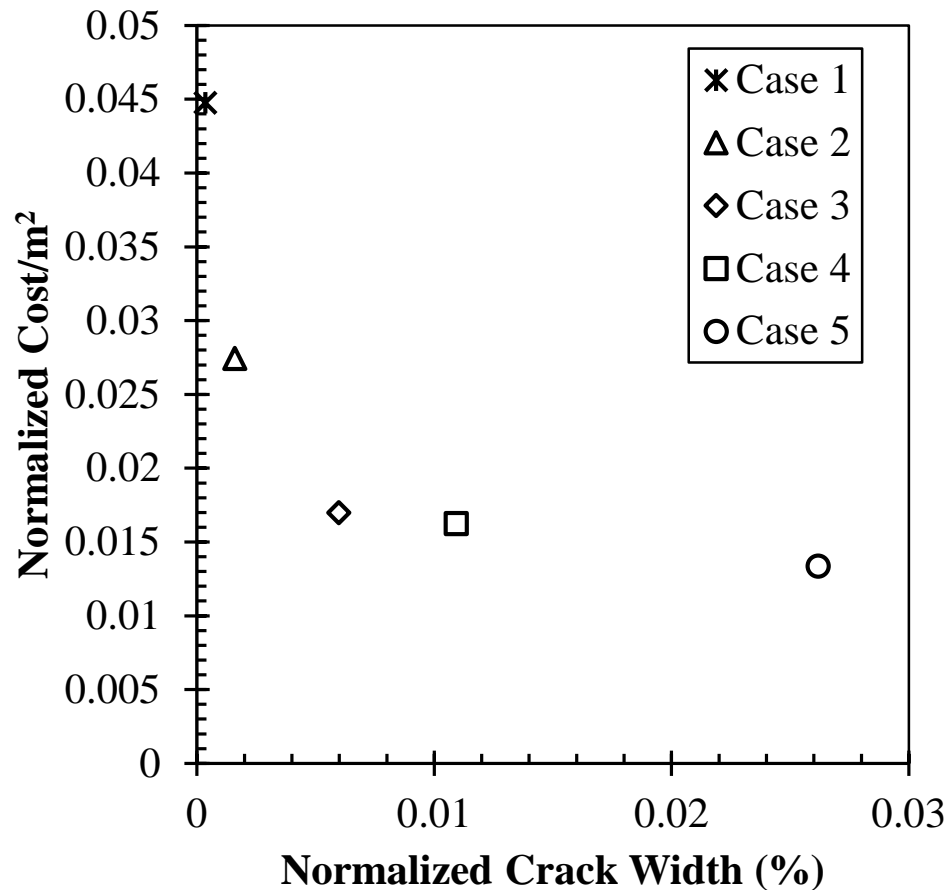
Figure 5.9 Normalized cost versus normalized crack width.

Similar to Figure 5.8, Figure 5.9 can used as a cost-benefit analysis guide during the design process. It allows the tracking of deformation with cost. This chart can be very useful when making decisions concerning acceptable cost and acceptable damage to adjacent structures due to excavation-induced distortions. For example, if cost is not the critical issue then from Figure 5.9, the engineer may opt for the section chosen in Case 3

136

(i.e. GU 6N) instead of that in Case 4 (i.e. CZ 67). Because Case 4 guarantees a diagonal crack width of 1.31mm, while GU 6N would permit 0.72mm but the normalized cost difference between the two is about 0.001GDP (PPP)/m^2. The cost difference is small compared to the anticipated damages that may be caused to adjacent building.

5.3.1   Prediction of Ground Movements

This subsection focused on determining the ground movements associated with the designed excavation support systems (i.e. Cases 1 to 5). The importance of the step is to allow the designer to do direct comparison with other methods in literature or the output of finite elements programs for excavation support systems. Furthermore, it is the only viable option for comparison given that no literature was found on the combined design of excavation support systems and excavation-induced distortions in adjacent structures. Table 5.5 is a summary of the various sections and their respective predicted maximum horizontal and maximum vertical ground movements.

Table 5.5 Predicted ground movements.

Case	Δl_c (mm)	Section type	Angular distortion,β $x10^{-3}$	$\delta_{V(max)}$ (mm)	$\delta_{H(max)}$ (mm)
1	0.5	AZ 39-700	0.99	11.92	25.19
2	1	SCZ 23	1.35	16.23	32.63
3	2	GU 6N	1.79	21.42	41.18
4	3	CZ 67	2.04	24.45	46.00
5	5	SKS 11	2.50	30.05	54.68

137

Because it is the ground movements that give rise to the distortions within the adjacent building, it is necessary to look at the relationship between the predicted ground distortions and the design normalized crack widths. Figure 5.10 is a plot of ground movements versus flexibility index.
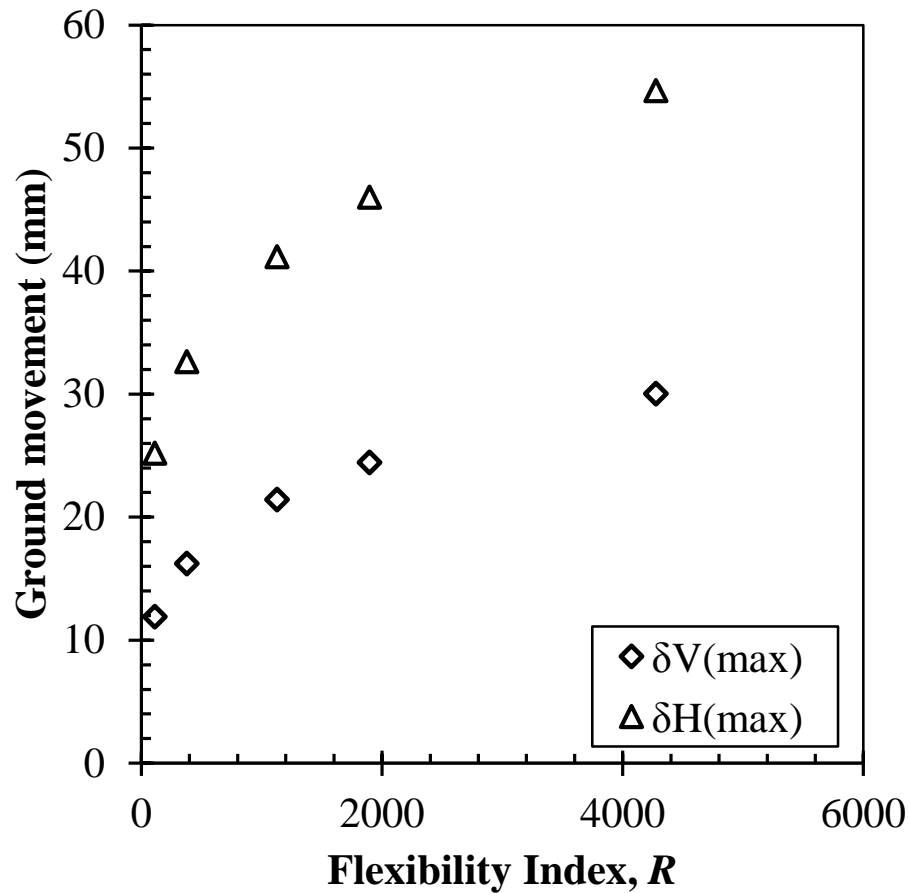
Figure 5.10 Distribution of ground movement with system flexibility index.

From Figure 5.10, a general pattern can be observed between system flexibility index and ground distortions. There seem to be a proportional relationship and it is reasonable. This agrees with the overall concept of excavation support stiffness or flexibility index because it is expected that as a system becomes more and more flexible, so should the

138

ground movements increase. Furthermore, the only means for the ground to deform is when the wall of the excavation system moves under the weight of the backfilled soil. Hence, the more the backfilled soil moves, the more the wall of the excavation support system should deform until equilibrium is attained. Conversely, a rigid support system can only allow a small amount of deformation resulting from wall movements and therefore the corresponding ground movement is little.

Similarly, it was of interest to explore the relationship between ground distortions and normalized cost, this is shown in Figure 5.11.
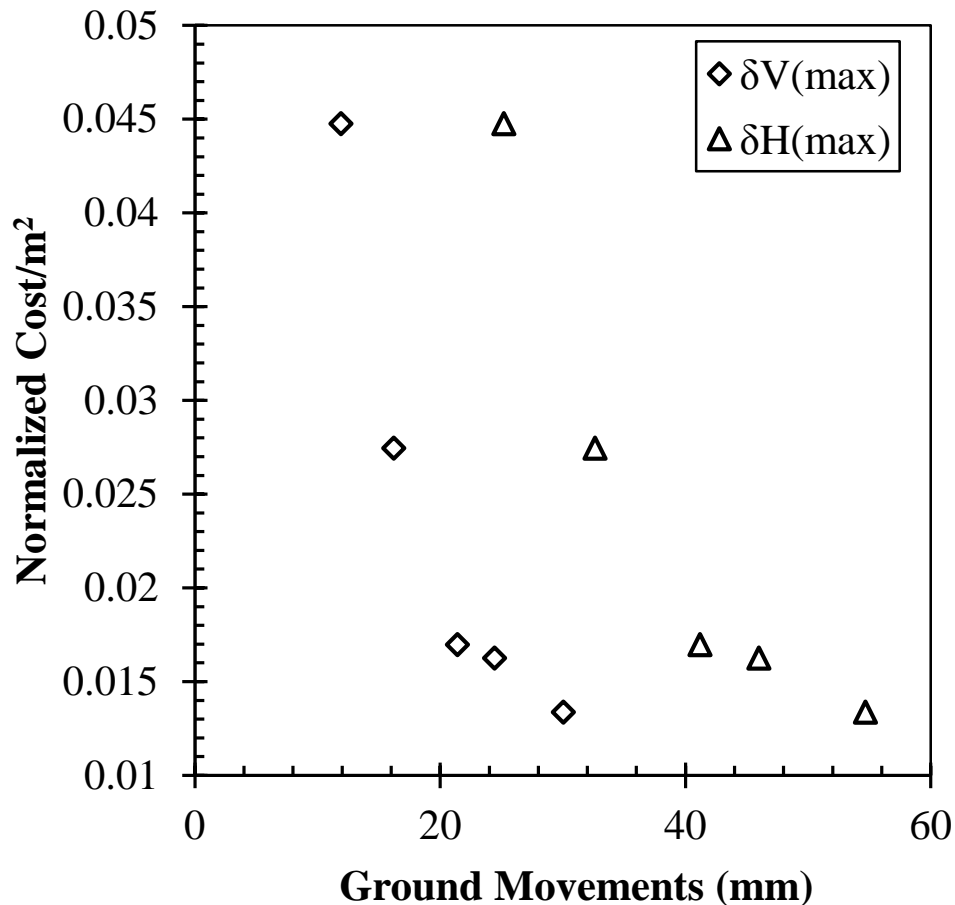
Figure 5.11 Distribution of normalized cost with ground movements.

139

The distribution in the above graph is just what is to be expected. There is a general decline in normalized cost as ground movements increases. It has already been shown that the flexibility index of the excavation support system determines its reaction to movements within the backfill soil. It has also been shown that these movements increases with increasing system flexibility index. All things being equal, decreasing the moments of inertia of the excavation support wall will increase the flexibility index. Subsequently, a less expensive section by unit weight will yield a higher flexibility index and also will allow higher ground distortions.

Further insight is given to the behavior between the design sections; normalized cost; and ground deformations through a plot of anticipated crack width and design moments of inertia, as shown in Figure 5.12.
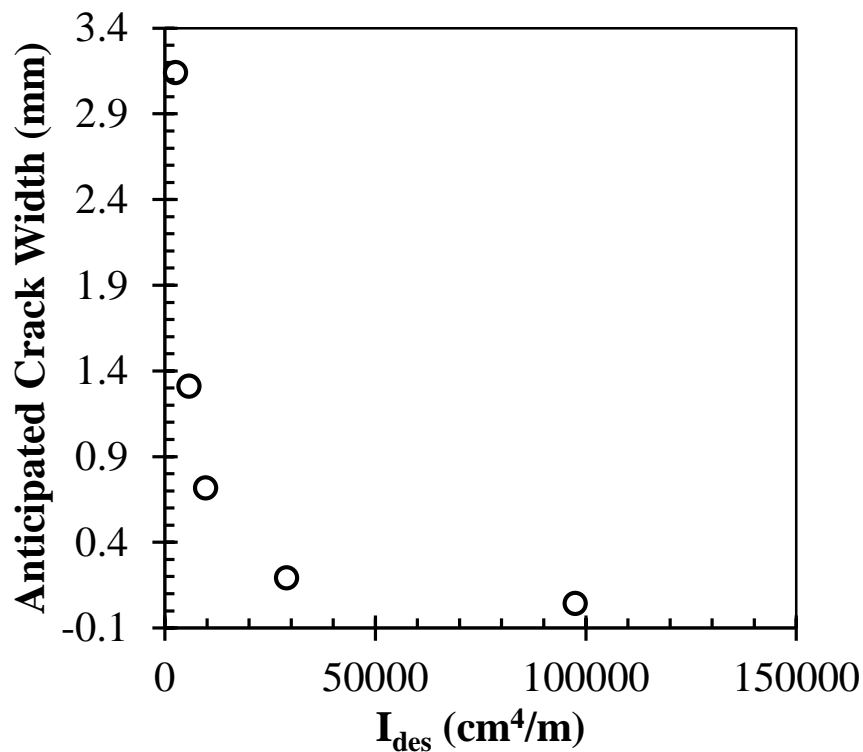
Figure 5.12 Distribution of anticipated crack with design moments of inertia.

140

5.3.2 Designing the remaining components of the excavation support system

This section deals with designing the remaining components of the excavation support system in accordance with the proposed method and will make use of steps 14 to 19 as detailed in chapter 3. The relevance of which is that the members (i.e. excavation support wall and struts) sized using this process would be used as input parameters for the 2D Plaxis model.

Table 5.6 is a summary of the wall moments; uniform loading; maximum wale moments; and the maximum strut loads. Various wales, and strut sections were sized based on the calculated moments and axial loads.

Table 5.6 Moments and axial loads used to design sections.

Case	Design Δl_c (mm)	Max. wall moments (kNm/m)	Equivalent uniform load (kN/m^2)	Max. wale moments (kNm/m)	Max. strut load (kN/m)
1	0.04	968.37	1626.53	3388.60	3968.73
2	0.19	422.11	709.00	1477.08	1729.96
3	0.72	155.19	260.66	543.05	636.01
4	1.31	142.77	239.81	499.60	585.13
5	3.14	84.67	142.22	296.29	347.01

The corresponding wall section properties used as input in 2D Plaxis is summarized on Table 5.7.

141

Table 5.7 Wall input properties in 2D Plaxis model.

Case	Design Δl_c (mm)	Wall section	A (cm²/m)	EA (kN/m)	EI (kPa/m)
1	0.04	AZ 39-700	240.00	4802400.00	195097.50
2	0.19	SCZ 23	145.40	2909454.00	57828.90
3	0.72	GU 6N	89.00	1780890.00	19349.67
4	1.31	CZ 67	85.35	1707853.50	11505.75
5	3.14	SKS 11	69.60	1392696.00	5102.55

The corresponding struts sections and their properties used in the model are shown on Table 5.8.

Table 5.8 Strut input properties in 2D Plaxis.

Case	Design Δl_c (mm)	Strut section	A (cm²/m)	EA (kN/m)	Design compressive strength (kN/m)
1	0.04	CHS 406.4x16.0	196.00	3921960.00	4135.96
2	0.19	CHS 193.7x16.0	89.30	1786893.00	1883.16
3	0.72	CHS 139.7x8.0	33.10	662331.00	697.53
4	1.31	CHS 101.6X10	28.80	576288.00	605.96
5	3.14	CHS101.6X5.6	16.90	338169.00	355.67

From Table 5.8, it can be seen that the design compressive strengths of the design strut sections are either greater than or equal to the strut loads from Table 5.6. This is shown on Figure 5.13.
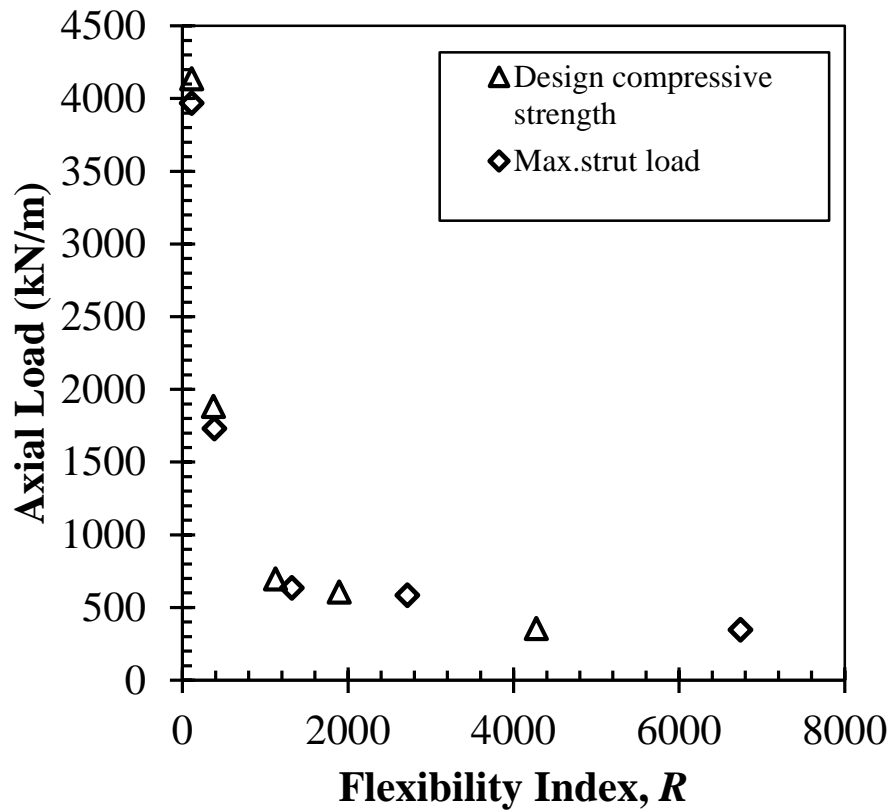
Figure 5.13 Comparison of design compressive strength and average strut load.

It should be noted that these are real A36 steel sections and their properties are readily available in manufacturer's data sheets. A summary of all the design sections, as used in 2D Plaxis, is provided on Table 5.9.

143

Table 5.9 Summary of all sections used in 2D Plaxis model.

Case	Design Δl_c (mm)	Wall section	Wale section	Strut section
1	0.04	AZ 39-700	W33x263	CHS 406.4x16.0
2	0.19	SCZ 23	W30x132	CHS 193.7x16.0
3	0.72	GU 6N	W24X68	CHS 139.7x8.0
4	1.31	CZ 67	W24X62	CHS 101.6X10
5	3.14	SKS 11	W12x87	CHS101.6X5.6

5.4   Assessment of performance of proposed method

This section will provide a side-by-side comparison of the prediction of the proposed method and the output (i.e. maximum horizontal and maximum vertical ground settlement) values from 2D Plaxis.

Section details in Tables 5.7 through 5.9 served as data for material input parameters (i.e. plates, and anchors) within the 2D finite element model. Analyses in 2D Plaxis was conducted on a case-by-case basis. And in each case the Hardening Soil model properties presented Table 5.1 was used for the simulation. In all the analyses within 2D Plaxis, the water table was assumed to be below the bottom of the excavation and drainage type "Undrained (A)" was used. A summary of the output values with respect to each case is shown on Table 5.10.

144

5.10 2D Plaxis-HSM ground movement values.

Case	Design Δl_c (mm)	Wall section	Wale section	Strut section	$\delta_{V(max)}$	$\delta_{H(max)}$
1	0.04	AZ 39-700	W33x263	CHS 406.4x16.0	47.6	34.46
2	0.19	SCZ 23	W30x132	CHS 193.7x16.0	50.64	39.8
3	0.72	GU 6N	W24X68	CHS 139.7x8.0	54.67	50.44
4	1.31	CZ 67	W24X62	CHS 101.6X10	55.5	53.08
5	3.14	SKS 11	W12x87	CHS101.6X5.6	60.75	61.65

As earlier indicated, the comparison would be done on based on the last two columns of the Table5.10 (i.e. $\delta_{V(max)}$ and $\delta_{H(max)}$). Based on this criterion, a summary of the results from both the proposed method and 2D Plaxis is in Figure 5.11.

Table 5.11 Ground movement comparison of proposed method and 2D Plaxis.

Case	Δl_c (mm)	Design Δl_c (mm)	$\delta_{V(max)}$ (mm) Inverse method	$\delta_{V(max)}$ (mm) 2D Plaxis	$\delta_{H(max)}$ (mm) Inverse method	$\delta_{H(max)}$ (mm) 2D Plaxis
1	0.5	0.37	11.92	47.6	25.19	34.46
2	1	0.69	16.23	50.64	32.63	39.80
3	2	1.76	21.42	54.67	41.18	50.44
4	3	2.19	24.45	55.5	46.00	53.08
5	5	2.38	30.05	60.75	54.68	61.65

145

5.4.1 Maximum horizontal ground movement

A graph of the maximum horizontal ground movement from both methods versus the design flexibility index is shown on Figure 1.14 for all the five cases.
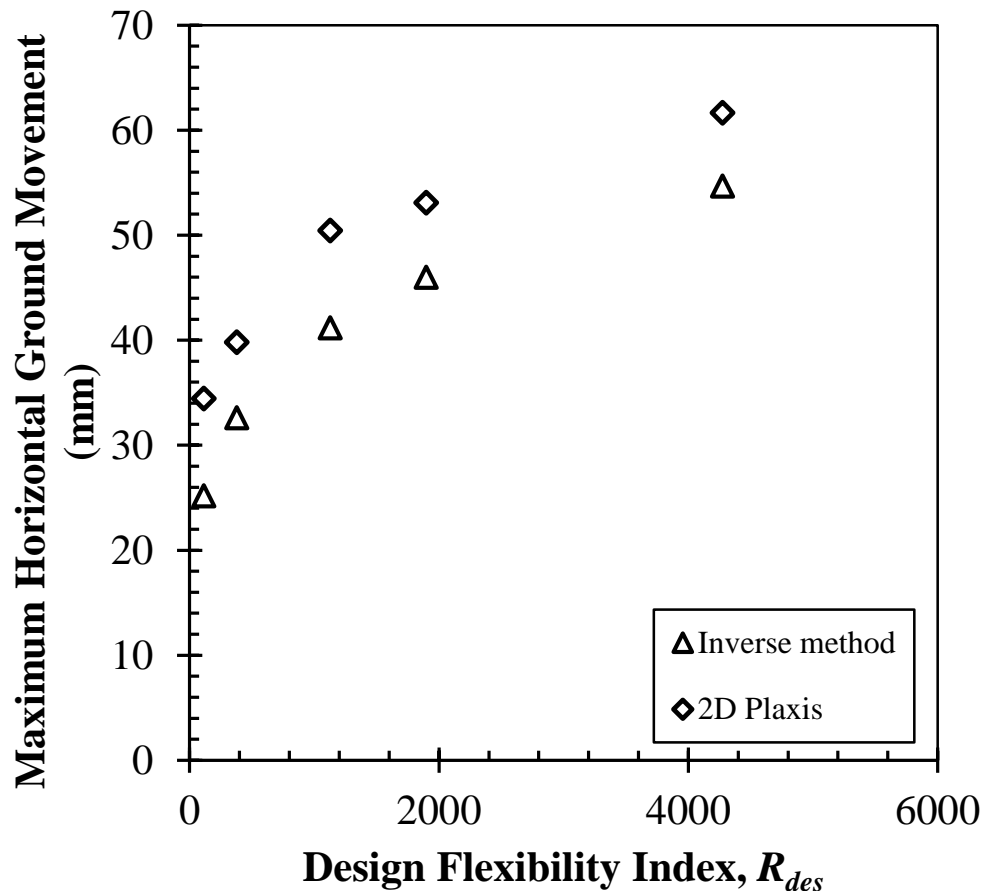
Figure 5.14 Comparison of maximum horizontal ground movements as predicted by inverse method versus prediction of 2D Plaxis model.

Figure 5.14 shows that the deformation-based approach consistently predicted values lesser than 2D Plaxis values. However, the predicted values compare favorably to 2D Plaxis values. It can also be observed that the difference between the predicted values and 2D Plaxis values had no particular pattern with the flexibility index. Generally, the

146

average difference was 7.95mm. To put this analysis into perspective, a simple Student t-statistic was used to find a 95% confidence interval for the mean difference of the two methods in predicting the maximum horizontal ground movements. A bar graph showing the head-to-head values with respect to the cases is shown in Figure 5.15.
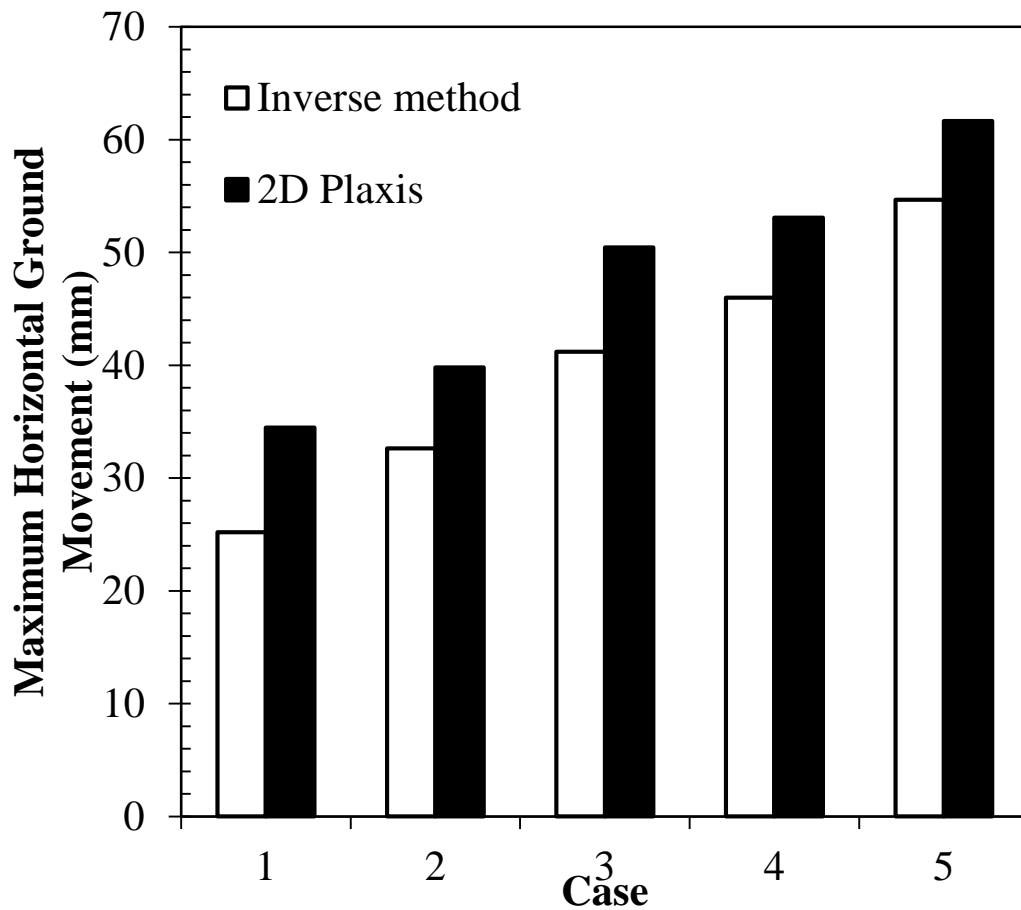
Figure 5.15 Comparison of maximum horizontal ground movement as predicted by inverse method versus 2D Plaxis model data.

Table 5.12 is a summary of statistical data on the results of the two methods.

147

Table 5.12 Statistical data on proposed inverse values and 2D Plaxis values for maximum horizontal ground movement.

	Inverse method	2D Plaxis
Mean	39.94	47.89
Standard deviation	10.26	9.68
Difference in mean	-7.95	
Standard error	6.31	
t-statistic at 95% C.I	2.13	
Max. error estimate	13.45	

Making the null hypothesis that the mean of the proposed method's prediction is not different from the mean of the 2D Plaxis values, a 95% confidence interval for the difference in mean is given by the range $(-21.40, 5.50)$. This implies that with 95% confidence, one can say that the average difference between the predicted values (i.e. maximum horizontal ground movement) using the proposed method and 2D Plaxis values is between -21.40mm (i.e. as much as 21.40mm less than 2D Plaxis values) and +5.50mm (i.e. as much as 5.50mm more than 2D Plaxis values).

5.4.2   Maximum vertical ground settlement

A graph of the maximum vertical ground settlement from both methods versus the design flexibility index is shown on Figure 5.16 for all the five cases.

148

Figure 5.16 Comparison of maximum vertical ground settlement as predicted by deformation-based method versus prediction of 2D Plaxis model.

Figure 5.16 shows that the 2D Plaxis model values were consistently greater than the predictions from the deformation-based design method. It was also observed that the difference between the 2D Plaxis data and the predicted values decreased with increasing relative flexibility. For example , for a design flexibility index of 112, the corresponding difference in 35.68mm (i.e. Case 1) while the difference is 30.70mm when the flexibility index is 4245 (i.e. Case 5). Generally, the average difference was 33.02mm.

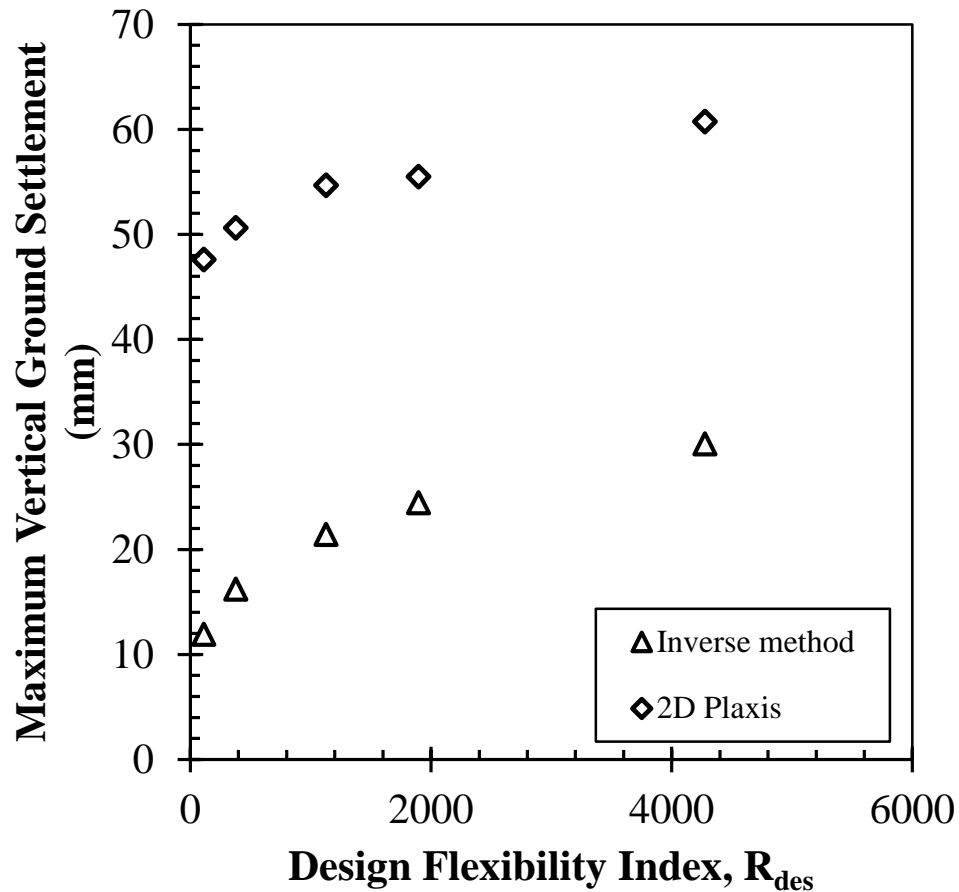A bar graph showing a side-by-side comparison of the maximum vertical settlement is shown in Figure 5.17.

149
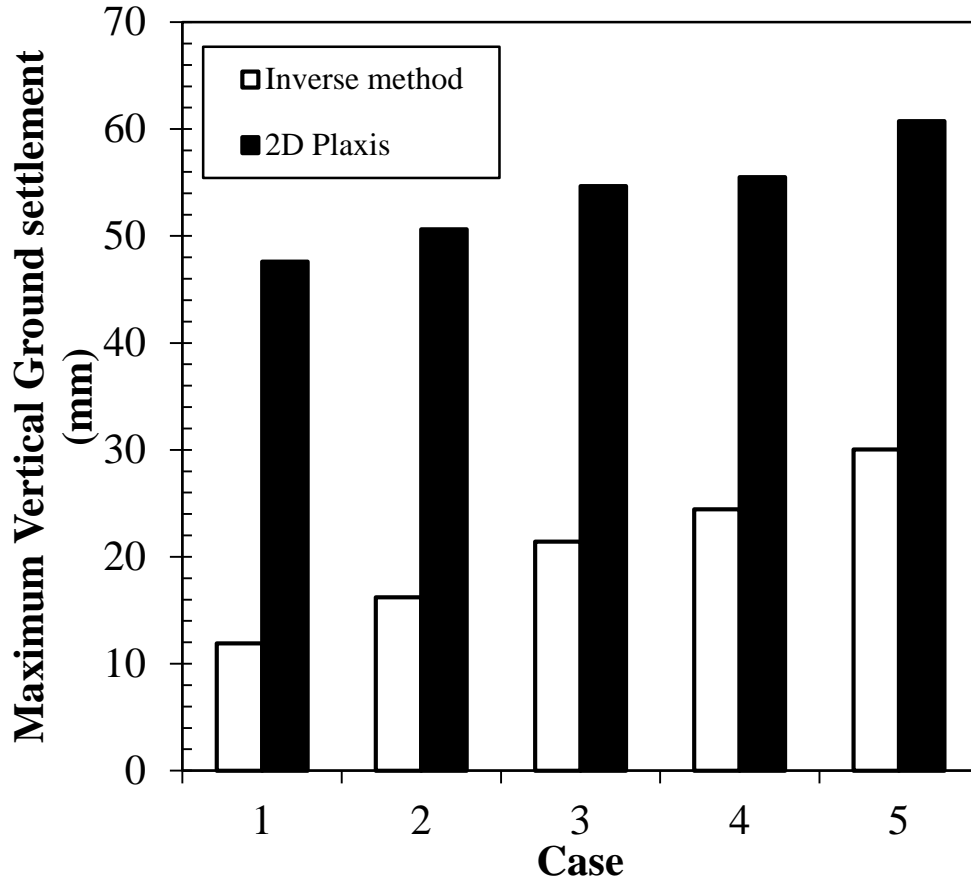
**Figure 5.17 Comparison of maximum vertical ground settlement as predicted by
deformation-based method versus prediction of 2D Plaxis model**

A summary of the statistical data on the results is shown on Table 5.13.

**Table 5.13 Statistical data on proposed deformation-based values and 2D Plaxis values for
maximum vertical ground settlement.**

	Inverse method	2D Plaxis
Mean	20.81	53.83
Standard deviation	6.31	4.48
Difference in mean	-33.02	
Standard error	3.46	
t-statistic at 95% C.I	2.13	
Max. error estimate	7.38	

150

As previously done, making the null hypothesis that the mean of the proposed method's prediction is not different from the mean of the 2D Plaxis values, a 95% confidence interval for the difference in mean is given by the range $(-40.40, -25.64)$. This implies that with 95% confidence, one can say that the average difference between the predicted values (i.e. maximum horizontal ground movement) using the proposed d method and 2D Plaxis values is between -40.40mm (i.e. as much as 40.40mm less than 2D Plaxis values) and -25.64mm (i.e. not less than 25.64mm below 2D Plaxis values).

It should be noted, as earlier indicated, that predicted values may seem different from the 2D Plaxis values, especially the maximum vertical ground settlement values. This may not represent the true situation on the ground. Furthermore, the assumptions within the 2D Plaxis program is beyond this research and may account for the disparities. Thus, only real case history data will provide credibility to the proposed method.

151

CHAPTER 6

6.0   Summary and Conclusion

6.1   Summary

The popularity of deep excavation in mostly urban areas is on the rise worldwide. This is principally due to the fact that space in urban areas is very limited. The situation is further compounded by the closeness of adjacent structures. The challenge, therefore, is to be able to undertake such necessary developmental projects while limiting the damage, caused to adjacent structures, due to the excavation-induced ground movements. This underscores the need to be able to accurately predict the damage to adjacent buildings due to excavation related ground movements. Though three-dimensional in nature, it is fairly accurate to estimate the distortions assuming plane strain conditions. This assumption is reasonable, given that the length of the deep excavation is very long compared to the ground movements along the longitudinal.

Typically, limits equilibrium requirements are used in designing deep excavation support systems. However, the problem associated with the approach is that it usually results in excessive ground movements and consequently unacceptable adjacent structure deformations. Additionally, current methods (both three-dimensional and two-dimensional) consider the design of the excavation support system apart from the damages caused to adjacent structures. This leaves much to be desired, since the ultimate goal is to limit the distortions in adjacent buildings.

A new deformation-based approach (sometimes referred to as the inverse design method) is proposed to address the problem of independent excavation support system

152

design and distortions induced in adjacent buildings. The proposed semi-empirical analytical approach will lead to the design of excavation support systems with the controlling factor being the acceptable deformation in adjacent buildings. The method also introduces a novel idea into the design of excavation support systems, hitherto nonexistent in current literature; known as the preliminary cost estimate. Thus, not only does the engineer design excavation support systems that automatically fulfills both equilibrium requirements and deformations induced in adjacent structures, but also can keep a finger on the cost of the decisions made in the design process. This provides a real-time cost check along the way. This ensures that designs not only meet engineering requirements, but also meets cost-benefits requirements.

A detailed literature review was the focus of Chapter 2. In Chapter 2, methods for predicting perpendicular ground movements and calculating crack widths were reviewed. The methods made use of relative flexibility, known in this research as flexibility index, and factor of safety against basal heave. Various models for deformation in adjacent structures were also presented. Additionally, the chapter reviewed cost comparison of different excavation support wall systems.

Chapter 3 focused on the analytic approach and development of the proposed deformation-based method. In Chapter 3, different excavation wall configurations (i.e. varying both horizontal and vertical strut spacing), were used to calculate flexibility index values given soil properties; excavation width; depth of excavation; varying moments of inertia of excavation support wall; and a constant Young's modulus of the support material. The calculated flexibility index was then used to predict the perpendicular ground movements or distortions. Assuming a rigid soil-structure

153

interaction, the ground distortions were then imposed on the adjacent structure to produce crack widths. The associated angular distortions were then used to calculate the maximum vertical settlement within an infill wall. Next, the maximum vertical settlement was related to the maximum horizontal ground movements using plot of case history data. The concept of rigidity deficit, a measure of the amount of strength needed to produce a desired deformation within an adjacent structure, was also introduced. Finally, the concept of preliminary cost was developed. Preliminary cost entails the cost of material and installation cost as a function of the unit weight of sheet pile wall. The chapter ends in a proposed design flow chart. The flow chart details all the necessary steps to the successful design of an excavation support system, which meets both deformation an equilibrium requirements.

In Chapter 4, a sensitivity analyses of the various formulations used in Chapter 3 were presented. The sensitivity analyses involved further investigation of the effects of flexibility factor on the calculation of crack widths; effect of frame structure on crack width; effect of factor of safety against basal heave on deformations; effect of different length-to-height ratios of infill wall; effect of moments of inertia of excavation support wall on flexibility index and crack width; and the effect of different undrained shear strength on flexibility index.

Chapter 5 presented a means to evaluate the proposed inverse design method. This was achieved using a two-dimensional finite element model created using 2D Plaxis. First, the proposed method was used to design all the members of an excavation support system as well as the preliminary costing. Then using the sized members' properties as input in 2D

154

Plaxis, the associated output ground deformations were recorded for comparison with the predicted ground movements using the proposed deformation-based method.

6.2   Conclusions

With regards to the detailed review of past literature, the following conclusions can be made:

- Typical excavation support systems are designed first and foremost to meet equilibrium requirements and then checks for ground deformations made

- The classical approach also relies on the apparent earth pressure diagrams proposed by Peck (1969). However, the apparent earth pressure approach should only be used in the calculation of strut loads, and are not valid for the calculation of bending moments in the excavation support wall.

- Excavation support system designs should be governed more by the damages induced in surrounding structures.

- The relationship between maximum horizontal ground movement and maximum vertical ground settlement is widely used due to substantial records in case history, thereby increasing its reliability.

- Ground settlement profiles can be predicted flexibility index.

- The assumption of "wished-in-place" wall is practical and widely supported by researchers.

- Structures only begin to exhibit signs of distress only when critical strains, which is an intrinsic property of the structural material, are overcome.

155

- The deep beam model for assessing damage in structures is still favorable due to its applicability to plane strain condition and requires parameters usually present in literature.
- A proper understanding of soil-structure interaction is vital to the efficient and cost effective design of excavation support systems.

Based on the semi-empirical deformation-based method of designing excavation support systems, the following can be concluded:

- It is possible to design an excavation support system with damage to adjacent building driving the design process.
- A design driven by damage to adjacent structures, automatically fulfills equilibrium requirements. This saves time and cost.
- Preliminary cost of an excavation support system can be optimized during the design phase of the excavation support system. This results in an efficient design and also an initial costing tool compared to traditional engineering design approaches for excavation support systems.

The following conclusions can be made from the sensitivity analyses:

- The end-condition of an infill wall determines, to a large extent, the amount of distortions experienced by the wall.
- Normalized crack width decreases with increasing length-to-height ratios.
- The Dulacska (1992) method can out predict or perform similarly to competing methods for calculating deformations (i.e. crack width) caused by ground movements.

156

- Normalized crack width is inversely proportional to the factor of safety against basal heave.

- Normalized crack width varies proportionally to the undrained shear strength of the soil.

- Normalized crack width is proportional to the flexibility index.

- Preliminary cost of an excavation support system is directly proportional to the unit weight of the sheet pile section.

Based on the method evaluation using 2D finite element software package (2D Plaxis), the following conclusions are made:

- For very long length of excavation, plane strain condition is valid. Thus a 2D finite element simulation, and by extension 2D excavation support modelling, is a very useful tool in studying excavation-induced deformations in adjacent structures.

- Maximum horizontal ground movements compared very favorably with the maximum horizontal ground movements from 2D Plaxis. A 95% confidence interval of the difference in mean shows that the proposed method can predict as much as 21.40mm below 2D Plaxis values and as much as 5.50mm more than 2D Plaxis values.

- The maximum vertical settlement from both methods indicates that the proposed inverse method consistently predicted values lower than those from the 2D Plaxis simulation. A 95% confidence interval of the difference in mean showed that the proposed method can predict as much as 40.40mm lower than 2D Plaxis simulation values.

157

- 2D Plaxis values are used solely for the purposes of showing the trend of ground distortions with system flexibility index. Differences may be due to assumptions, within 2D Plaxis, beyond this research.

- True case history data would be needed to test the prediction capabilities of the proposed method.

Given the complexity involved with soil-structure interaction and the prediction of excavation-induced distortions in adjacent building, the deformation-based design method indeed presents a strong case for future researchers. The proposed method is largely successful in not only creating a solution driven by deformation in adjacent structures, but also provides an optimized design process. It has also incorporated a costing aspect during the design phase. The benefit is that, business decisions can be made in a timely fashion because design need not be complete before costing proves that the project is unprofitable. Notwithstanding, further research is needed to verify the method using real case history data.

158

APPENDIX A

www.manaraa.com

A.0   Two-dimensional (2D) Finite element simulation of deep excavation

A.1   Introduction

A complete 2D FE simulation of a submerged construction of an excavation is presented herein. The software package used is PLAXIS 2D AE. This appendix presents the full details as presented by the software manufacturers for the construction of a submerged excavation.

The wall is "wished-in-place". The excavation is 25m wide and the final depth is 12.2m. It extends in the longitudinal direction for a large distance, so that plane strain condition is applicable. The sides of the excavation are supported by a sheet pile wall approximately 30m long and are braced by horizontal struts at horizontal interval of 5m. The entire stratum is assumed to be uniform and of medium clay (Figure A.1).

Since the geometry is symmetric, only one half (in this case only the left side) is considered in the analysis. The excavation process is simulated in five separate excavation stages. The sheet pile wall is modeled by means of a plate. The interaction between the wall and the soil is modelled at both sides by means of interfaces. The interfaces allow for the specification of reduced wall friction compared to the friction in the soil. The strut is modelled as a spring element for which the normal stiffness is a required input parameter.
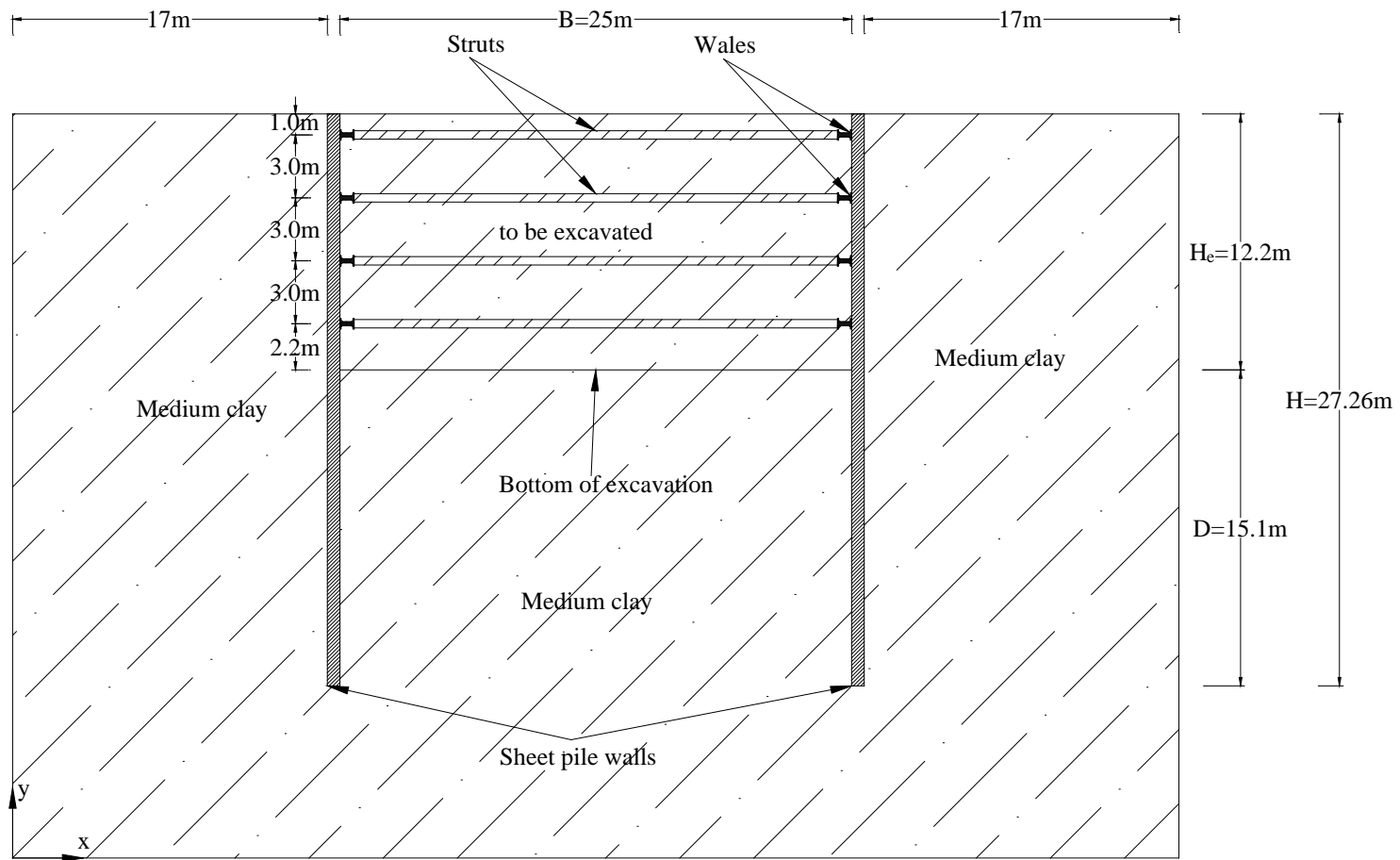
160

Figure A.1-Geometry of 2D Plaxis simulation

A.2   Input

The geometry of the model is created by following the steps:

A.2.1   General Settings

- Start the Input program and select Start a new Project from the Quick select dialog box.

- In the Project tabsheet of the Project properties window, enter an appropriate title.

- In the Model tabsheet keep the default options for Model (Plane strain), and Elements (15-Node).

- Set the model dimensions to $x_{min} = 0.0$m, $x_{max} = 30$m, $y_{min} = 0.0$m, and $y_{max} = 30.0$m.

- Keep the default values for units and constants and press OK to close the Project properties window.

A.2.2   Definition of soil stratigraphy

To define the soil stratigraphy:

Create a borehole at $x = 0$m. The Modify soil layers window pops up.

- Add the uniform soil layer by setting the top level to 30m and the bottom level to 0m.

- Set the Head in the borehole to 0m. This model assumes water table is below bottom of excavation.

One data set is created for the medium clay layer as follows:

162

- Click the Materials button on the Modify soil layers window. The Material sets window pops up where the Soil and interfaces option is selected by default as the Set type.

- Click the New button in the Material sets window to create a new data set.

- Enter an appropriate name for the medium clay layer and select Soft soil as the Material model. Set the Drainage type to Undrained (A).

- Enter the properties of the uniform soil layer as listed in Table A.2.1. In the General

Table A.2.1- Material properties of medium clay layer

Parameter	Unit	Undrained Medium clay
γ_{unsat}	kN/m^3	18.1
γ_{sat}	kN/m^3	18.1
$k_x = k_z$	m/day	0.00015
k_y	m/day	0.00009
E_{50}^{ref}	kN/m^2	6550
E_{oed}^{ref}	kN/m^2	4000
E_{ur}^{ref}	kN/m^2	19650
c^{ref}	kN/m^2	0
φ	°	29
ψ	°	0
υ_{ur}	-	0.2
p^{ref}	kN/m^2	100
m	-	1
K_0^{nc}	-	0.55
c_{inc}	kN/m^3	0
y_{ref}	m	0
C_k	-	1E+15
R_f	-	0.95
$T\ strength$	kN/m^2	0
R_{interf}	-	1
$\delta\text{-}inter$	m	0

163

Parameter and Flow tabsheets.

- Click the Interfaces tab. Select the Manual option in the Strength drop-down menu. Enter a value of 1.0. This implies that the interface has the same strength properties as the soil.

A.2.3 Definition of Structural Elements

The creation of sheet pile or diaphragm walls, strut, and excavation levels is described below.

- Click the Structures tab to proceed with the input of structural elements in the Structures mode

To define the diaphragm wall:

- o Click the Create structure button in the side toolbar.

- o In the expanded menu select the Create plate option

- In the draw area move the cursor to positon (17.5, 30) at the upper horizontal line and click. Move 27.26 m down (17.5, 2.74) and click. Click the right mouse button to finish the drawing.

Click the Show materials button in the side toolbar. Set the Set type parameter in the Material sets window to Plates and click the New button. Enter an appropriate name as an Identification of the data set and enter the properties as given Table A.2.2. Set the Poisson's ratio for all plates to 0.32 (i.e. A36 steel).

164

Table A.2.2- Material properties of the diaphragm wall (Plate)

Case	Wall section	Unit wgt (psf)	EA (kN/m)	EI (kPa/m)
1	AZ 39-700	38.59	4.80E+06	1.95E+05
2	SCZ 23	23.35	2.91E+06	5.78E+04
3	GU 6N	14.336	1.78E+06	1.93E+04
4	CZ 67	13.72	1.71E+06	1.15E+04
5	SKS 11	11.26	1.39E+06	5.10E+03

- Click OK to close the data set.

- Drag any of the Diaphragm wall data set to the wall in the geometry and drop it as soon as the cursor indicates that dropping is possible.

- Click OK to close the Material sets window.

To define interfaces:

- Right-click the plate representing the diaphragm wall. Point to Create and click on the Positive interface option in the appearing menu (Figure A.2.1). In the same way assign a negative interface as well.

It should be noted that in order to identify interfaces at either side of a geometry line, a positive sign or negative sign is added. This sign has no physical relevance or influence on the results.

To define the excavation levels

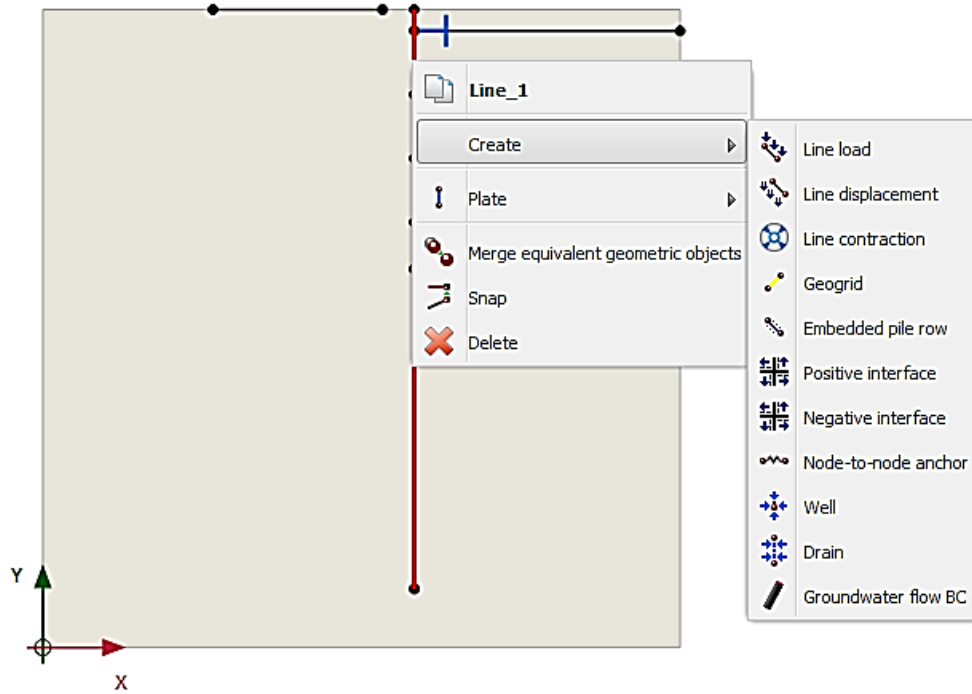Click the Create line button in the side toolbar.

165

Figure A.2.1- Positive interface assignment to existing geometry

- To define the first excavation stage move the cursor to positon (17.5, 29.0) at the wall and click. Move the cursor 12.5m to the right (30.0, 29.0) and click again. Click the right mouse button to finish drawing the first excavation stage.

- To define the second excavation stage move the cursor to position (17.5, 26.0) and click. Move to (30.0, 26.0) and click again. Click the right mouse button to finish drawing the second excavation stage.

- Similarly for third, and fourth excavations follow previous step using the coordinates (17.5, 23.0) to (30.0, 23.0) and (17.5, 20.0) to (30.0, 20.0) respectively.

- The fifth and final excavation is defined by clicking the position (17.5, 17.8) at the wall. Move the cursor 12.5m to the right (30.0, 17.8) and click again. Click the right mouse button to finish the excavation levels.

166

To define the strut:

Click the Create structure button in the side toolbar and select the Create fixed-end anchor button in the expanded menu.

- Move the cursor to (17.5, 29.0) and click the left mouse button. A fixed-end anchor is added, being represented by a rotated T with a fixed size.

Click the Show materials button in the side toolbar. Set the Set type parameter in the Material sets window to Anchor and click the New button. Enter an appropriate name as an Identification of the data set and enter the properties as given in Table A.2.3. Close OK to close the data set.

It should be noted that the Spacing out of plane, $L_{spacing}$, is the same for all configurations and equal to the horizontal strut spacing, $s_H = 5.0m$. And the Young's modulus of elasticity of A36 steel is $E = 200.1GPa$.

- Click OK to close the Material sets window.

Table A.2.3- Material Properties of struts (anchors)

Case	Wall section	Strut section	EA of strut (kN/m)
1	AZ 39-700	CHS 406.4x16.0	3.92E+06
2	SCZ 23	CHS 193.7x16.0	1.79E+06
3	GU 6N	CHS 139.7x8.0	6.62E+05
4	CZ 67	CHS 101.6X10	5.76E+05
5	SKS 11	CHS101.6X5.6	3.38E+05

- Make sure that the fixed-end anchor is selected in the draw area.

- In the Selection explorer assign the material data set to the strut by selecting the corresponding option the Material drop-down menu.

- The anchor is oriented in the model according to the $Dirction_x$ and $Direction_y$ parameters in the Selection explorer. The default orientation is valid in this simulation.

- Enter an Equivalent length of 12.5 m corresponding to half the width of the excavation (Figure A.2.2)
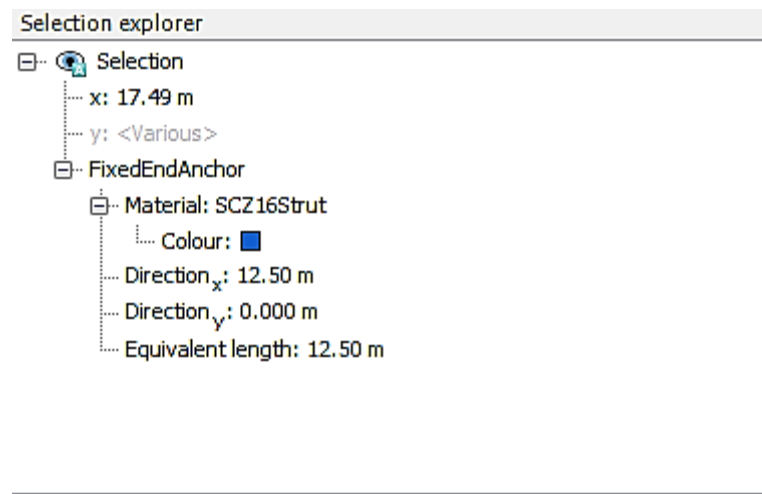

Figure A.2.2- Parameters for fixed-end anchors in the Selection explorer.

A.2.4   Mesh Generation

- Proceed to Mesh mode.

Create the mesh. Use the default option for the Element distribution parameter (medium).

View the mesh. The resulting mesh is displayed in Figure A.2.3

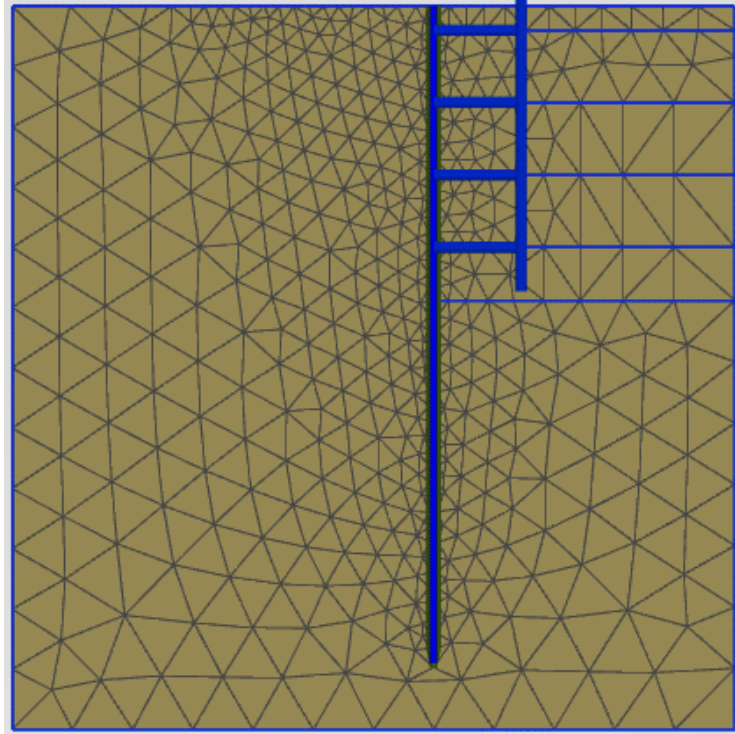- Click on the Close tab to close the Output.

Figure A.2.3- A sample generated mesh

A.2.5   Calculations

In practice, the construction of an excavation is a process that can consist of several phases. First, the wall is installed to the desired depth. Then some excavation is carried out to create space to install an anchor or a strut. Then the soil is gradually removed to the final depth of the excavation. Special measures are usually taken to keep any water out of the excavation. Props may sometime s be used to support the retaining wall.

In Plaxis, these processes are simulated with the Staged construction loading type available in the General subtree of the Phases window. It enables the activation or deactivation of weight, stiffness and strength of selected components of the finite element model.

169

- Click on the Staged construction tab to proceed with the definition of the calculation phases.
- The initial phase has already been introduced. Keep type as K_0 procedure. Make sure all the soil volumes are active and all the structural elements and load are inactive.

Phase 1: Activate plate

In the Phases explorer click the Add phase button to introduce a new phase.

- The default settings are valid for this phase. In the model the full geometry is active except for the wall, interfaces, and strut.

Click the Select multiple objects button in the side toolbar. In the appearing menu point Select line and click on the Select plates option.

- In the draw area define a rectangle including all the plate elements
- Right-click the wall in the draw area and select the Activate option from the appearing menu. The wall is now visible in the color that is specified in the material dataset.
- Make sure all the interfaces in the model are active.

Phase 2: First excavation stage (1m from surface)

In the Phases explorer click the Add phase button to introduce a new phase.

- A new calculation phase appears in the Phases explorer. Note that the program automatically presumes that the current phase should start from the previous one and the same objects are active.

170

- The default settings are valid for this phase. In the Staged construction mode all the structure elements except the fixed-end anchor are active.

- In the draw area right-click the top right cluster and select the Deactivate option in the appearing menu. Figure A.2.4 displays the model for the first excavation phase.
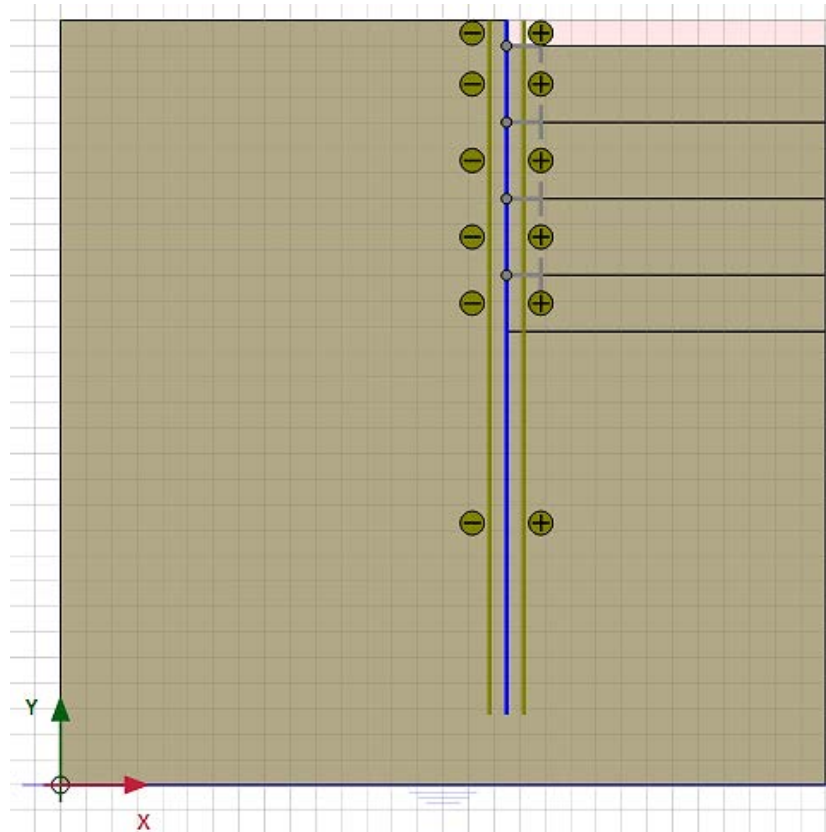

Figure A.2.4- Model view for the first excavation phase

Phase 3: Installation of first strut level 1m below surface

Add a new phase.

- Activate the strut. The strut should turn the set color (in this case blue) to indicate it is active.

171

Phase 4: Second excavation (to 4m depth from surface)

Add a new phase

- Deactivate the second cluster from the top on the right side of the mesh. It should be the topmost active cluster (Figure A.2.5)
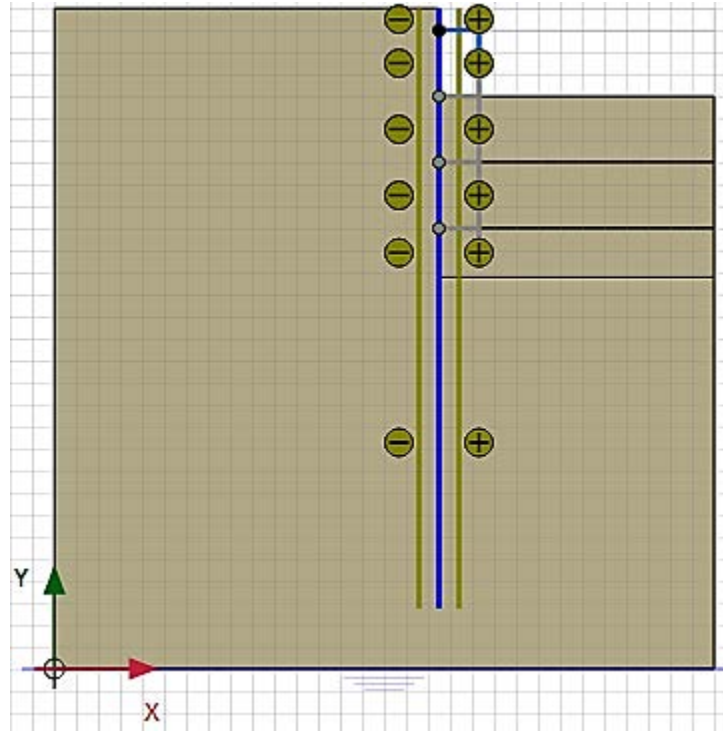

Figure A.2.5- Model for the second excavation phase

Phase 5: Installation of second level of strut (4m below surface)

Add a new phase.

- Activate the strut. The strut should turn the set color (in this case blue) to indicate it is active.

172

Phase 6: Third excavation (to 7m depth from surface)

Add a new phase

- Deactivate the third cluster from the top on the right side of the mesh. It should be the topmost active cluster (Figure A.2.6)
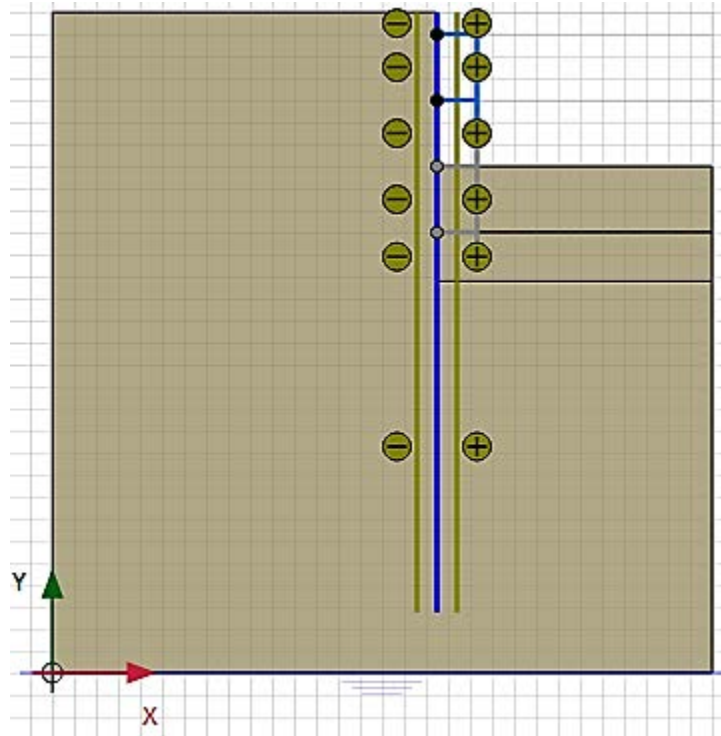

Figure A.2.5- Model for the third excavation phase

Phase 7: Installation of third level of strut (7m below surface)

Add a new phase.

- Activate the strut. The strut should turn the set color (in this case blue) to indicate it is active.

173

Phase 8: Fourth excavation (to 10m depth from surface)

Add a new phase

- Deactivate the third cluster from the top on the right side of the mesh. It should be the topmost active cluster (Figure A.2.7)
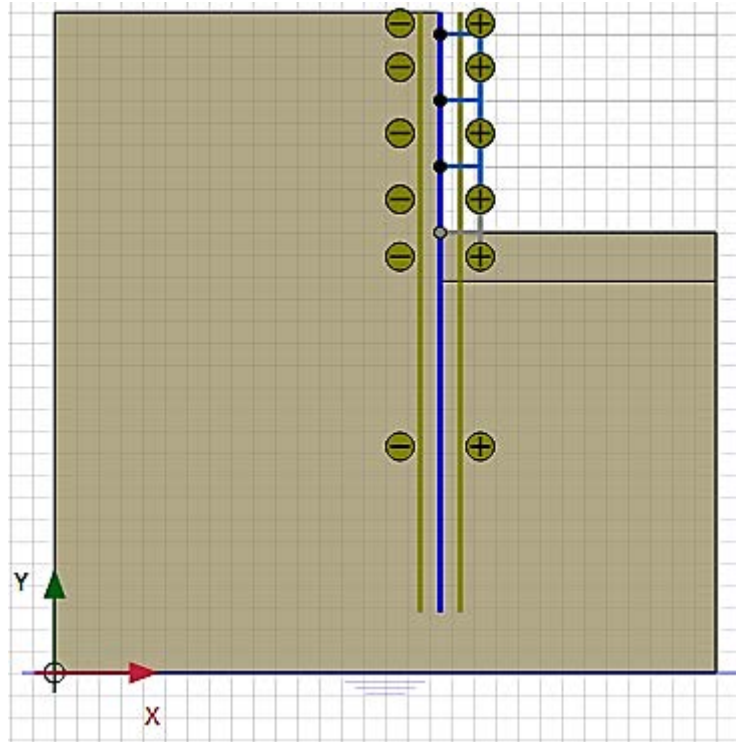

Figure A.2.7- Model for the fourth excavation phase

Phase 9: Installation of last level of strut (10m below surface)

Add a new phase.

- Activate the strut. The strut should turn the set color (in this case blue) to indicate it is active.

174

Phase 10: Last excavation (to 12.2m depth from surface)

Add a new phase

- In the final calculation stage the excavation of the last layer inside the pit is simulated. Deactivate the fifth cluster from the top on the right side of the mesh (Figure A.2.8).
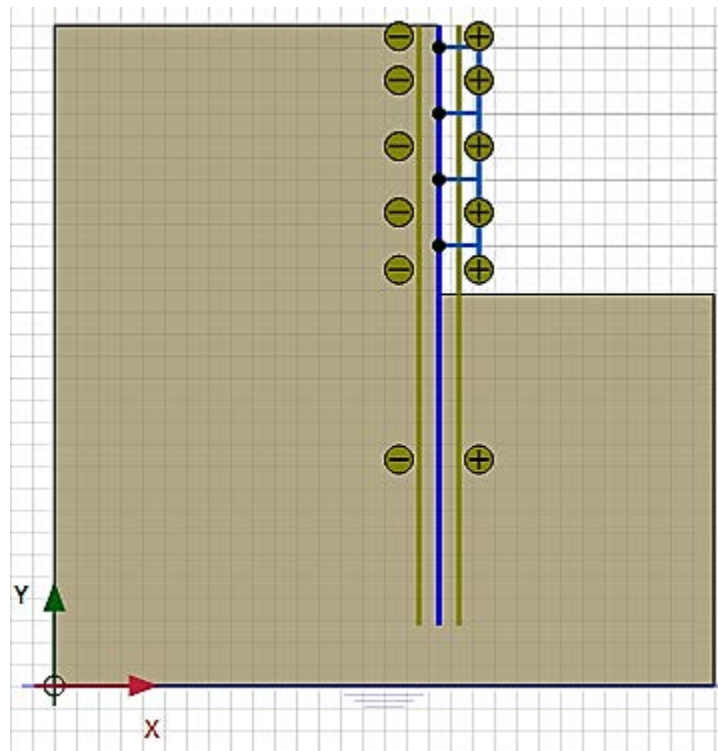
Figure A.2.8- Model for the final excavation phase

The calculation definition is now complete. Before starting the calculation it is suggested that you select nodes or stress points for a later generation of load-displacement curves or stress and diagrams. To do this, follow the steps below.

Click the Select points for curves button in the side toolbar. The connectivity plot is displayed in the Output program and the Select points window is activated.

175

- Select some nodes on the wall at points where large deflections can be expected. The nodes located near that specific location are listed. Select the convenient one by checking the box in front of it in the list. Close the Select points window (Figure A.2.9)
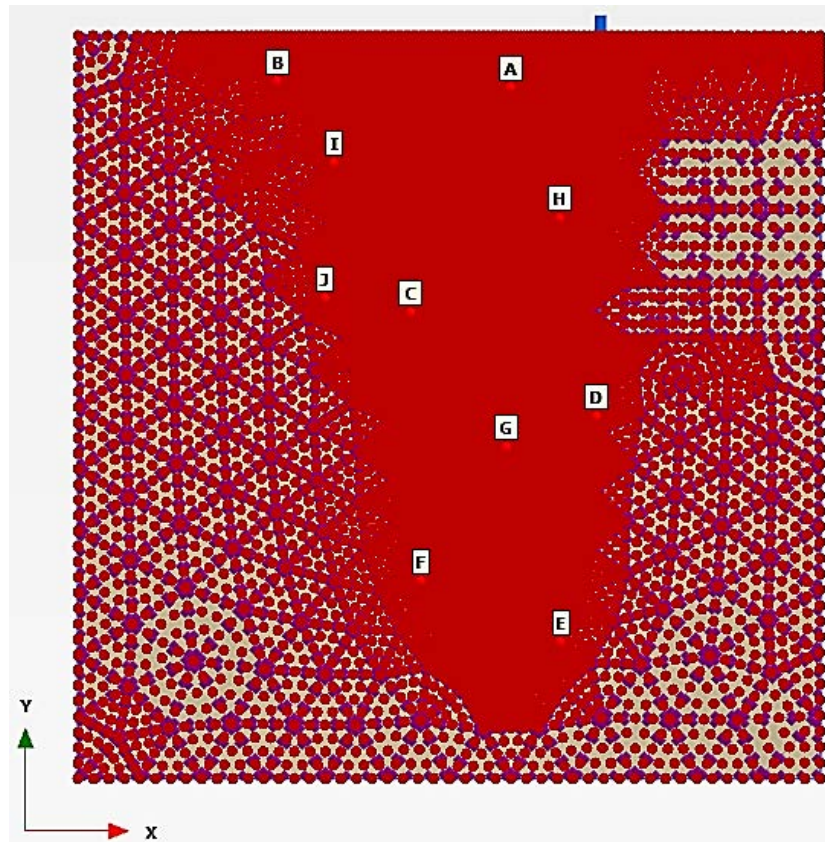

Figure A.2.9- Selection of points of interest for ground movements

- Click on the Update tab to close the Output program and go back to the Input program.

Calculate the project

During a Staged construction calculation phase, a multiplier called $\Sigma Mstage$ is increased from 0.0 to 1.0. This parameter is displayed on the calculation info window. As soon as

$\Sigma Mstage$ has reached the value 1.0, the construction stage is completed and the calculation phase is finished. If a Stage construction calculation finishes while $\Sigma Mstage$ is smaller than 1.0, the program will give a warning message. The most likely reason for not finishing a construction stage is that a failure mechanism has occurred, but there can be other causes as well. See the Reference Manual, available on software manufacturer's website, for more information about Stage construction.

A.2.6   Results

As earlier indicated the interest of this research is on the displacements, thus only maximum horizontal and maximum vertical values will be featured.

To examine the results of this project follow these steps;

- Click the final calculation phase in the Calculations window.

Click the View calculation results button on the toolbar. As a result, the Output program is started, showing the deformed mesh (scaled up) at the end of the selected calculation phase, with an indication of the maximum displacement.

The results for the various configurations are shown below:

177

Figure A.2.10 Case 1: Maximum horizontal ground movements.

Figure A.2.11 Case 1: Maximum vertical ground settlement.

Figure A.2.12 Case 2: Maximum horizontal ground movements.

Figure A.2.13 Case 2: Maximum vertical ground settlement.

Figure A.2.14 Case 3: Maximum horizontal ground movements.

Figure A.2.15 Case 3: Maximum vertical ground settlement.

Figure A.2.16 Case 4: Maximum horizontal ground movements.

184

Figure A.2.17 Case 4: Maximum vertical ground settlement.

Figure A.2.18 Case 5: Maximum horizontal ground movements.

Figure A.2.19 Case 5: Maximum vertical ground settlement.

APPENDIX B

B.0   RSMeans Cost Data

B.1   RSMeans 2014 Bare Costs

Shoring

3 - Timber Shoring

3.10 Building Shoring		Crew	Daily Output	Labor-Hours	Unit	Material	2014 Bare Costs Labor	Equipment	Total	Total Incl O&P
BUILDING SHORING										
Shoring, existing building, with timber, no salvage allowance		B-51	2.20	21.818	M.B.F.	760	805	123	1,688	2,225
On cribbing with 35 ton screw jacks, per box and jack		"	3.60	13.333	Jack	71	495	75	641	920
16 - Sheet Piling										
6.10 Sheet Piling Systems										
SHEET PILING SYSTEMS										
Sheet piling steel, not incl. wales, 22 psf, 15' excav., left in place		B-40	10.81	5.920	Ton	1,450	272	355	2,077	2,425
Drive, extract & salvage	R314116-40		6	10.667		505	490	635	1,630	2,025
20' deep excavation, 27 psf, left in place			12.95	4.942		1,450	227	295	1,972	2,275
Drive, extract & salvage	R314116-45		6.55	9.771		505	450	585	1,540	1,900
25' deep excavation, 38 psf, left in place			19	3.368		1,450	155	201	1,806	2,075
Drive, extract & salvage			10.50	6.095		505	280	365	1,150	1,400
40' deep excavation, 38 psf, left in place			21.20	3.019		1,450	139	180	1,769	2,025
Drive, extract & salvage			12.25	5.224	▼	505	240	310	1,055	1,275
15' deep excavation, 22 psf, left in place			983	.065	S.F.	16.95	3	3.89	23.84	27.50
Drive, extract & salvage			545	.117		5.65	5.40	7	18.05	22.50
20' deep excavation, 27 psf, left in place			960	.067		21.50	3.07	3.98	28.55	32.50
Drive, extract & salvage			485	.132		7.35	6.05	7.85	21.25	26
25' deep excavation, 38 psf, left in place			1000	.064		31.50	2.94	3.82	38.26	43.50
Drive, extract & salvage			553	.116	▼	10.05	5.30	6.90	22.25	27
Rent steel sheet piling and wales, first month					Ton	305			305	335
Per added month						30.50			30.50	33.50
Rental piling left in place, add to rental						1,150			1,150	1,275
Wales, connections & struts, 2/3 salvage						475			475	525
High strength piling, 50,000 psi, add						63			63	69.50
55,000 psi, add						81			81	89
Tie rod, not upset, 1-1/2" to 4" diameter with turnbuckle						2,100			2,100	2,300
No turnbuckle						1,625			1,625	1,800
Upset, 1-3/4" to 4" diameter with turnbuckle						2,375			2,375	2,600
No turnbuckle					▼	2,050			2,050	2,250
Lightweight, 18" to 28" wide, 7 ga., 9.22 psf, and										
7 ga., 8.6 psf, minimum					Lb.	.79			.79	.87
Average						.90			.90	.99
Maximum					▼	1.05			1.05	1.16
Wood, solid sheeting, incl. wales, braces and spacers,	R314116-40									
drive, extract & salvage, 8' deep excavation		B-31	330	.121	S.F.	1.76	4.71	.66	7.13	9.90
10' deep, 50 S.F./hr. in & 150 S.F./hr. out			300	.133		1.81	5.20	.73	7.74	10.80
12' deep, 45 S.F./hr. in & 135 S.F./hr. out			270	.148		1.87	5.75	.81	8.43	11.85
14' deep, 42 S.F./hr. in & 126 S.F./hr. out			250	.160		1.92	6.20	.88	9	12.70
16' deep, 40 S.F./hr. in & 120 S.F./hr. out			240	.167		1.98	6.50	.91	9.39	13.20
18' deep, 38 S.F./hr. in & 114 S.F./hr. out			230	.174		2.05	6.75	.95	9.75	13.75
20' deep, 35 S.F./hr. in & 105 S.F./hr. out			210	.190		2.12	7.40	1.04	10.56	14.95
Left in place, 8' deep, 55 S.F./hr.			440	.091		3.18	3.54	.50	7.22	9.50
10' deep, 50 S.F./hr.			400	.100		3.34	3.89	.55	7.78	10.30
12' deep, 45 S.F./hr.			360	.111		3.53	4.32	.61	8.46	11.20
14' deep, 42 S.F./hr.			335	.119		3.74	4.64	.65	9.03	12
16' deep, 40 S.F./hr.			320	.125		3.97	4.86	.69	9.52	12.60
18' deep, 38 S.F./hr.			305	.131		4.23	5.10	.72	10.05	13.30
20' deep, 35 S.F./hr.			280	.143	▼	4.54	5.55	.78	10.87	14.40
Alternate pricing, left in place, 8' deep			1.76	22.727	M.B.F.	715	885	125	1,725	2,300
Drive, extract and salvage, 8' deep		▼	1.32	30.303	"	635	1,175	166	1,976	2,700
For treated lumber add cost of treatment to lumber										

621

Figure B.1- Bare costs

189

Figure B.2- Reference table

APPENDIX C

C.0 Comparison Retaining Wall Design and Cost Study: Steel Sheet Piling vs. Various

Walls by NASSPA, 2009

1.1 Conceptual Model

Wall Properties

$H := 19 \cdot ft$ Exposed Wall height

$L := 100 \cdot ft$ Wall Length

1.1.1 Soil and Site Parameters

Retained Soil - Existing above Excavation Level

$\gamma := 120 \cdot pcf$ Soil Density

$\phi f := 30 \cdot deg$ Angle of internal friction

$\delta := 0$ Angle of friction between soil and wall or per AASHTO table 5.5.2B

$\beta := 90 \cdot deg$ Batter of Wall, where 90 degrees is vertical except at Concrete Modular Units

$\alpha := 18 \cdot deg$ Slope of Retained Soil (approx 1:3 slope)

$c := 0$ Soil Cohesion

Foundation Soil - Below Excavation Level - same as Retained Soil
above Excavation Level

Design Standard - AASHTO Standard Specifications for Highway
Bridges - 17th Edition 2002 - Allowable Strength Design

Figure C.1- Model parameters

NORTH AMERICAN STEEL SHEET PILING ASSOCIATION
RETAINING WALL STUDY
Section 1.2 Summary of Costs and Construction Time
All Walls

Retaining Wall Type	Construction Duration (Days)	Total Cost for 100 ft. Wall		Cost per Linear Ft.		Cost per Square Ft.	
Grouted Anchor Steel Sheet Pile Wall	13	$	90,607	$	906.07	$	47.69
Cast-In-Place Reinforced Concrete Wall	47	$	258,572	$	2,585.72	$	136.09
Concrete Modular Unit Gravity Wall	31	$	144,741	$	1,447.41	$	76.18
Mechanically Stabilized Earth Wall	35	$	181,593	$	1,815.93	$	95.58
Soldier Pile and Lagging Wall	26	$	171,856	$	1,718.56	$	90.45
Slurry Wall*	64	$	400,145	$	4,001.45	$	210.60

*Concept model - not typical application for slurry wall but included in study to give comprehensive range of options

Figure C.2- Summary of costs and construction time of all walls

193

NORTH AMERICAN STEEL SHEET PILING ASSOCIATION
RETAINING WALL STUDY
Section 1.2 Summary of Costs and Construction Time
All Walls

Retaining Wall Type	Construction Duration (Days)	Total Cost for 100 ft. Wall	Cost per Linear Ft.	Cost per Square Ft.
Grouted Anchor Steel Sheet Pile Wall	13	$ 90,607	$ 906.07	$ 47.69
Cast-In-Place Reinforced Concrete Wall	47	$ 258,572	$ 2,585.72	$ 136.09
Concrete Modular Unit Gravity Wall	31	$ 144,741	$ 1,447.41	$ 76.18
Mechanically Stabilized Earth Wall	35	$ 181,593	$ 1,815.93	$ 95.58
Soldier Pile and Lagging Wall	26	$ 171,856	$ 1,718.56	$ 90.45
Slurry Wall*	64	$ 400,145	$ 4,001.45	$ 210.60

*Concept model – not typical application for slurry wall but included in study to give comprehensive range of options

Figure C.3-Summary of costs and construction time for cast-in-place reinforced concrete wall

NORTH AMERICAN STEEL SHEET PILING ASSOCIATION
RETAINING WALL STUDY
Section 1.3 Summary of Costs and Construction Time, Each Wall

Concrete Modular Unit Gravity Wall

Pay Item No.	Item		Unit	Quantity	Daily Output (unit/day)	Time (day)	Unit Cost		Cost	
07	Backfill structural	105 H.P., 150 ft. haul, sand &gravel	LCY	2,791.0	670	5	$	2.02	$	5,637.82
08	Borrow loading	Select granular fill	BCY	2,724.0	NA	-	$	13.86	$	37,754.64
09	Compaction, riding, vibrating roller	12 in. lift, 2 passes	ECY	2,724.0	5200	1	$	0.23	$	626.52
10	Compaction, walk behind, vibrating plate	12 in. lift, 2 passes	ECY	117.0	560	1	$	0.78	$	91.26
12	Excavation, trench, common earth	14 ft to 20 ft deep, 1.5 cy hdraulic backhoe	BCY	2,944.0	480	7	$	3.86	$	11,363.84
16	Geotextile for subsurface drainage	Fabric, laid in trench, adverse conditions	SY	300.0	1600	1	$	2.18	$	654.00
18	Forms in place, footing	Continuous wall, plywood, 2x	SFCA	400.0	440	1	$	2.80	$	1,120.00
21	Reinforcing steel, A615 Gr 60	10 - 50 ton job #3 to #7 bars	TN	21.5	2.1	10	$	2,825.00	$	60,737.50
23	Concrete, ready mix	Normal weight, 3500 psi	CY	146.5	NA	-	$	114.00	$	16,701.00
24	Placing concrete, footings	Continuous, shallow, direct chute	CY	128.0	120	2	$	21.00	$	2,688.00
25	Placing concrete, footings	Continuous, shallow pumped	CY	18.5	150	1	$	28.00	$	518.00
27	Placing concrete	with crane	CY	128.0	95	2	$	53.50	$	6,848.00
	Totals					31			$	144,740.58
							Cost per LF		$	1,447.41
							Cost per SF		$	76.18

6 of 78

Figure C.4-Summary of costs and construction time for concrete modular unit gravity wall

NORTH AMERICAN STEEL SHEET PILING ASSOCIATION
RETAINING WALL STUDY
Section 1.3 Summary of Costs and Construction Time, Each Wall

Mechanically Stabilized Earth Wall

Pay Item No.	Item		Unit	Quantity	Daily Output (unit/day)	Time (day)	Unit Cost		Cost
07	Backfill structural	105 H.P., 150 ft. haul, sand &gravel	LCY	3,593.0	670	6	$	2.02	$ 7,257.86
08	Borrow loading	Select granular fill	BCY	3,593.0	NA	-	$	13.86	$ 49,798.98
09	Compaction, riding, vibrating roller	12 in. lift, 2 passes	ECY	3,593.0	5200	1	$	0.23	$ 826.39
10	Compaction, walk behind, vibrating plate	12 in. lift, 2 passes	ECY	117.0	560	1	$	0.78	$ 91.26
12	Excavation, trench, common earth	14 ft to 20 ft deep, 1.5 cy hdraulic backhoe	BCY	3,593.0	480	8	$	3.86	$ 13,868.98
16	Geotextile for subsurface drainage	Fabric, laid in trench, adverse conditions	SY	438.9	1600	1	$	2.18	$ 956.80
21	Reinforcing steel, A615 Gr 60	10 - 50 ton job, # 3 to # 7 bars	TN	7.1	2.1	4	$	2,825.00	$ 20,057.50
22	Welded wire fabric	6x6, W4xW4, 58psf/csf	CSF	193.0	27	8	$	94.00	$ 18,142.00
23	Concrete, ready mix	Normal weight, 3500 psi	CY	11.1	NA	-	$	114.00	$ 1,265.40
25	Placing concrete, footings	Continuous, shallow pumped	CY	600.0	150	4	$	28.00	$ 16,800.00
29	Precast concrete wall panels	10 in. thick	SF	2,100.0	1550	2	$	22.68	$ 47,628.00
30	Galvanizing steel in shop	1 ton to 20 tons	TN	5.6	NA	-	$	875.00	$ 4,900.00
	Totals					35			$ 181,593.17
							Cost per LF	$	1,815.93
							Cost per SF	$	95.58

7 of 78

Figure C.5-Summary of costs and construction time for mechanically stabilized earth wall

NORTH AMERICAN STEEL SHEET PILING ASSOCIATION
RETAINING WALL STUDY
Section 1.3 Summary of Costs and Construction Time, Each Wall

Soldier Pile and Lagging Wall

Pay Item No.	Item		Unit	Quantity	Daily Output (unit/day)	Time (day)	Unit Cost	Cost
05	Grouted Anchors 1" dia		LF	350.0	120	3	$ 20.20	$ 7,070.00
04	Anchors		TN	0.5	NA	-	$ 2,700.00	$ 1,269.00
07	Backfill structural	105 H.P., 150 ft. haul, sand &gravel	LCY	2,266.0	670	4	$ 2.02	$ 4,577.32
08	Borrow loading	Select granular fill	BCY	2,266.0	NA	-	$ 13.86	$ 31,406.76
09	Compaction, riding, vibrating roller	12 in. lift, 2 passes	ECY	2,266.0	5200	1	$ 0.23	$ 521.18
10	Compaction, walk behind vibrating plate	12 in. lift, 2 passes	ECY	106.0	560	1	$ 0.78	$ 82.68
11	Excavation, trench, common earth	6 ft to 10 ft deep, 1.5 cy hydraulic backhoe	BCY	968.0	600	2	$ 3.10	$ 3,000.80
12	Excavation, trench, common earth	14 ft to 20 ft deep, 1.5 cy hydraulic backhoe	BCY	1,298.0	480	3	$ 3.86	$ 5,010.28
14	Driven piles, H sections	HP14x89 to 50 ft length	VLF	420.0	510	1	$ 76.50	$ 32,130.00
15	Driven piles, complete pile driving setup	Mobilization, large	EA	1.0	0.27	4	$ 22,000.00	$ 22,000.00
16	Geotextile for subsurface drainage	Fabric, laid in trench, adverse conditions	SY	233.3	1600	1	$ 2.18	$ 508.59
21	Reinforcing steel, A615 Gr 60	10 - 50 ton job, # 3 to # 7 bars	TN	7.5	2.1	4	$ 2,825.00	$ 21,187.50
29	Precast concrete wall panels	10 in. thick	SF	1,900.0	1550	2	$ 22.68	$ 43,092.00
	Totals					26		$ 171,856.11
							Cost Per LF	$ 1,718.56
							Cost Per SF	$ 90.45

8 of 78

Figure C.6-Summary of costs and construction time for soldier pile and lagging wall

NORTH AMERICAN STEEL SHEET PILING ASSOCIATION
RETAINING WALL STUDY
Section 1.3 Summary of Costs and Construction Time, Each Wall

Slurry Wall

Pay Item No.	Item		Unit	Quantity	Daily Output (unit/day)	Time (day)	Unit Cost	Cost
07	Backfill structural	105 H.P., 150 ft. haul, sand &gravel	LCY	515.9	670	1	$ 2.02	$ 1,042.12
08	Borrow loading	Select granular fill	BCY	515.9	NA	-	$ 13.86	$ 7,150.37
10	Compaction, walk behind vibrating plate	12 in. lift, 2 passes	ECY	515.9	560	1	$ 0.78	$ 402.40
12	Evacuation, trench, common earth	14 ft to 20 ft deep, 1.5 cy hydraulic backhoe	BCY	515.9	480	2	$ 3.86	$ 1,991.37
16	Geotextile for subsurface drainage	Fabric, laid in trench, adverse conditions	SY	288.9	1600	1	$ 2.18	$ 629.80
17	Slurry Trench, excavated in wet soils	Backfilled w/3ksi concrete, no reinforcement	CF	11,691.0	333	36	$ 23.50	$ 274,738.50
20	Steel framed plywood	16ft to 20ft high	SFCA	2,000.0	400	5	$ 8.15	$ 16,300.00
21	Reinforcing steel, A615 Gr 60	10 - 50 ton job, # 3 to # 7 bars	TN	32.7	2.1	17	$ 2,825.00	$ 92,377.50
23	Concrete, ready mix	Normal weight, 3500 psi	CY	37.0	NA	-	$ 114.00	$ 4,218.00
26	Placing concrete, walls	15 in thk, pumped	CY	37.0	120	1	$ 35.00	$ 1,295.00
	Totals					64		$ 400,145.07
							Cost Per LF	$ 4,001.45

Figure C.7-Summary of costs and construction time for slurry wall

APPENDIX D

D.0 Hand Calculations of design sections

WALL DESIGN

													--------->Recalculation				
-------->Forward																	
Δl_c (mm)	L(m)	$\Delta l_c/L$ (%)	R	s_v	$s_h/s_v I$	s_h	s_h/s_v	I_{rqd} (cm^4/m)	Type	I_{des}(cm^4/m	lb/s.f	NC/m^2	STATUS	$s_h/s_v I$	R	β	$\Delta l_c/L$ (%)	Δl_c (mm)	STATUS
1.00	12	0.008	385.75	2.44	7251.525	5	2.05	28258.61	SCZ 23	28900	23.35	0.027	OK	7090.59	377.18	0.001352	0.0016	0.19	OK

LOAD CALCS

S_{des} (cm^3/m)	M_{max} (kN-m/m)	p (kN/m^2)	$M_{maxwale}$ (kN-m/m)	$P_{maxstrut}$ (kN/m)
1700	422	709	1477	1730

WALE DESIGN

S_{rqd} (cm^3/m)	Type	S_{des} (cm^3/m)	STATUS
5949	W30x132	6227.06	OK

STRUT DESIGN

					TRIAL SECTION				STATUS
Required	A_{rqd} =	0.0069672 m^2			Type	A(cm^2/m)			OK
		70 cm^2			CHS 193.7	89.3			

Compressive Strength Check

				r_x =	6.31 cm	B =	25 m
K =	1			r_y =	6.31 cm		
ϕ_c =	0.85			t =	7.01 cm		
λ_c =	0.044			D =	19.37 cm		
Q =	1						
F_{cr} =	248095 kPa			STATUS			
Available	$F_{available}$ =	1883 kN----------	>1730 kN	OK			

Figure D.1- Case 2

200

		-------->Forward													--------->Recalc				
WALL DESIGN	Δl_c (mm)	L(m)	$\Delta l_c/L$ (%)	R	s_v	$s_h/s_v/I$	s_h	s_h/s_v	I_{rqd} (cm^4/m)	Type	I_{des}(cm^4/m)	lb/s.f	NC/m^2	STATUS	$s_h/s_v/I$	R	β	$\Delta l_c/L$ (%)	Δl_c (mm)	STATUS
	2.00	12	0.017	1322.60	2.44	24863	5	2.05	8242	GU 6N	9670	14.336	0.017	OK	21191	1127	0.001785	0.00597	0.72	OK

LOAD CALCS	S_{des} (cm^3/m)	M_{max} (kN-m/m)	p (kN/m^2)	$M_{maxwale}$ (kN-m/m)	$P_{maxstrut}$ (kN/m)
	625	155	261	543	636

WALE DESIGN	S_{rqd} (cm^3/m)	Type	S_{des} (cm^3/m)	STATUS
	2187.05	W24X68	2523.598	OK

STRUT DESIGN

				TRIAL SECTION		STATUS
Required	A_{rqd} =	0.00256 m^2		Type	A(cm^2/m)	OK
		26 cm^2		CHS 139.7	33.1	

Compressive Strength Check

			r_x =	4.66 cm	B =	25 m
K =	1		r_y =	4.66 cm	
ϕ_c =	0.85		t =	0.8 cm	
λ_c =	0.060		D =	13.97 cm	
Q =	1			
F_{cr} =	247924 kPa			STATUS
Available	$F_{available}$ =	698 kN---------- >637 kN		OK

Figure D.2- Case 3

www.manaraa.com

WALL DESIGN

	-------->Forward													-------->Recalc					
	Δl_c (mm)	L(m)	$\Delta l_c/L$ (%)	R	s_v	$s_h/s_v/I$	s_h	s_h/s_v	I_{rqd} (cm⁴/m)	Type	I_{des}(cm⁴/m)	lb/s.f	NC/m²	STATUS	$s_h/s_v/I$	R	β	$\Delta l_c/L$ (%)	Δl_c (mm)	STATUS
	3.00	12	0.025	2719.27	2.44	51119	5	2.05	4009	CZ 67	5750	13.72	0.016	OK	35638	1896	0.002037	0.01092	1.31	OK

LOAD CALCS

S_{des} (cm³/m)	M_{max} (kN-m/m)	p (kN/m²)	$M_{maxwale}$ (kN-m/m)	$P_{maxstrut}$ (kN/m)
575	143	240	500	585

WALE DESIGN

S_{rqd} (cm³/m)	Type	S_{des} (cm³/m)	STATUS
2012	W24X62	2163.084	OK

STRUT DESIGN

				TRIAL SECTION			STATUS
Required	A_{rqd} =	0.00236	m²	Type	A(cm²/m)		OK
		24	cm²	CHS 101.6	28.8		

Compressive Strength Check

			r_x =	3.26 cm	B =	25 m
	K =	1	r_y =	3.26 cm		
	ϕ_c =	0.85	t =	1 cm		
	λ_c =	0.086	D =	10.16 cm		
	Q =	1				
	F_{cr} =	247533 kPa			STATUS	
Available	$F_{available}$ =	606 kN----------	>586 kN		OK	

Figure D.3- Case 4

	-------->Forward													-------->Recalc					
WALL DESIGN	Δl_c (mm)	L(m)	$\Delta l_c/L$ (%)	R	s_v	$s_h/s_v/I$	s_h	s_h/s_v	I_{rqd} (cm⁴/m)	Type	$_{des}$(cm⁴/m)	lb/s.f	NC/m²	STATUS	$s_h/s_v/I$	R	β	$\Delta l_c/L$ (%)	Δl_c (mm)	STATUS
	0.50	12	0.004	112.51	2.44	2115	5	2.05	96890	AZ 39-700	97500	38.59	0.045	OK	2102	112	0.000993	0.00036	0.04	OK

LOAD CALCS	S_{des} (cm³/m)	M_{max} (kN-m/m)	p (kN/m²)	$M_{maxwale}$ (kN-m/m)	$P_{maxstrut}$ (kN/m)
	3900	968	1627	3389	3969

WALE DESIGN	S_{rqd} (cm³/m)	Type	S_{des} (cm³/m)	STATUS
	13647	W33x263	15059.71	OK

STRUT DESIGN

				TRIAL SECTION		STATUS
Required	$A_{rqd} =$	0.01598	m²	Type	A(cm²/m)	OK
		160	cm²	CHS 406.4	196.0	

Compressive Strength Check

			$r_x =$	13.8	cm	B = 25 m
K =	1		$r_y =$	13.8	cm	
$\phi_c =$	0.85		t =	1.6	cm	
$\lambda_c =$	0.020		D =	40.64	cm	
Q =	1					
$F_{cr} =$	248257	kPa		STATUS		
Available	$F_{available} =$	4136	kN----------	>3969 kN	OK	

Figure D.4- Case 1

WALL DESIGN	Δl_c (mm)	L(m)	$\Delta l_c/L$ (%)	R	s_v	$s_h/s_v/I$	s_h	s_h/s_v	I_{rqd} (cm⁴/m)	Type	I_{des}(cm⁴/m)	lb/s.f	NC/m²	STATUS	$s_h/s_v/I$	R	β	$\Delta l_c/L$ (%)	Δl_c (mm)	STATUS
--------->Forward															--------->Recalc					
	5.00	12	0.042	6742.28	2.44	126746	5	2.05	1617	SKS 11	2550	11.26	0.013	OK	80360	4275	0.002504	0.02618	3.14	OK

LOAD CALCS	S_{des} (cm³/m)	M_{max} (kN-m/m)	p (kN/m²)	$M_{maxwale}$ (kN-m/m)	$P_{maxstrut}$ (kN/m)
	341	85	142	296	347

WALE DESIGN	S_{rqd} (cm³/m)	Type	S_{des} (cm³/m)	STATUS
	1193	W12x87	1933.7	OK

STRUT DESIGN

			TRIAL SECTION		STATUS
Required	A_{rqd} =	0.00140 m²	Type	A(cm²/m)	OK
		14 cm²	CHS101.6x	16.9	

Compressive Strength Check

			r_x =	3.4 cm	B = 25 m
K =	1		r_y =	3.4 cm	
ϕ_c =	0.85		t =	0.56 cm	
λ_c =	0.082		D =	10.16 cm	
Q =	1				
F_{cr} =	247595 kPa			STATUS	
Available	$F_{available}$ =	356 kN----------	>348 kN	OK	

Figure D.5- Case 5

APPENDIX E

E.1 Rigidity deficit values at various vertical strut spacing

R	s_v= 0.5m	s_v= 1m	s_v= 2m	s_v= 3m	s_v= 4m	s_v=5m
	$(s_h/s_v \cdot I)$					
0	0	0	0	0	0	0
5	2238.36	559.59	139.90	62.18	34.97	22.38
50	22383.62	5595.90	1398.98	621.77	349.74	223.84
100	44767.23	11191.81	2797.95	1243.53	699.49	447.67
200	89534.47	22383.62	5595.90	2487.07	1398.98	895.34
400	179068.94	44767.23	11191.81	4974.14	2797.95	1790.69
500	223836.17	55959.04	13989.76	6217.67	3497.44	2238.36
750	335754.26	83938.57	20984.64	9326.51	5246.16	3357.54
900	402905.11	100726.28	25181.57	11191.81	6295.39	4029.05
1000	447672.35	111918.09	27979.52	12435.34	6994.88	4476.72
1500	671508.52	167877.13	41969.28	18653.01	10492.32	6715.09
2000	895344.70	223836.17	55959.04	24870.69	13989.76	8953.45
3000	1343017.04	335754.26	83938.57	37306.03	20984.64	13430.17
4000	1790689.39	447672.35	111918.09	49741.37	27979.52	17906.89
5000	2238361.74	559590.44	139897.61	62176.72	34974.40	22383.62
7500	3357542.61	839385.65	209846.41	93265.07	52461.60	33575.43
9000	4029051.13	1007262.78	251815.70	111918.09	62953.92	40290.51
10000	4476723.48	1119180.87	279795.22	124353.43	69948.80	44767.23
12000	5372068.18	1343017.04	335754.26	149224.12	83938.57	53720.68
15000	6715085.22	1678771.31	419692.83	186530.15	104923.21	67150.85
17000	7610429.92	1902607.48	475651.87	211400.83	118912.97	76104.30
20000	8953446.96	2238361.74	559590.44	248706.86	139897.61	89534.47
22000	9848791.66	2462197.92	615549.48	273577.55	153887.37	98487.92
25000	11191808.71	2797952.18	699488.04	310883.58	174872.01	111918.09
30000	13430170.45	3357542.61	839385.65	373060.29	209846.41	134301.70
35000	15668532.19	3917133.05	979283.26	435237.01	244820.82	156685.32
40000	17906893.93	4476723.48	1119180.87	497413.72	279795.22	179068.94
45000	20145255.67	5036313.92	1259078.48	559590.44	314769.62	201452.56
46000	20592928.02	5148232.00	1287058.00	572025.78	321764.50	205929.28
48000	21488272.72	5372068.18	1343017.04	596896.46	335754.26	214882.73
50000	22383617.41	5595904.35	1398976.09	621767.15	349744.02	223836.17
52000	23278962.11	5819740.53	1454935.13	646637.84	363733.78	232789.62
54000	24174306.80	6043576.70	1510894.18	671508.52	377723.54	241743.07
55000	24621979.15	6155494.79	1538873.70	683943.87	384718.42	246219.79
57000	25517323.85	6379330.96	1594832.74	708814.55	398708.19	255173.24
58000	25964996.20	6491249.05	1622812.26	721249.89	405703.07	259649.96
60000	26860340.89	6715085.22	1678771.31	746120.58	419692.83	268603.41

206

REFERENCES

Attewell, P. B. (1978). "Large ground movements and structural damage caused by tunneling below the water table in a silty alluvial clay." *Proc., Conf. on Large Ground Movements and Structures, Cardiff, July 1977 , James D. Geddes, ed., Pentech Press, London*. Cardiff, 307–355.

Bjerrum, L. (1963). "Allowable settlements of structures." *Proc. European Conf. on Soil Mechanics and Foundation Engineering, Vol. 2, Weisbaden*, 135-137.

Boone, S. J. (2003). "Design of deep excavations in urban environments." Ph.D. thesis, Univ. of Toronto, Toronto, Canada.

Boone, S. J. Westland, J., and Nusink, R. (1999). "Comparative evaluation of building responses to an adjacent braced excavation ." *Can. Geotech. J., 36*, 210–223.

Boone, S.J. (2001). "Assessing construction and settlement-induced building damage: a return to fundamental principles." *Underground Construction, Institution of Mining and Metalurgy*. London, 559-570.

Boscardin, M. D., and Cording, E. J. (1989). "Building response to excavation-induced settlement." *J. Geotech. Eng., 115(1),* 1-21.

Boscardin, M. D., Cording, E. J., and O'Rourke, T. D. (1979) "Case studies of building behavior in response to adjacent excavation." *Univ. of Illinois Rep. for the U.S. Dept. of Transportation, Rep. No. UMTA-IL-06-0043-78-2, Washington D.C*.

Bozozuk, M. (1962) "Soil shrinkage damages shallow foundations at Ottawa Canada." *The Engrg. J., Canada*, 33-37.

207

Bryson, L. S. and Kotheimer, M. J. (2011). "Cracking in Walls of a Building Adjacent." *J. Perform. Constr. Facil.*, 491-503.

Bryson, L. S. (2002). "*Performance of a stiff excavation support system in soft clay and the response of an adjacent building*." Northwestern Univ., Ph.D. thesis. Evanston, IL.

Burland, J. B., and Wroth, C. P. (1974). "Settlement of buildings and associated damage." *Proc., Conf. on Settlement of Structures, Pentech, London*, 611–654.

Calvello, M. (2002)"Inverse Analysis of a Supported Excavation through Chicago Glacial Clays." *PhD Thesis, Northwestern University, Evanston, IL.*

Clough, G. W., and O'Rourke, T. D. (1990). "Construction induced movements of in situ walls." *Geotechnical Special Publication No. 25, ASCE, Reston, VA, 439–470.*

Fang, H-Y. (1991). "*Foundation Engineering Handbook.*" 2nd edition, Van Nostrand Reinhold, New York, NY 10003.

Finno, R. J. and Bryson, L. S. (2002). "Response of Building Adjacent to Stiff Excavation Support System in Soft Clay." *Journal of Performance of Constructed Facilities, ASCE,16(1),* 10-20.

Finno, R. J., Blackburn, J. T., and Roboski, J. F. (2007). "Threedimensional effects for supported excavations in clay." *J. Geotech. Geoenviron. Eng., 133(1)*, 30-36.

Finno, R. J., Voss, F. T., Jr., Rossow, E., and Blackburn, J. T. (2005). "Evaluating Damage Potential in Buildings Affected by Excavations." *J. Geotech. Geoenviron. Eng., 131(10),* 1199-1210.

Fjeld, S. (1963). "Settlement damage to a concrete-framed structure." *Proc. Eur. Conf. on Soil Mech. and Found. Engrg., Vol. I*, Norwegian Geotechnical Institute, Oslo, 37-45.

Gere, J. M., and Timoshenko, S. (1984). "*Mechanics of materials.*" 2nd Ed, Boston, MA, TWS Publishers.

Halim, D., and Wong, K.S. (2012). "Prediction of Frame Structure Damage Resulting from Deep Excavation ." *Journal of Geotechnical and Geoenvironmental Engineering,* 138(12), 1530-1536.

Kotheimer, M. J., and Bryson, L. S. (2009). "Damage approximation method for excavation-induced damage to adjacent buildings." *International Foundations Congress and Equipment Expo (IFCEE09),ASCE*. Reston, VA, 8.

Koutsoftas, D. C., Frobenius, P., Wu, C. L., Meyersohn, D. and Kulesza, R. (2000). "Deformations during Cut-and-Cover Construction of MUNI Metro Turnback Project." *Journal of Geotechnical and Geoenvironmental Engineering, ASCE,* 126(4), 344-359.

PLAXIS. (2015). "2D-1-Tutorial." *Plaxis 2D Tutorial Manual*, 31-45.

Meyerhoff, G. G. (1956). "Discussion of the allowable settlements of buildings",by A. W. Skempton and D. H. MacDonald. *Proc., Institute of Civil Engineers, Part II, Vol 5*, 774.

EIC Group. (2009). "Retaining Wall Comparison Technical Report". 420 Route 46 East, Suite 1 Fairfield, NJ 07004, 3-9.

209

O'Rourke, T. D., Cording, E. J., and Boscardin, M. D. (1976). "The ground movements related to braced excavations and their influence on adjacent structures." *Univ. of Illinois Rep. for the U.S. Dept. of Transportation ,Rep. No. DOT-TST-76T-22, Washington D.C.*

Ou, C. Y., Hsieh, P. G., and Chiou, D. C. (1993). "Characteristics of ground surface settlement during excavation ." *Can. Geotech. J.,* 30(5), 758–767.

Ou, C.-Y., Liao, J.-T., and Cheng, W.-L. (2000). "Building response and ground movements induced by a deep excavation." *Geotechnique,* 50(32), 209-220.

Peck, R. B., and Reed, W. C. (1954). "Engineering properties of Chicago subsoils." *Bulletin No. 423, Engineering Experiment Station, Univ. of Illinois, Urbana, III*.

Polshin, D. E., and Tokar, R. A. (1957). "Maximum allowable nonuniform settlement of structures." *Proc., 4th Int. Conf. on Soil Mechanics and Foundation Engineering, London,*1, 402–405.

RSMeans. (2014). "RSMeans Building Construction Cost Data." Norwell, MA: Reed Construction Data, LLC, 621-853.

Schanz, T. and Vermeer, P. A. (1996). "Angles of Friction and Dilatancy of Sand." *Geotechnique,* 46(1), 145-151.

Schuster, M., Kung, G. T. C., Juang, C. H., and Hashash, Y. M. A. (2009). "Simplified model for evaluating damage potential of buildings adjacent to a braced excavation ." *J. Geotech. Geoenviron. Eng.,* 135(12), 1823–1835.

Skempton, A. W., and McDonald, D. H. (1956). "Allowable settlement of buildings." *Proc., Institute of Civil Engineers,* Part III, Vol. 5, 727-768.

Son, M., and Cording, E. J. (2005). "Estimation of building damage due to excavation-induced ground movements ." *J. Geotech. Geoenviron. Eng.,* 131(2), 162–177.

Son, M., and Cording, E.J. (2011). "Responses of Buildings with Different Structural Types to Excavation-Induced Ground Settlements ." *Journal of Geo- technical and Geoenvironmental Engineering,* 137(4), (2011).

VITA

Sekyi Kobina Intsiful is from Sekondi in the Western Region of Ghana. He attended Kwame Nkrumah University of Science and Technology in Kumasi, Ashanti Region, earning himself a BSc. in Civil Engineering. With the first degree he worked with the government of Ghana for a mandatory one year, as Civil Engineer with the Ghana Irrigation Development Authority between 2008 and 2009. Subsequent work experience were in structural analysis of building, telecommunication mast foundations, and water treatment. After over four years of industry experience, he entered the civil engineering master's program hosted by the Civil Engineering Department at the University of Kentucky in August, 2013. In 2014, he was offered the teaching/research assistant in the same department under the direction of L. Sebastian Bryson, Ph.D., P.E.